Site NGHP-01-03

By T. Collett, M. Riedel, J. Cochran, R. Boswell, J. Presley, P. Kumar, A. Sathe,
A. Sethi, M. Lall, and the National Gas Hydrate Program Expedition 01 Scientists

Scientific Investigations Report 2012–5054

U.S. Department of the Interior
U.S. Geological Survey

Contents

Figures

Tables

Site NGHP-01-03

By T. Collett, M. Riedel, J. Cochran, R. Boswell, J. Presley, P. Kumar, A. Sathe, A. Sethi, M. Lall, and the National Gas Hydrate Program Expedition 01 Scientists

Background and Objectives

Site NGHP-01-03 (Prospectus Site GDGH05-A) is located at 15° 53.8919' N, 81° 53.9678' E in the Krishna-Godavari (KG) Basin (fig. 1). The water depth is ~1,076 m.

The objectives of the work carried out at this site follow the general objectives of NGHP Expedition 01:

- Study the occurrence of gas hydrate and establish the background geochemical, geological, geophysical, and microbiological baselines for gas hydrate proxy-studies;
- Define the relationship between the sedimentology and structure of the sediments and the occurrence and concentration of gas hydrate;
- Calibrate remote sensing data such as seismic data by acquiring LWD/MWD and wire-line log data as well as VSP data for time-depth imaging.

Two seismic lines were available in the vicinity of Site NGHP-01-03: line AD-94-16 (SW-NE) and line AD-94-17 (NW-SE). Line AD-94-16 is located about 250 m SW of Site NGHP-01-03 (fig. 2). On the primary line AD-94-17 (fig. 3) a BSR can be identified at Site NGHP-01-03 at a depth of ~1.72 s TWT, whereas there is no clear evidence for a BSR on the crossing line AD-94-16 (fig. 4). Using a uniform velocity of 1,580 m/s and a seafloor depth of 1.45 s TWT, this corresponds to a depth of the BSR of ~209 mbsf.

The general stratigraphy is characterized by seafloor-parallel to slightly inclined beds to a depth of ~125 mbsf. A strong reflection marks the base of this unit and is most likely an unconformity. Below this unconformity the sediments are dipping to the northwest at an apparent dip of 3°. Below the BSR, these dipping layers show signs of gas-charging indicated by the strong seismic reflectivity. The location of this site avoids the strongest seismic amplitudes and was approved to a maximum depth of 350 mbsf.

Operations

This operations summary covers the Leg 2 transit from Site NGHP-01-02 (KGGH03-A) to Site NGHP-01-03 (GDGH05-A), the third Chennai port call at the beginning of Leg 3B, the transit to Site NGHP-01-03, and drilling/coring operations for Holes NGHP-01-03A through NGHP-01-03C (fig. 4). Schedule details and statistics for this site can be found as Appendixes:

- Appendix 1: NGHP Expedition 01 Operations Schedules
- Appendix 2: NGHP Expedition 01 Operations Statistics

Included in the Glossary is a list of standard or commonly used operations terms and acronyms.

Hole NGHP-01-03A

The first hole of Site NGHP-01-03 was drilled on Leg 2 of NGHP Expedition 01 as the third hole in a 12-hole LWD/MWD transect. The 4.8 NMI transit from Site NGHP-01-02 (KGGH03-A) was completed in 1.0 hr, the vessel was switched from cruise mode to DP control, and a positioning beacon was deployed at the prospectus coordinates. The LWD/MWD tools were assembled, the nuclear source was loaded, and the drill string was lowered to a depth of 150.0 mbrf. The tools were function tested at that depth and the Minitron was turned on. The pipe trip then continued to the sea floor, the drill string was spaced out for spudding, and a tag of the sea floor indicated a mudline depth of 1,092.0 mbrf. After offsetting the vessel two meters north of the prospectus coordinates, Hole NGHP-01-03A was spudded at 0915 hr on May 22. LWD/MWD drilling continued at a controlled rate of 18.8 m/h (average net ROP including connection time) to a total depth of 300.0 mbsf. The hole was displaced with 92 barrels of weighted 10.5 ppg Sepiolite mud and the drill string was retracted to 23 mbsf. LWD/MWD logging resumed from that point up to the sea floor. After recovering the drill string, the data were downloaded, the nuclear source was removed, batteries were changed out, and the BHA was racked back in the derrick. The vessel was switched from DP to cruise mode and got underway for Site NGHP-01-04 (KGGH01-A) at 1015 hr on May 23.

Hole NGHP-01-03B

Leg 3B of the five-leg NGHP Expedition 01 began after completing a 3.4 day port call in Chennai. This was the third Chennai port call and was primarily used for a drilling contractor crew change, some changes to the science compliment, and taking on general supplies. The port call was interrupted briefly (~1 hr) while the vessel was relocated from its arrival berth at Quay 3 South (coal dock) to the Chokhani International North Pier. Once port call activities were completed, the last line was released at 1530 hr on June 28 and the vessel got underway for

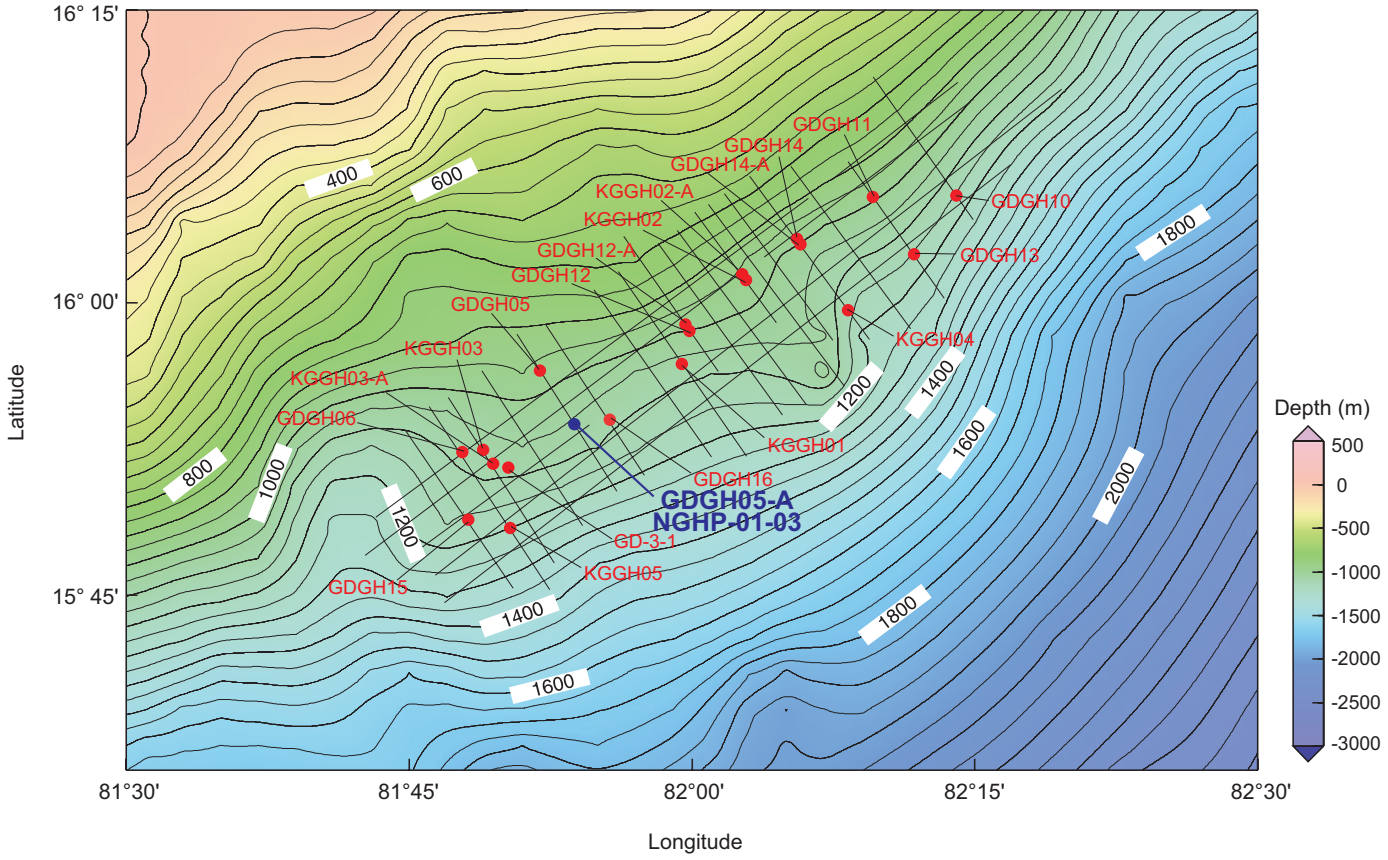

Figure 1. Location of Site NGHP-01-03 (Prospectus Site GDGH05-A) in the Krishna-Godavari (KG) Basin.

Site NGHP-01-03 (GDGH05-A). The 192.0 NMI sea voyage was made at an average speed of 10.1 knots and ended at 1000 hr on 29 June. The vessel was switched from cruise mode to DP control at 1023 hr and a positioning beacon was deployed at the Hole NGHP-01-03A location coordinates. The ice bath was installed in the moon pool and a standard two-stand APC/XCB BHA was made up with a LFV and a typical 11-7/16" APC/XCB C-3 TCI roller cone bit.

Hole NGHP-01-03B was to focus on continuous APC/XCB coring with a few select pressure cores within the gas hydrate stability field. Temperature measurements were also to be taken using the APCT–3, APCT, and DVTP systems to define a thermal gradient from sea floor to TD.

The vessel was offset 10 meters to the SW of Hole NGHP-01-03A while the drill string was tripped to bottom. The bit was positioned at a depth of 1,085.0 mbrf and the first attempt at spudding Hole NGHP-01-03B was made. This attempt was unsuccessful when a full core was recovered making it impossible to accurately determine the mudline. The drill string was raised 4.0 m to 1,081.0 mbrf and Hole NGHP-01-03B was spudded at 1610 hr on June 29, 2006, establishing a sea floor depth of 1,085.1 mbrf. The PDR depth for this site, corrected to the rig floor DES, was 942.4 mbrf. APC Core NGHP-01-03B-01H was on-deck at 1600 hr and APC coring continued through Core NGHP-01-03B-07H to a depth of 62.4 mbsf.

Temperature measurements were taken using the APCT–3 shoe on Cores NGHP-01-03B-03H, NGHP-01-03B-05H, and NGHP-01-03B-07H (24.4 mbsf, 43.4 mbsf, and 62.4 mbsf, respectively).

After switching to the XCB system, Cores NGHP-01-03B-08X through NGHP-01-03B-12X to 104.9 mbsf set up the first PCS Core NGHP-01-03B-13P recovered from 105.9 mbsf. Five more XCB Cores NGHP-01-03B-14X through NGHP-01-03B-18X to 151.7 mbsf were cut and the first DVTP temperature measurement was taken at that depth. Three XCB Cores NGHP-01-03B-19X through NGHP-01-03B-21X to 174.9 mbsf set up the second PCS Core NGHP-01-03B-22P cored to 175.9 mbsf. This was followed by the first FPC Core NGHP-01-03B-23Y to 176.9 mbsf. Three additional XCB Cores NGHP-01-03B-24X through NGHP-01-03B-26X to 198.9 mbsf set up the final series of pressure cores. The third PCS Core NGHP-01-03B-27P advanced to a depth of 199.9 mbsf and the first HRC Core NGHP-01-03B-28E reached 200.9 mbsf. Two more XCB cores NGHP-01-03B-29X-30X were then cut to 220.3 mbsf before deploying the DVTP for the fifth temperature measurement in the hole. The last five XCB cores NGHP-01-03B-31X through NGHP-01-03B-39X were recovered advancing the hole to a total depth of 300.0 mbsf before deploying the DVTP for one last temperature measurement. The sinker bars

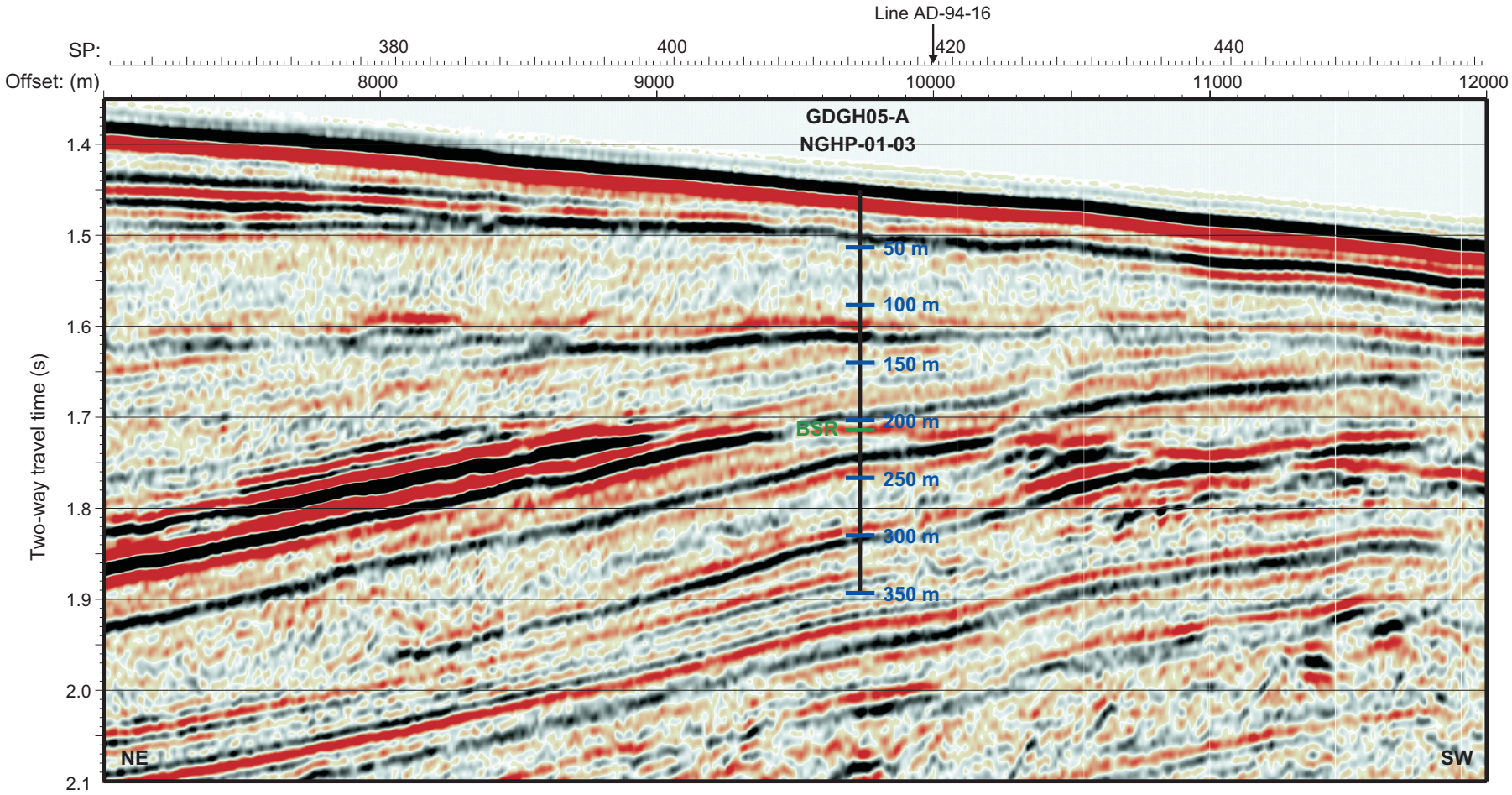

Figure 2. Map showing all holes occupied at Site NGHP-01-03 (GDGH05-A).

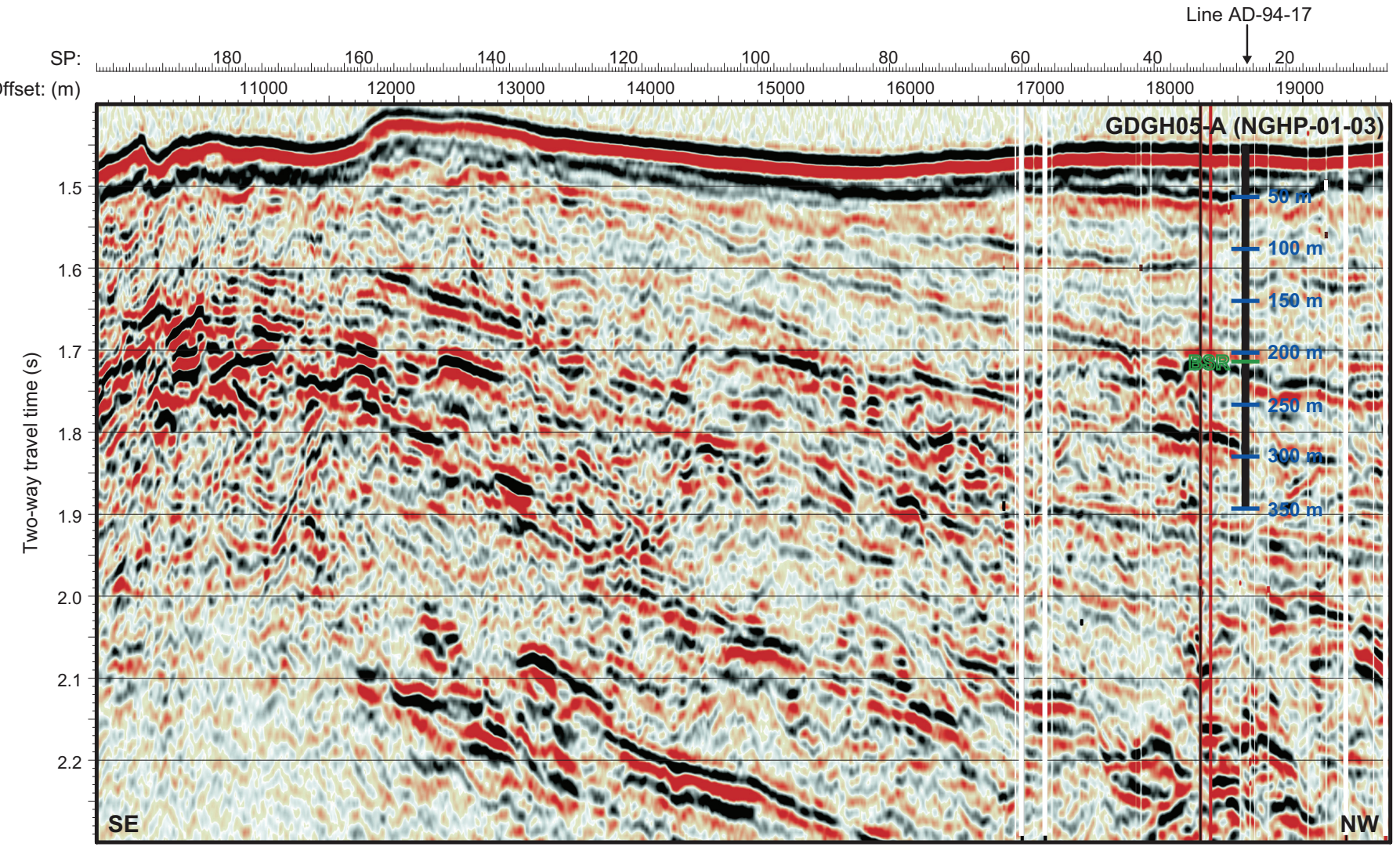

Figure 3. Section of 2D seismic line AD-94-17 in the vicinity of Site NGHP-01-03 (Prospectus Site GDGH05-A) showing predicted formation tops and BSR depth (209 mbsf) based on a uniform seismic velocity of 1,580 m/s. [BSR, bottom-simulating reflector; mbsf, meters below sea floor; m/s, meters per second]

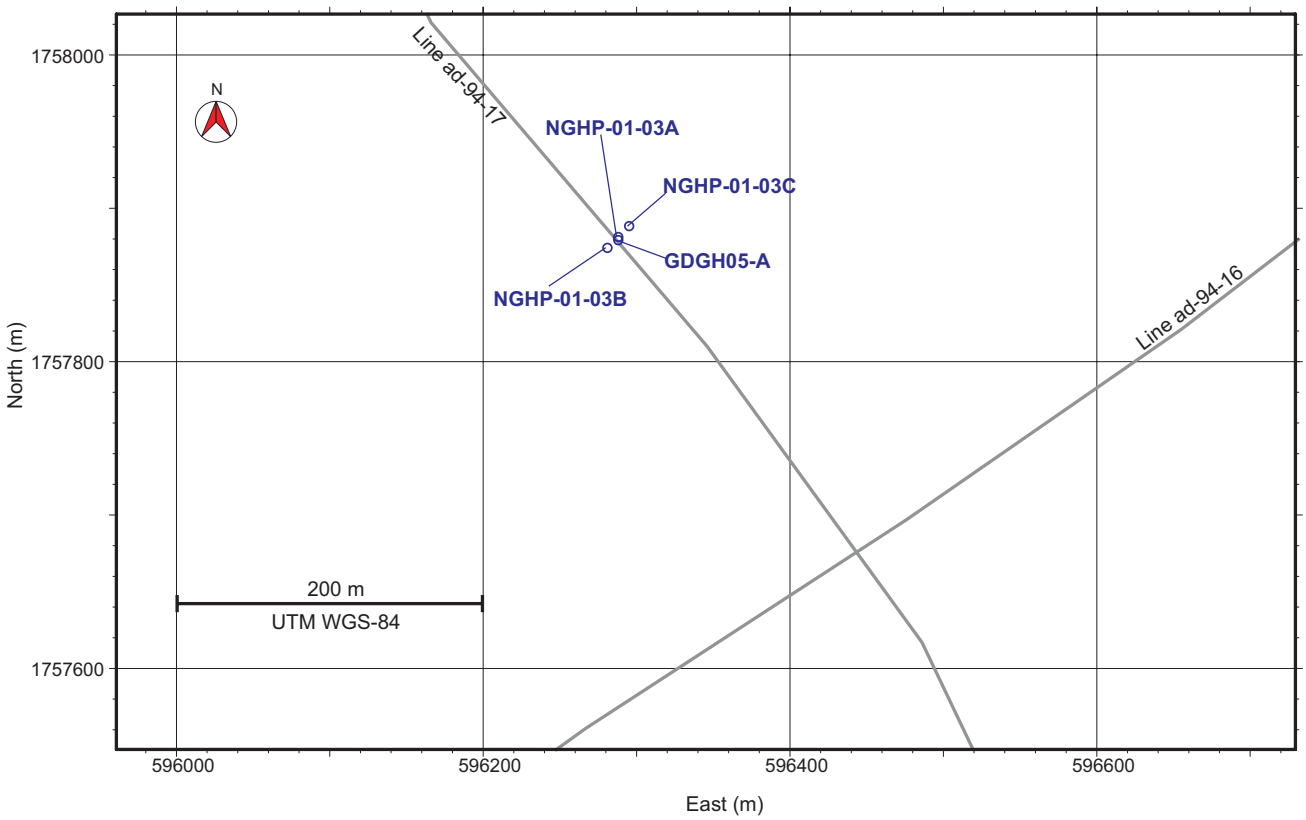

Figure 4. Section of seismic line AD-94-16 around Site NGHP-01-03 (Prospectus Site GDGH05-A) showing predicted formation tops and BSR depth (209 mbsf) based on a uniform seismic velocity of 1,580 m/s. [BSR, bottom-simulating reflector; mbsf, meters below sea floor; m/s, meters per second]

(wire-line core barrel retrieval system) were removed from the drill pipe for all cores beginning with NGHP-01-03B-36X due to elevated (550 PSI) pump pressure.

All three PCS deployments included successful recovery of data with the PCS Methane tool. Penetration rates with the XCB varied between 12.8 and 57.6 m/h and excluding partial cores, which skew the data, recovery ranged from as little as 10 percent to as much as 102 percent. The hole was displaced with 92 barrels of 10.5 ppg weighted mud and the drill string was pulled out of the hole. Hole NGHP-01-03B officially ended when the bit cleared the sea floor at 2230 hr on July 1, 2006.

Whirlpaks (microbeads) commonly used for microbiological contamination control were not used for coring; however, accelerated core barrel handling protocols were used for all core barrels (APC, XCB, and PCS) deployed in this hole. All APC/XCB core barrels were laid down immediately upon arrival at the rig floor before making another drill pipe connection or deploying the next core barrel. Once at the rig floor any PCS core barrel showing signs of proper actuation was placed in the moon pool ice bath.

Hole NGHP-01-03C

Hole NGHP-01-03C was intended to be a "tools" hole primarily for deployment of specialty pressure-coring systems targeted to sample areas of high gas hydrate interest. Limited APC coring was to be conducted through the SMI. Wire-line logging was scheduled after drilling/coring the hole to total depth.

The vessel was offset 10 meters to the NE of Hole NGHP-01-03A and the bit was positioned at a depth of 1,082.0 mbrf. The first spud attempt failed to recover anything but water so the drill string was lowered 4.0 m and Hole NGHP-01-03C was ultimately spudded at 0025 hr on July 2, 2006, establishing a sea floor depth of 1,086.0 mbrf. APC coring continued through Core NGHP-01-03C-03H to a depth of 28.5 mbsf.

The hole was then drilled to a depth of 170.0 mbsf where pressure coring commenced. Whether to wash with open ended pipe or deploy an XCB center bit was left to the discretion of the driller and coring technician dependent upon the degree of formation induration.

A total of seven pressure cores (each approximately 1-meter advance) were cut using the PCS, FPC, and HRC pressure-coring systems. Each pressure core was preceded by a drilled interval and the hole was swept with a 10-15 bbl Sepiolite mud pill prior to each deployment. PCS Core NGHP-01-03C-04P advanced from 170.0 to 171.0 mbsf followed by a drilled interval of 4.0 m. FPC Core NGHP-01-03C-05Y advanced from 175.0 to 176.0 mbsf followed by a drilled interval of 4.0 m. During this drilled interval there were some stuck pipe and hole problems. These were attributed to a lack of adequate hole cleaning due to the short duration core intervals (5–10 minutes and 1.0 m advance) coupled with the short intermediate drilled intervals (45 minutes and 4.0 m advance). After that incident, more attention was paid to ensuring that cuttings were adequately flushed from the hole. HRC Core NGHP-01-03C-06E advanced from 180.0 to 181.0 mbsf followed by a drilled interval of 3.0 m. PCS Core NGHP-01-03C-07P advanced from 184.0 to 185.0 mbsf followed by a drilled interval of 5.0 m. FPC Core NGHP-01-03C-08Y advanced from 190.0 to 191.0 m followed by a drilled interval of 5.0 m. FPC Core NGHP-01-03C-09Y advanced from 196.0 to 197.0 m followed by another PCS Core NGHP-01-03C-10P which advanced from 197.0 to 198.0 m. A drilled interval of 102.0 m extended the hole to a total depth of 300.0 mbsf.

For all HYACINTH pressure-coring systems (FPC and HRC), a 15–20 minute wait period was employed at the mudline on the way in the hole and again during retrieval. This was to cool the core barrels down thus aiding in keeping any entrained gas hydrate within the stability field. At the rig floor, all pressure core barrels (PCS, FPC, and HRC) showing signs of proper actuation were placed in the moon pool ice bath prior to processing.

Five hours were spent conducting a wiper trip to ~60 mbsf and back and a final DVTP temperature measurement was taken at TD. The hole was displaced with 110 barrels of 10.5 ppg weighted mud. The drill string was then tripped setting the EOP at 58.0 mbsf.

At 1815 hr on July 3, 2006, rig-up for logging began. The first logging run was made with the triple combo tool suite. This tool string reached only 79.0 mbsf before encountering resistance. The drill string was raised up a single joint of drill pipe and the tools were eventually worked all the way to TD. The triple combo string was recovered by 0130 on July 4. The FMS-Sonic tool string was then made up and deployed; however, it was still not possible to pass 68.0 mbsf. As before, the pipe was raised one single joint; however, this time the tools still were unable to pass the borehole obstruction. The logging tools were recovered, laid out, and the EOP was lowered to 106.0 mbsf which, based upon the caliper logs, was past the known tight spots located in the upper portion of the hole. The FMS-Sonic tool suite was deployed a second time and this time reached all the way to TD at 300.0 mbsf. By 1200 hr the second tool string was recovered. The third and final logging run was dedicated to zero offset VSP measurements. Following IODP mammal watch (daylight operations only) protocols the VSP tool string was deployed and reached an obstruction at 104.0 mbsf. After some effort the tools were worked down to 120.0 mbsf but could not be advanced beyond that point. The tools were recovered back to the bit and three hours were spent getting back into the pipe. Eventually the VSP tools were recovered and further VSP logging efforts were cancelled for this hole.

The drill string was pulled clear of the sea floor at 1650 hr and by 1730 hr the drill string was recovered and the rig was secured for transit.

Initial attempts to release the positioning beacon during the pipe trip had been unsuccessful; however, after shutting down the main screws, the beacon release command was acknowledged and by 2000 hr the beacon was recovered. Control was switched from DP to cruise mode at 2023 hr, all thrusters and hydrophones were secured, and at 2042 hr the vessel headed for Site NGHP-01-07 (KGGH06-A).

Lithostratigraphy

Site NGHP-01-03 is located in the Krishna-Godavari (KG) Basin, along the eastern continental margin of India. A total of three holes were drilled at Site NGHP-01-03. Hole NGHP-01-03A was drilled for LWD data collection. Hole NGHP-01-03B was cored to 300 mbsf. Hole NGHP-01-03C was spot cored to 198 mbsf, then drilled and wire-line logged to a total depth of 300 mbsf (see “Operations”).

We classify the sedimentary sequence recovered at Holes NGHP-01-03B and NGHP-01-03C as one lithostratigraphic unit with two Subunits (Unit Ia and Ib) based on sedimentological criteria (for example, variations in sedimentary structure and grain size or biogenic and lithologic components) and physical property and downhole logging data (for example, magnetic susceptibility and LWD density; see figs. 5 and 6, and Site NGHP-01-03 Visual Core Descriptions in the supplemental data files). We also integrate the core data with the available seismic data to help define and interpret the stratigraphic sequence. For the 0–210 mbsf interval, the lithostratigraphy recovered at Site NGHP-01-03 is similar to the lithostratigraphy previously drilled at Sites NGHP-01-05, NGHP-01-10, and NGHP-01-12 on the Krishna-Godavari slope. One notable exception is that Sites NGHP-01-10 and NGHP-01-12 contain significantly less silt/sand laminae and beds than Sites NGHP-01-03 and NGHP-01-05. In addition,

Figure 5 (following page). Lithostratigraphic summary of Hole NGHP-01-03B. [BSR, bottom simulating reflector; RAB, resistivity-at-bit; SMI, sulfate-methane interface] Note: Colored intervals exceed symbol size when there is a range in the occurrence. Center point of each symbol represents depth of occurrence, therefore colored bars may slightly exceed core recovery; see Site NGHP-01-03 Visual Core Descriptions for the expanded scale, detailed core descriptions and Site NGHP-01-03 Oversized Figures for the enlarged version of this summary.

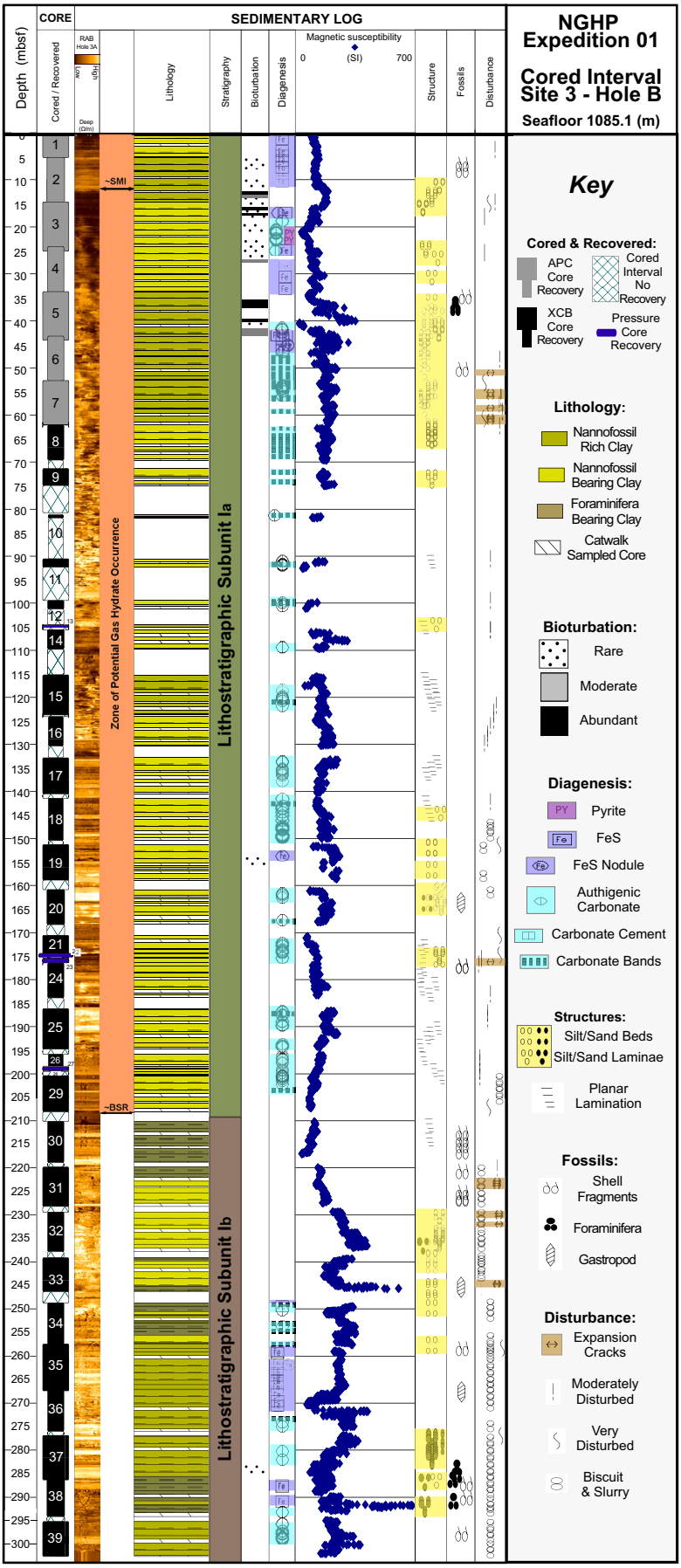
NGHP Expedition 01
Cored Interval
Site 3 - Hole B
Seafloor 1085.1 (m)
Depth (mbsf)
CORE
Cored / Recovered
SEDIMENTARY LOG
RAB Hole 3A
Low
High
Deep (Ωm)
Lithology
Stratigraphy
Bioturbation
Diagenesis
Magnetic susceptibility
0
(SI)
700
Structure
Fossils
Disturbance
~SMI
~BSR
Zone of Potential Gas Hydrate Occurrence
Lithostratigraphic Subunit Ia
Lithostratigraphic Subunit Ib
Key
Cored & Recovered:
APC Core Recovery
Cored Interval No Recovery
XCB Core Recovery
Pressure Core Recovery
Lithology:
Nannofossil Rich Clay
Nannofossil Bearing Clay
Foraminifera Bearing Clay
Catwalk Sampled Core
Bioturbation:
Rare
Moderate
Abundant
Diagenesis:
Pyrite
FeS
FeS Nodule
Authigenic Carbonate
Carbonate Cement
Carbonate Bands
Structures:
Silt/Sand Beds
Silt/Sand Laminae
Planar Lamination
Fossils:
Shell Fragments
Foraminifera
Gastropod
Disturbance:
Expansion Cracks
Moderately Disturbed
Very Disturbed
Biscuit & Slurry

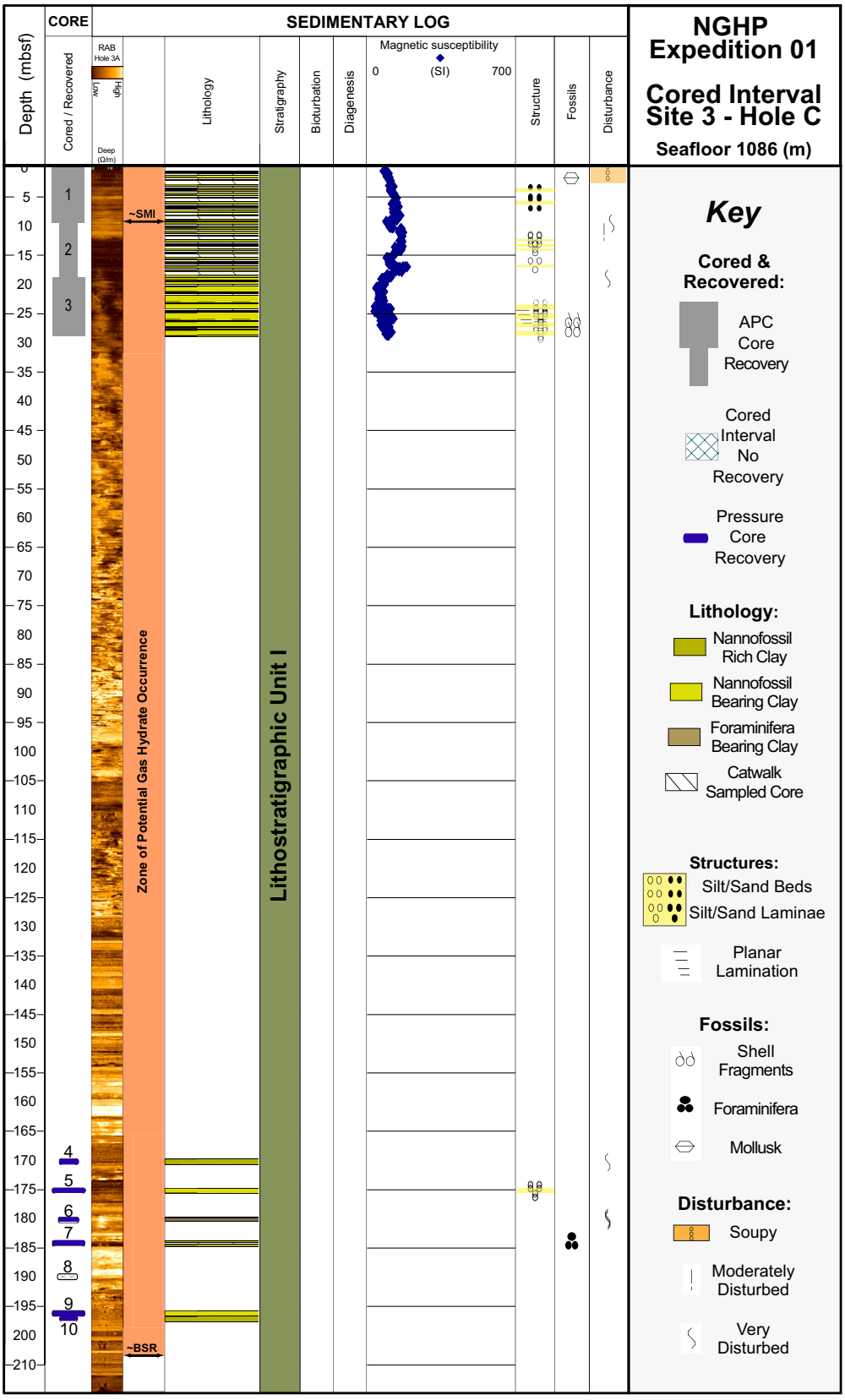

Figure 6. Lithostratigraphic summary of Hole NGHP-01-03C. [BSR, bottom simulating reflector; RAB, resistivity-at-bit; SMI, sulfate-methane interface] Note: Colored intervals exceed symbol size when there is a range in the occurrence. Center point of each symbol represents depth of occurrence; therefore colored bars may slightly exceed core recovery; see Site NGHP-01-03 Visual Core Descriptions for the expanded scale, detailed core descriptions and Site NGHP-01-03 Oversized Figures for the enlarged version of this summary.

because Site NGHP-01-03 was cored to a greater TD (300 mbsf), a new section of stratigraphy that was apparently not reached at Sites NGHP-01-05, NGHP-01-10, or NGHP-01-12 was recovered. This section is distinct from Lithostratigraphic Unit I as defined elsewhere throughout the KG Basin. Therefore, Site NGHP-01-03 Subunit Ia is correlative with Unit I and the new, distinctive interval encountered at Site NGHP-01-03 is designated Lithostratigraphic Subunit Ib (see below; figs. 5 and 6, and Site NGHP-01-03 Visual Core Descriptions in the supplemental data files).

Similar to other KG Basin sites, we observed cyclicity in the RGB color scans of the cores and a lack of *Discoaster* spp. in the record here. Both of these suggest that the age of the stratigraphy is Quaternary. Additional postcruise biostratigraphy, however, may help further constrain the history of deposition throughout the entire KG Basin.

Lithostratigraphic Units

Lithostratigraphic Unit Ia

Intervals: Hole NGHP-01-03B, Sections NGHP-01-03B-01H-1 to NGHP-01-03B-29X-CC; Hole NGHP-01- 03C, Sections NGHP-01-03C-01H-1 to NGHP-01-03B-10P-1

Depth: Hole NGHP-01-03B, 0–210.6 mbsf; Hole NGHP-01-03C, 0–198 mbsf

Age: Quaternary

Core recovery was good at Hole NGHP-01-03B for the upper 69 mbsf and moderate in the interval from 115 mbsf to bottom of the hole. Core recovery was the poorest from 69 mbsf to 115 mbsf because of apparent coring problems that were likely induced by gas hydrate, as interpreted from moderate increases in resistivity values on the LWD data (figs. 5 and 6, and Site NGHP-01-03 Visual Core Descriptions in the supplemental data files). Core recovery at Hole NGHP-01-03C was limited to APC cores from 0–28.5 mbsf and then spot pressure cored between 170–197 mbsf (see "Operations"). Designation of Lithostratigraphic Subunit Ia in both holes was based on sediment characteristics, physical property data, LWD/MWD data, and available seismic data. Lithostratigraphic Subunit Ia is composed of nannofossil-bearing-to-rich clay that ranges in color from dark olive gray (5Y 3/2) to very dark gray (2.5Y 3/1) to black (5Y 2.5/1). Terrestrial organic matter is common (trace to 5 percent) in smear slides taken throughout Subunit Ia (tables 1 and 2). Thin (0.2–3.0 cm) silt/sand laminae and beds are abundant in discrete zones throughout the Subunit at Site NGHP-01-03 (fig. 7), similar to those observed at Site NGHP-01-05, but in contrast to those at Sites NGHP-01-10 and NGHP-01-12, where silts are infrequent. Similar to Site NGHP-01-05, Site NGHP-01-10, and Site NGHP-01-12, Site NGHP-01-03 is likely Quaternary to recent in age (see "Lithostratigraphy" in "Site NGHP-01-05"); however, postcruise biostratigraphic work will help constrain the age of the Unit I (Subunits Ia and Ib) stratigraphy.

Shell fragments, visible foraminifera tests, and gastropod shells occur sporadically throughout Subunit Ia (figs. 5 and 6, and Site NGHP-01-03 Visual Core Descriptions in the supplemental data files). Authigenic carbonate precipitates in the form of nodules, bands, and fine-grained precipitates (fig. 8) are common throughout Subunit Ia below 16 mbsf (figs. 5 and 6, and Site NGHP-01-03 Visual Core Descriptions in the supplemental data files). Bioturbated zones are most easily seen when highlighted by iron sulfide precipitates (figs. 5 and 6 and, Site NGHP-01-03 Visual Core Descriptions in the supplemental data files) and thus only occur sporadically in Subunit Ia. Downcore magnetic susceptibility measurements (figs. 5 and 6, and Site NGHP-01-03 Visual Core Descriptions in the supplemental data files) throughout the subunit show variability patterns similar to those at Sites NGHP-01-05, NGHP-01-10, and NGHP-01-12; however, the consistent increase in susceptibility observed at Sites NGHP-01-05, NGHP-01-10, and NGHP-01-12, from 50 mbsf to 150 mbsf is not as pronounced at Site NGHP-01-03. Magnetic iron sulfides (likely gregite and(or) pyrrhotite) have been observed in gas-hydrate-bearing sediments offshore western North America (Musgrave and others, 2006) and may be responsible for some of the magnetic susceptibility highs observed here. At Site NGHP-01-03, we observe magnetic iron sulfide nodules (fig. 9) that are either gregite or pyrrhotite, confirming their suspected presence throughout much of the stratigraphy in the Krishna-Godavari Basin. Magnetic susceptibility is also high in stratigraphic intervals containing abundant sand and silt beds, which often contain magnetite grains (opaque minerals in smear slide; see, for example, Trehu and others, 2003).

The zones of highest magnetic susceptibility appear coincident with the abundant silt/sand zones in Subunit Ia. This is in contrast to Sites NGHP-01-10 and NGHP-01-12, where most of the susceptibility highs are associated with an abundance of iron sulfides, observed bioturbation, and authigenic carbonate (see "Lithostratigraphy" in "Sites NGHP-01-10, 12, and 13"). At Sites NGHP-01-05, NGHP-01-10, and NGHP-01-12, the magnetic susceptibility may be responding mainly to magnetic minerals precipitated during diagenetic processes possibly associated with gas hydrates (see "Lithostratigraphy" in "Sites NGHP-01-10, 12, and 13"). Because there was significantly less gas hydrate observed at Site NGHP-01- 03 than at Sites NGHP-01-10, and NGHP-01-12, and more silt and sand layers, perhaps the variation in magnetic susceptibility at Site NGHP-01-03 reflects primary depositional variability (due to magnetic minerals present in sand and silt beds) more than diagenetic effects.

The major lithologies of Lithostratigraphic Subunit Ia determined from smear slides are primarily clay-sized (80–100 percent) grains with minor amounts of silt-sized grains (up to 20 percent) and generally no sand (tables 1 and 2). Minor lithologies described in smear slides included silt/sand beds (tables 3 and 4) and iron monosulfide rich zones. The major nonbiogenic components of Subunit Ia are feldspar, quartz, and clay and opaque minerals. Opaque grains, mostly sulfides in irregular and framboidal forms or heavy minerals, are common in all grain sizes, and typically comprise trace

Table 1. Smear slide data for Hole NGHP-01-03B.

Sample reference		Texture			Mineral								
Core, section, depth (cm, in section)	Lithology	Sand	Silt	Clay	Quartz	Feldspar	Mica	Heavy minerals	Clay minerals	Volcanic glass	Glauco-nite	Iron sulfides	Authigenic carbonates
Hole NGHP-01-03B													
1H-1,102	D		3	97					95				
1H-3,127	D		10	90	trace				91				
2H-1,84.5	M		10	90	7	1	trace		46				1
2H-3,80	D		3	97	1	trace		2	86			trace	1
2H-7,40	D		5	95	2	trace	trace		86				1
3H-1,130	M		40	60	25	3	1	7	52	1		2	
3H-4,52	M		4	96	3	trace			85			4	3
3H-7,39	D		7	93	1	1			89	trace		3	1
4H-2,122	M		95	5	50	10	2	14	22			trace	trace
4H-4,60	D		1	99	1	trace	trace	trace	93			trace	1
4H-7,50	M		trace	>99	trace			trace	98				
5H-3,50	D		5	95	2				80				1
5H-4,60	D		5	95	trace				88				
5H-4,81.5	M		90	10	80	5		5	3			5	
6H-1,68	D		1	99	2	trace			80			2	
6H-5,50	D		5	95	5				77				2
7H-1,77	D		15	85	3	1			82			2	2
7H-4,58	D		5	95				2	75				2
8X-1,80	D		10	90	10	2		5	81				
8X-4,21	D		5	95	5	1		2	85				
9X-2,22.5	D		10	90	5				82			4	trace
10X-1,25	D		5	95	2		trace		90				
11X-2,42	D		10	90	5				89				trace
12X-1,52	D		5	95	2	trace		2	90				
13P-1,49.5	D		10	90	1	1			82				
14X-2,45	M		10	90	5	trace	trace	1	89			trace	trace
15X-3,60	D		7	93	5	2			73	1		2	1
15X-6,40	M		7	93	5	1	trace	2	69	1			2
17X-1,102	D		10	90			trace		87				1
18X-1,76	D		10	90	2		trace		85			3	
18X-4,80	D		5	95	1				86			1	1
19X-3,68	D			100	1				85			3	
19X-5,10	M	10	90		48	20	10	10				10	
20X-1,50	D		5	95	1				85			2	trace
20X-4,7	M		100		80	10	2					5	3
21X-2,37	D			100					90			1	
21X-3,34	D		1	99					94			1	
22P-1,60	D		1	99	2				88				
23Y-1,61	D		10	90	2				88				
23Y-1,48.5	M	90	10		83	10	1	2		trace		2	
24X-2,60	D		10	90	5	1	trace	1	83		trace	trace	trace
24X-5,50	D		2	98	1	trace	trace	trace	98			trace	trace
25X-7,56	D		4	96	2	trace	trace	trace	92			trace	trace
25X-4,132	D		2	98	1	trace	trace	trace	92			trace	1
26X-3,60	D		2	98	1	1	trace	trace	98				trace
27P-1,60	D		1	99	2				90				
29X-3,40	D		1	99	1		trace		90			trace	trace
30X-2,40	D		3	97	3	trace	trace	trace	93		trace	trace	
30X-5,120	D		1	99	1	trace	trace	trace	96			trace	1
31X-1,100	D		2	98	1		trace		94				
31X-4,80	D		3	97	2		trace		89				
32X-2,33	D		20	80	10	2	1		72			2	
32X-3,43	M	10	90		80	17	1					1	
33X-2,95	D		1	99				1	90				
33X-6,74	M	10	90		50	20		20					
33X-2,55	D		10	90	3				90			2	
34X-1,64	D		10	90	2	1			85				
34X-2,65	D		10	90	10				80				
34X-4,128	D		25	75	5				83			5	
35X-3,47	D		2	98	1		trace		76			trace	1
35X-4,80	D	2	13	85	5	2	1	3	64			2	1
35X-6,103	D		2	98					75			trace	trace
36X-5,116	D		1	99	trace	trace	trace		84			trace	1
37X-3,32	D	10	15	75	20	5	2		72			1	trace
37X-4,110	D		3	97	2	trace	trace	trace	86				2
37X-7,30	M		5	95	2	trace	1	trace	80			trace	1
38X-2,120	D		20	80	10	1	3		75			trace	trace
38X-4,80	D		1	99	trace	trace			64			trace	1
38X-5,16	D		10	90	2	1	trace	trace	90			trace	2
39X-1,80	D		5	95	3	trace	1	trace	80				
39X-5,120	D		1	99	1				70			trace	trace

Table 1. Smear slide data for Hole NGHP-01-03B.—Continued

Sample reference		Biogenic							Comments
Core, section, depth (cm, in section)	Lithology	Fora-minifera	Nanno-fossils	Carbonate shell fragments	Diatoms	Radio-larians	Sponge spicules	Plant debris	
Hole NGHP-01-03B—Continued									
1H-1,102	D		5	trace				trace	
1H-3,127	D		8					1	
2H-1,84.5	M	3	40					2	
2H-3,80	D	1	8	trace				1	
2H-7,40	D		9	trace				2	
3H-1,130	M	1	6					2	from silt layer
3H-4,52	M	trace	3				trace	2	from iron sulfide layer
3H-7,39	D		5	trace					
4H-2,122	M		1					1	from silt, possible glauconite
4H-4,60	D		5					trace	
4H-7,50	M	trace	2						
5H-3,50	D	1	14					2	
5H-4,60	D		12					trace	
5H-4,81.5	M	2							iron sulfides in shell fragments
6H-1,68	D		15					1	
6H-5,50	D		15					1	
7H-1,77	D		9					1	
7H-4,58	D		20					1	
8X-1,80	D		2						
8X-4,21	D		7						
9X-2,22.5	D		8					1	rock fragments
10X-1,25	D		8					trace	
11X-2,42	D		5					1	
12X-1,52	D		5					1	
13P-1,49.5	D		15					1	
14X-2,45	M	trace	5						
15X-3,60	D		11					5	
15X-6,40	M		20	trace			trace		
17X-1,102	D		10					2	
18X-1,76	D		8					2	
18X-4,80	D		9					2	
19X-3,68	D		10					1	
19X-5,10	M							2	from silt layer
20X-1,50	D		9					3	
20X-4,7	M								from silt layer
21X-2,37	D		9					trace	
21X-3,34	D		5					trace	
22P-1,60	D		8					2	
23Y-1,61	D		8					2	
23Y-1,48.5	M			2					trace blond sand
24X-2,60	D	trace	10					trace	
24X-5,50	D		1						
25X-7,56	D		6						coarser silt grains than previous cores
25X-4,132	D		6					trace	
26X-3,60	D							trace	
27P-1,60	D		8						
29X-3,40	D		9					trace	
30X-2,40	D	1	3					trace	trace pyroxene
30X-5,120	D	trace	2					trace	possilbe trace pyroxene and garnet
31X-1,100	D		3	1				1	
31X-4,80	D		8					1	from light colored clay
32X-2,33	D		5					8	
32X-3,43	M			1					from silt/sand layer
33X-2,95	D	trace	8	1					from light colored clay
33X-6,74	M			10					from silt layer
33X-2,55	D		2					3	from dark colored clay
34X-1,64	D		8	2				2	from light colored clay
34X-2,65	D		2					8	from dark colored clay
34X-4,128	D		2					5	large woody debris in silt fraction
35X-3,47	D	2	20					trace	
35X-4,80	D	2	15	2				3	3% plant debris
35X-6,103	D	trace	25						
36X-5,116	D	trace	15						
37X-3,32	D	trace	trace					trace	possible zircon
37X-4,110	D	trace	10					trace	from dark colored clay
37X-7,30	M	1	15						
38X-2,120	D	9	2						
38X-4,80	D	trace	35						
38X-5,16	D	trace	5					trace	
39X-1,80	D	1	15						
39X-5,120	D	trace	29						

Note: M = minor lithology, D = dominant lithology

Table 2. Smear slide data for Hole NGHP-01-03C.

Core, section, depth (cm, in section)	Lithology	Sand	Silt	Clay	Quartz	Feldspar	Mica	Heavy minerals	Clay minerals	Volcanic glass	Glauco-nite	Iron sulfides
Hole NGHP-01-03C												
1H-4,78	D	trace	5	95	2	trace	trace		88		1	
1H-1,82	D		7	93	2		1	trace	76			trace
1H-5,5	M	40	20	40	40	10	5	1	43			1
1H-cc,10	D		5	95	2	1	2		65			trace
2H-2,85	D	trace	2	98	1	trace	trace		84			
2H-3,75	D	trace	3	97	2	trace	1	trace	81			1
3H-1,110	D		2	98	1		1		92			
3H-7,70	D		2	98	1				90			
4P-1,42	D		1	99					83			
5Y-1,55	D		1	99	1		1		85			2
6E-1,25	D		15	85	5	1		1	86			2
7P-1,24	D	2	7	91	3	1	trace	3	70	1		2
10P-1,33	D	3	10	87	2	1		5	67	1		2
9Y-1,-	D		7	93	3	1		2	80	1		trace

amounts of the total sediment in the clays, but higher percentages in the silts (tables 1 and 2). The total biogenic component of the sediment is dominated by calcareous nannofossils, which comprise 5–40 percent of the total (biogenic and nonbiogenic) sediment grains (table 1 and 2). Foraminifera are common in the coarse fractions (>63 μm) of the sediments and often visible with the naked eye on the split core surfaces. Terrestrial organic matter was also observed in smear slides as trace to 5 percent throughout the sediments of Subunit Ia.

Subunit Ib

Intervals: Hole NGHP-01-03B, Sections NGHP-01-03B-30X-1 to NGHP-01-03B-39X-CC.

Depth: Hole NGHP-01-03B, 210.6–300.0 mbsf

Designation of Lithostratigraphic Subunit Ib in Hole NGHP-01-03B was based on sedimentological characteristics, physical properties, LWD data, and available seismic data. Lithostratigraphic Subunit Ib differs from Subunit Ia in the main constituents in the clays. In addition, the magnetic susceptibility and LWD density also show a marked increase at 210.6 m that correspond to the change in the lithology near this boundary. These changes serve to delineate Subunit Ia from Subunit Ib. Lithostratigraphic Subunit Ib is composed of alternating zones of nannofossil-bearing-to-rich clays and foraminifera-bearing clays that ranges in color from black (N 2.5/1) to greenish black (10Y 2.5; figs. 5 and 10). The slightly lighter colored clays are often more enriched in calcareous nannofossils and(or) foraminifera (table 1). Terrestrial organic matter is slightly more common (trace to 8 percent) in smear slides taken throughout Subunit Ib (table 1). Other mineral grains present in smear slides were similar in abundance to their occurrence in Subunit Ia (tables 1 and 2). Thin (0.2–3.0 cm) silt and sand laminae and beds are abundant in discrete zones throughout Subunit Ib (fig. 8). Authigenic carbonates and iron sulfides (fig. 10) are also abundant in Subunit Ib. In the interval between ~260 mbsf and ~272 mbsf, abundant iron sulfides and a lack of carbonates and sands and silts may be responsible for the slightly higher background magnetic susceptibility (as compared to Subunit Ia). The highest magnetic susceptibility zones throughout Subunit Ib, however, correspond well with the occurrence of sand and silt beds (fig. 5 and Site NGHP-01-03 Visual Core Descriptions in the supplemental data files). Gastropods, shell fragments, and visible foraminifera are rare to common throughout Subunit Ib.

Gas-Hydrate Occurrence

The presence of gas hydrate was inferred from small increases in resistivity on the LWD RAB data at Site NGHP-01-03; however, no gas hydrate was recovered on the catwalk or in the pressure cores and no significant IR anomalies were detected. Gas-hydrate-bearing sediment was not observed at this site; however, gas hydrate may have been disseminated within the pore spaces or fracture fills and dissociated completely during recovery.

Inorganic Geochemistry

The main objectives of the inorganic geochemistry program at this site were to (1) constrain the fluid and gas source(s), subsurface hydrology (transport mechanisms and migration pathways), and biogeochemical reactions associated with subsurface gas hydrates; and (2) quantify the content and distribution of gas hydrate based on dissolved chloride concentrations and determine the relationship between the regional hydrogeochemistry and gas-hydrate distribution. The primary objective of the high-resolution sampling in Hole C at Site NGHP-01-03 was to characterize the sulfate-methane interface (SMI) for future

Table 2. Smear slide data for Hole NGHP-01-03C.—Continued

Core, section, depth (cm, in section)	Authigenic carbonates	Fora-minifera	Nanno-fossils	Carbonate shell fragments	Diatoms	Radio-larians	Sponge spicules	Plant debris	Comments
Hole NGHP-01-03C—Continued									
1H-4,78	trace	1	7					1	foraminifera as test fragments
1H-1,82		1	20						
1H-5,5	trace	trace	trace						
1H-cc,10	trace		30						
2H-2,85		trace	15					trace	trace fish remains
2H-3,75		trace	15					trace	foraminifera as test fragments
3H-1,110			5	1				trace	
3H-7,70			8				trace	1	
4P-1,42			15					2	
5Y-1,55			9	1				1	
6E-1,25			2					3	
7P-1,24	1	1	15				trace	3	
10P-1,33	2	trace	15				2	3	
9Y-1,-	1		10				trace	2	

Note: M = minor lithology, D = dominant lithology.

geochemical modeling studies and to provide supporting data and samples for studies on the microbial dynamics of the SMI. The interstitial water (IW) geochemistry data are tabulated in tables 5 and 6, and illustrated in figures 11 and 12.

A total of 101 whole-round samples were collected for IW analyses at Site NGHP-01-03 in the Krishna-Godavari Basin offshore the eastern margin of the Indian Peninsula (59 samples from Hole NGHP-01-03B and 42 samples from Hole NGHP-01-03C). Whole-round lengths ranged from 10 to 40 cm, with longer sections subsampled from cores recovered deeper within the hole. Longer whole-rounds were collected at this site than Sites NGHP-01-05 and NGHP-01-10 because the sediments were more consolidated, thus more dewatered producing less pore fluid from an equivalent length of sample. Samples were collected from Hole NGHP-01-03B at a frequency of three samples per core in the upper 10 m, two whole-round samples per core to the seismically inferred BSR (~209 mbsf), and one sample per core beneath the BSR. In addition to routine catwalk whole-round sampling, two PCS pressure cores were sampled from Hole NGHP-01-03B. Samples were collected at higher spatial resolution in Hole NGHP-01-03D to better define the SMI to quantify the magnitude of anaerobic methane oxidation (AMO) at this site, as well as for future geochemical and microbiological studies. In the high-resolution hole (Hole NGHP-01-03C), eighteen samples were taken per core (three samples per section) from the seafloor to ~10 m below the SMI. Below the SMI, one whole-round sample was collected from a pressure core at 184.35 mbsf. The whole-round sampling program was coordinated with both the organic geochemistry and microbiology sampling programs. In addition to the general whole-round sampling scheme, intervals with IR anomalies were sampled on the catwalk. The IR anomaly whole-round samples were immediately transferred to the chemistry laboratory, taken out of the core liner, split in half, and imaged with a hand-held IR camera. The sediment section containing the IR anomaly was then separated from the split whole-round sample and squeezed. If the sediment IR anomaly was heterogeneous, the lithologies were separated (that is, silt and clay) and squeezed separately to determine the percent pore space gas-hydrate occupancy of each sediment type. Pressure cores were sub-sampled for interstitial water squeezing based on X-ray logs.

Interstitial Water Chloride—Gas-Hydrate Distribution

Chloride (Cl^-) concentrations at this site vary from 572 mM to 517 mM with the greatest variability in concentrations occurring between 28.8 mbsf and the BSR at 209 mbsf (fig. 11A). Chloride concentrations decrease from 556 mM at 2.29 mbsf to 554 mM at 19 mbsf. Chloride then increases to the maximum value of 572 mM (2.3 percent greater than modern seawater value) at 38.3 mbsf. The elevated Cl^- concentrations between 30 and 40 mbsf likely reflect buried interglacial seawater with an average Cl^- concentration of ~579 mM in diffusional communication with the pore waters from sediments immediately above and below the Cl^- maxima. The Cl^- maxima within this depth interval are not likely to be related to localized gas hydrate formation because there is no evidence of gas hydrates between the seafloor and 40 mbsf in the downhole resistivity logs at Site NGHP-01-03 (see "Downhole logging"). Much of the Cl^- concentration depth profile between 60 mbsf and the BSR is dominated by concentrations near the modern seawater value or slightly depleted relative to modern seawater. The depleted Cl^- concentrations may reflect low concentrations of gas hydrate disseminated in the sediments within the gas hydrate stability zone at this site. Superimposed on the relatively constant Cl^- is a distinct Cl^- minimum occurring at 164.4 mbsf. The lowest Cl^- minimum of 517 mM (7.5 percent lower than modern seawater value) was collected from an IR anomaly identified on the catwalk corresponding to this depth. The extent of Cl^- dilution coupled with background

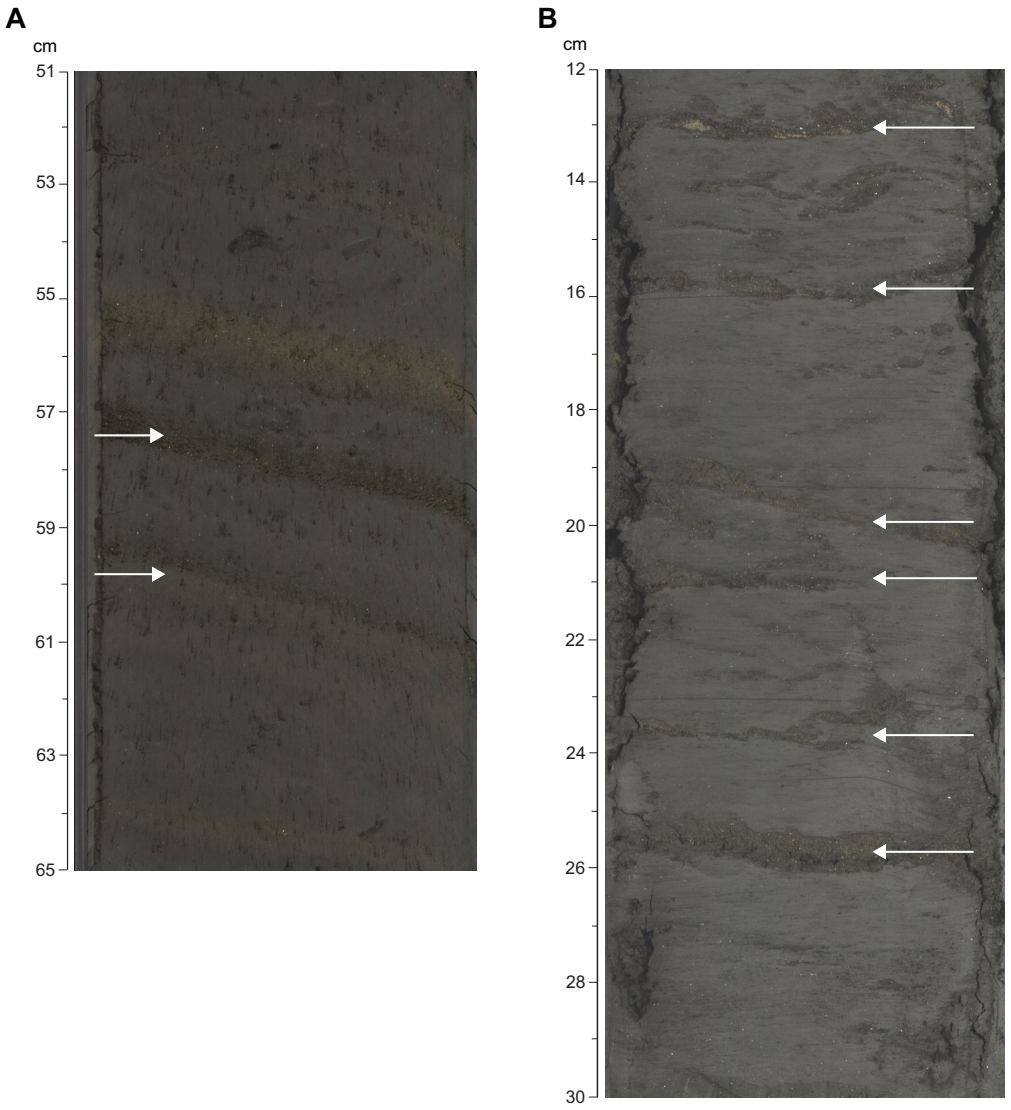

Figure 7. Silt beds typical of those observed in both Lithostratigraphic Subunits IIa and IIb. Silt layers shown by arrows. A, Section NGHP-01-03B-07H-5, 51–66 cm; also notice the authigenic carbonate band above the uppermost silt layer. B, Section NGHP-01-03B-20X-3, 11.5-30 cm.

Cl^- concentrations will be used to calculate the amount of pore space occupied by gas hydrate at this site. Below the BSR, Cl^-concentrations become less variable and range between 553 and 543 mM, defining the background Cl^- concentration depth profile at Site NGHP-01-03.

Overall, the Cl^- concentrations at this site indicate little gas-hydrate accumulation in comparison to Sites NGHP-01-05 and NGHP-01-10. They suggest that gas hydrate is more diffuse at Site NGHP-01-03 than at Site NGHP-01-10 and is mainly disseminated within the sediments, rather than along fractures as observed at Site NGHP-01-10, with discrete zones of higher gas-hydrate concentrations occurring along coarser grained sediment layers such as silts to very fine sands (see "Lithostratigraphy"). Based on the low gas-hydrate concentrations inferred from the Cl^- concentration depth profile and resistivity logs, Site NGHP-01-03 can serve as an ideal background location for site comparisons in the Krishna-Godavari Basin. Site NGHP-01-03 reference profiles will be integral in shore-based modeling efforts aimed at constraining the content and distribution of gas hydrate based on dissolved chloride concentrations, the relationship between the regional hydrogeochemistry and gas-hydrate distribution, and the biogeochemical reactions associated with subsurface gas hydrates.

Sulfate Concentrations and the SMI

The primary objectives of the high-resolution sampling in the upper 30 m of sediments at this site were to characterize the sulfate-methane interface (SMI) for future geochemical modeling of methane fluxes and to provide supporting data and samples for studies on the microbial dynamics of the sulfate-methane interface. Above the interface, sulfate-reducing microbial communities utilize interstitial sulfate to oxidize sedimentary organic matter, reducing sulfate to sulfide and producing bicarbonate. Below the interface,

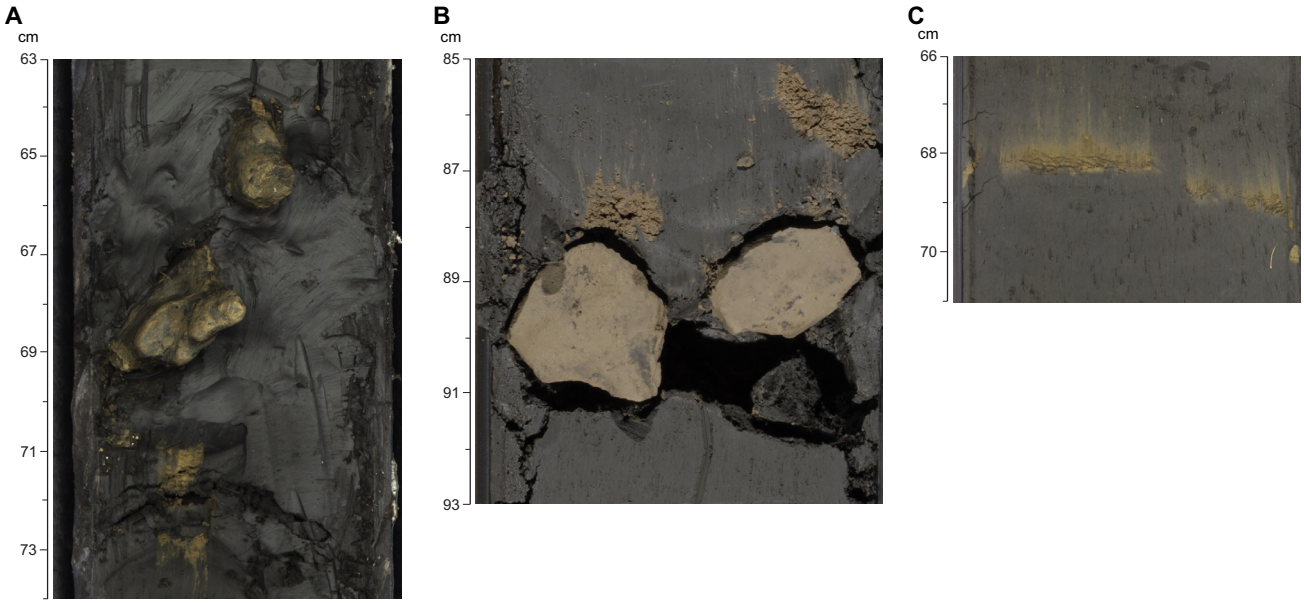

Figure 8. Authigenic carbonate nodules and bands. A, Section NGHP-01-03C-09Y-1, 63–74 cm; the branching shapes imply formation in burrows. B, Section NGHP-01-03B-18X-2, 84–93 cm; notice the additional fine grained carbonate precipitates just above the nodules. C, A semi-horizontal band from Section NGHP-01-03B-07H-5, 65.5–71.5 cm.

methanogens generate methane. At the interface, in some environments (especially diffusive settings), microorganisms reduce sulfate and oxidize methane by anaerobic methane oxidation (AMO). The net biogeochemical process is described by:

$$CH_4 + SO_4^{2-} \rightarrow HCO_{3-} + H_2O$$

(Reeburgh, 1976). When methane oxidation by AMO is complete, usually in diffusional settings, but not necessarily in advection-dominated environments, all of the methane fluxing upward is consumed before entering the water column. AMO also drives precipitation of authigenic carbonates, affecting carbon chemistry both above and below the SMI. The $d^{13}C$ of dissolved inorganic carbon produced by anaerobic methane oxidation is depleted with respect to that produced by oxidation of organic matter by sulfate. Samples for shore-based carbon isotopic analyses were preserved to be used to constrain the presence and relative magnitude of AMO occurring at Site NGHP-01-03. High-resolution microbiological samples were also collected from the seafloor across the SMI.

In Hole NGHP-01-03B, the SMI is located at ~12 mbsf (fig. 11C), whereas the SMI is located at 8.9 mbsf in Hole NGHP-01-3C (fig. 12A and 12B). At Site NGHP-01-03B, sulfate is 12.5 mM at 2.9 mbsf and is totally depleted by 12 mbsf, whereas SO_4^{2-} decreases steadily from 21.2 mM at 0.9 mbsf to zero by 8.9 mbsf at Hole NGHP-01-3C. Concomitant with the depleted SO_4^{2-} at these two depths is a rise in headspace methane values from concentrations below the detection limit (see "Organic Geochemistry"), constraining the depth of the sulfate methane interface (SMI) at ~9 mbsf. Below the SMI, sulfate remains depleted with a few minor excursions up to 0.7 mM at depth. These excursions most likely represent contamination of the whole-round samples collected for interstitial

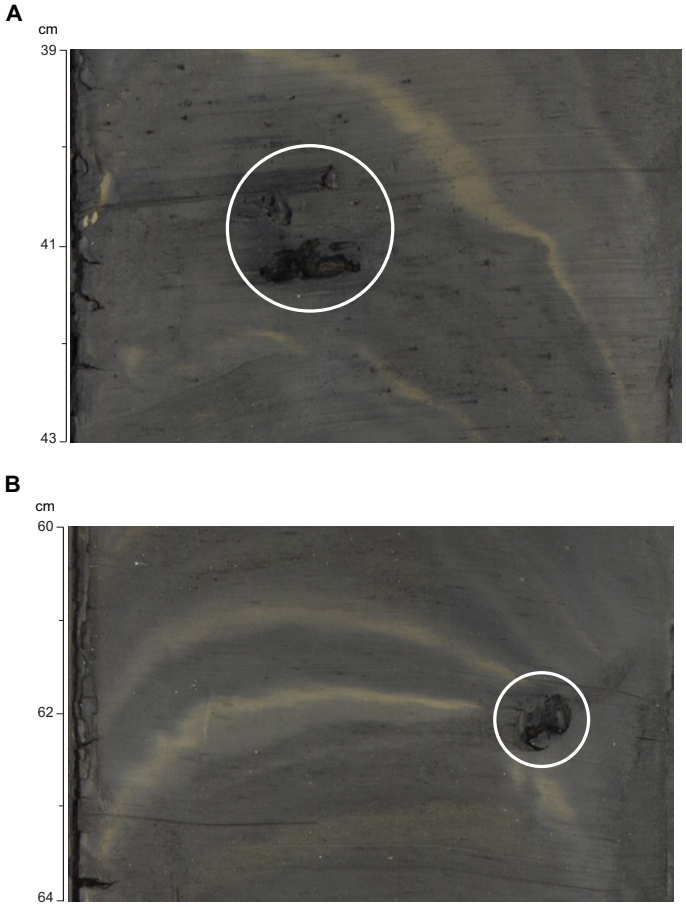

Figure 9. Magnetic iron sulfide nodules A, Section NGHP-01-03B-06H-2, 39–43 cm; B, Section NGHP-01-03B-06H-2, 60–64 cm. Notice in both A and B, the authigenic carbonate bands (light brown); deformation due to APC coring. [APC, Advance Piston Core]

Table 3. Silt laminae and beds at Hole NGHP-01-03B.

Core, section	Position start	Position end	Depth top (mbsf)	Depth base (mbsf)	Type	Core, section	Position start	Position end	Depth top (mbsf)	Depth base (mbsf)	Type
NGHP-01-03B											
2H-5	27	27	11.67	11.67	silt laminae	5H-7	52	52	43.42	43.42	silt laminae
2H-5	46	46	11.86	11.86	silt laminae	5H-7	53	53	43.43	43.43	silt laminae
2H-5	50	50	11.90	11.90	silt laminae	5H-7	68	68	43.58	43.58	silt laminae
2H-5	53	53	11.93	11.93	silt laminae	5H-7	72	72	43.62	43.62	silt laminae
2H-6	70	70	13.60	13.60	silt laminae	6H-1	45	48	43.85	43.88	multiple silt beds
2H-6	110	110	14.00	14.00	silt laminae	6H-1	50	54	43.90	43.94	multiple silt beds
2H-7	1	1	14.41	14.41	silt laminae	6H-1	98	150	44.38	44.90	multiple silt laminae
2H-7	6	6	14.46	14.46	silt laminae	6H-2	71	101	45.61	45.91	multiple silt laminae
2H-7	16	16	14.56	14.56	silt laminae	6H-2	103	109	45.93	45.99	multiple silt laminae
2H-7	23	23	14.63	14.63	silt laminae	7H-2	14	18	54.54	54.58	multiple silt laminae
2H-7	32	32	14.72	14.72	silt laminae	7H-2	63	69	55.03	55.09	silt bed
2H-7	34	34	14.74	14.74	silt laminae	7H-2	80	150	55.20	55.90	multiple silt laminae
2H-7	35	35	14.75	14.75	silt laminae	7H-3	0	12	55.90	56.02	multiple silt laminae
2H-7	44	44	14.84	14.84	silt laminae	7H-3	46	53	56.36	56.43	multiple silt laminae
2H-7	49	49	14.89	14.89	silt laminae	7H-3	88	88	56.78	56.78	silt laminae
2H-7	50	50	14.90	14.90	silt laminae	7H-3	101	103	56.91	56.93	multiple silt laminae
2H-7	56	56	14.96	14.96	silt laminae	7H-4	0	18	57.40	57.58	multiple silt laminae
3H-1	125	150	16.15	16.40	multiple silt laminae	7H-4	27	33	57.67	57.73	multiple silt laminae
3H-2	5	5	16.45	16.45	silt laminae	7H-5	0	150	58.90	60.40	multiple silt laminae
3H-2	20	20	16.60	16.60	silt laminae	8X-1	19	19	71.89	71.89	silt laminae
3H-2	25	25	16.63	16.63	silt laminae	8X-1	20	20	71.90	71.90	silt laminae
4H-1	50	50	24.90	24.90	silt laminae	8X-1	22	22	71.92	71.92	silt laminae
4H-1	107	107	25.47	25.47	silt laminae	8X-1	24	24	71.94	71.94	silt laminae
4H-1	109	109	25.49	25.49	silt laminae	8X-1	33	34	72.03	72.04	silt laminae
4H-5	78	78	31.18	31.18	silt laminae	8X-1	100	100	72.70	72.70	silt laminae
5H-2	84	84	35.68	36.24	silt bed	8X-1	127	127	72.97	72.97	silt laminae
5H-2	89	89	35.68	35.68	silt bed	8X-2	52	85	73.72	74.05	multiple silt laminae
5H-2	106	106	36.46	36.46	silt laminae	8X-2	110	110	74.30	74.30	silt laminae
5H-4	21	21	38.61	38.61	silt laminae	8X-2	121	121	74.41	74.41	silt laminae
5H-5	23	24	40.13	40.14	silt laminae	8X-2	125	125	74.45	74.45	silt laminae
5H-5	30	30	40.20	40.20	silt laminae	8X-3	39	39	75.09	75.09	silt laminae
5H-5	33	33	40.23	40.23	silt laminae	8X-3	51	51	75.21	75.21	silt laminae
5H-5	34	34	40.24	40.24	silt laminae	8X-3	59	59	75.29	75.29	silt laminae
5H-5	36	36	40.26	40.26	silt laminae	8X-3	73	73	75.43	75.43	silt laminae
5H-5	39	39	40.29	40.29	silt laminae	8X-3	80	80	75.50	75.50	silt laminae
5H-5	49	50	40.39	40.40	silt laminae	8X-3	82	82	75.52	75.52	silt laminae
5H-5	67	67	40.57	40.57	silt laminae	19X-1	59	64	152.29	152.34	multiple silt laminae
5H-5	69	69	40.59	40.59	silt laminae	19X-1	73	76	152.43	152.46	multiple silt laminae
5H-5	72	73	40.62	40.63	silt laminae	19X-5	9	10	157.05	157.06	silt bed
5H-5	76	76	40.66	40.66	silt laminae	20X-1	20	21	161.50	161.51	silty clay
5H-5	81	82	40.71	40.72	silt laminae	20X-1	56	62	161.86	161.92	silty clay
5H-5	89	90	40.79	40.80	silt laminae	20X-3	2	2	163.82	163.82	silt bed
5H-5	92	92	40.82	40.82	silt laminae	20X-3	12	26	163.92	164.06	multiple sand beds
5H-5	107	107	40.97	40.97	silt laminae	20X-4	3	3	164.63	164.63	silty clay
5H-5	114	115	41.04	41.05	silt laminae	20X-4	8	8	164.68	164.68	silty clay
5H-5	118	118	41.08	41.08	silt laminae	20X-4	14	14	164.74	164.74	silty clay
5H-5	128	128	41.18	41.18	silt laminae	20X-4	52	52	165.12	165.12	silty clay
5H-5	132	132	41.22	41.22	silt laminae	20X-4	90	96	165.50	165.56	silty clay
5H-5	142	142	41.32	41.32	silt laminae	21X-4	15	15	175.65	175.65	silt laminae
5H-5	143	143	41.33	41.33	silt laminae	21X-4	54	54	176.04	176.04	silt laminae
5H-6	5	5	41.45	41.45	silt laminae	22P-1	0	80	174.90	175.70	multiple silt laminae
5H-6	35	35	41.75	41.75	silt laminae	23Y-1	10	10	176.00	176.00	sand laminae
5H-6	66	66	42.06	42.06	silt laminae	23Y-1	42	52	176.32	176.42	multiple sand laminae
5H-6	71	71	42.11	42.11	silt laminae	32X-1	127	128	231.17	231.18	sand laminae
5H-6	88	91	42.28	42.31	silt rich bed	32X-2	2	2	231.22	231.22	sand laminae
5H-7	0.5	0.5	42.91	42.91	silt laminae	32X-2	84	88	232.04	232.08	multiple sand laminae
5H-7	15	15	43.05	43.05	silt laminae	32X-4	26	26	234.46	234.46	silt laminae
5H-7	36	36	43.26	43.26	silt laminae	32X-4	60	83	234.80	235.03	multiple silt laminae

Table 3. Silt laminae and beds at Hole NGHP-01-03B.—Continued

Core, section	Position start	Position end	Depth top (mbsf)	Depth base (mbsf)	Type	Core, section	Position start	Position end	Depth top (mbsf)	Depth base (mbsf)	Type
NGHP-01-03B—Continued											
32X-4	118	129	235.38	235.49	multiple silt laminae	37X-2	88	88	278.61	278.61	sand bed
32X-4	133	150	235.53	235.70	multiple silt laminae	37X-2	89	89	278.62	278.62	sand bed
32X-5	0	22	235.70	235.92	multiple silt laminae	37X-2	90	90	278.63	278.63	sand bed
32X-5	35	47	236.05	236.17	multiple silt laminae	37X-2	123	123	278.96	278.96	sand laminae
32X-5	75	76	236.45	236.46	silt laminae	37X-2	142	142	279.15	279.15	sand laminae
32X-5	93	93	236.63	236.63	silt laminae	37X-3	31	34	279.54	279.57	multiple sand laminae
32X-6	18	18	236.88	236.88	silt laminae	37X-3	40	40	279.63	279.63	sand laminae
32X-6	35	50	237.05	237.20	multiple silt laminae	37X-3	46	46	279.69	279.69	sand laminae
32X-6	64	65	237.34	237.35	silt laminae	37X-3	62	62	279.85	279.85	sand laminae
33X-1	6	6	239.66	239.66	silt laminae	37X-3	63	63	279.86	279.86	sand laminae
33X-2	1	1	239.24	239.24	silt laminae	37X-4	5	6	280.78	280.79	sand laminae
33X-2	10	14	239.33	239.37	multiple silt laminae	37X-4	30	50	281.03	281.23	multiple sand laminae
33X-3	13	16	241.21	241.24	multiple silt laminae	37X-4	72	77	281.45	281.50	multiple sand laminae
33X-6	35	36	245.43	245.44	silt laminae	37X-4	85	87	281.58	281.60	multiple sand laminae
33X-6	103	104	246.11	246.12	silt laminae	37X-4	104	112	281.77	281.85	multiple sand laminae
34X-2	20	25	250.30	250.35	multiple silt laminae	37X-4	143	144	282.16	282.17	sand laminae
35X-1	24	24	258.24	258.24	silt laminae	37X-5	18	18	282.41	282.41	sand laminae
37X-2	9	10	277.82	277.83	sand laminae	37X-5	30	34	282.53	282.57	multiple sand laminae
37X-2	24	25	277.97	277.98	sand bed	37X-5	63	65	282.86	282.88	multiple sand laminae
37X-2	56	56	278.29	278.29	sand laminae	38X-1	118	118	287.38	287.38	silt laminae
37X-2	78	78	278.51	278.51	sand bed	38X-5	8	9	292.24	292.25	sand laminae
37X-2	84	84	278.57	278.57	sand bed	38X-5	85	100	293.01	293.16	multiple sand laminae
37X-2	85	85	278.58	278.58	sand bed						

Table 4. Silt laminae and beds at Hole NGHP-01-03C.

Core, section	Position start	Position end	Depth top (mbsf)	Depth base (mbsf)	Type
NGHP-01-03C					
1H-4	4	5	4.54	4.55	sand bed
1H-5	5	6	6.05	6.06	sand bed
2H-3	13	16	12.63	12.66	multiple silt laminae
2H-3	34	34	12.84	12.84	silt laminae
2H-3	109	109	13.59	13.59	silt laminae
2H-4	16	16	14.16	14.16	silt laminae
2H-6	10	14	17.1	17.1	multiple silt laminae
3H-4	74	90	23.61	23.61	multiple silt laminae
3H-5	6	6	25.12	25.12	silt laminae
3H-5	8	8	25.12	25.12	silt laminae
3H-5	21	21	25.12	25.12	silt laminae
3H-5	66	67	25.12	25.12	silt laminae
3H-5	75	75	25.12	25.12	silt laminae
3H-5	97	97	25.12	25.12	silt laminae
3H-5	123	123	25.12	25.12	silt laminae
3H-6	14	14	26.64	26.64	silt laminae
3H-6	21	21	26.71	26.71	silt laminae
3H-7	4	4	28.04	28.04	silt laminae
3H-7	8	8	28.08	28.08	silt laminae
3H-7	13	13	28.13	28.13	silt laminae
3H-7	28	28	28.28	28.28	silt laminae
3H-7	55	55	28.55	28.55	silt laminae
3H-cc	7	7	29.15	29.15	silt laminae
3H-cc	12	13	29.15	29.15	silt laminae
5Y-1	0	5	175.28	175.28	multiple silt laminae
5Y-1	21	26	175.28	175.28	multiple silt laminae
5Y-1	73	77	175.28	175.28	multiple silt laminae
5Y-1	80	81	175.28	175.28	silt laminae

water analyses by seawater circulating in the borehole during drilling. The 4.9 mM sulfate value at 199 mbsf corresponds to a PCS pressure-core sample contaminated by seawater during collection.

In typical continental margin sediments with low upward advection rates, the downward sulfate flux is nearly balanced by upward methane flux under conditions of high upward methane diffusion (such as is present in gas-hydrate terranes) and relatively low sulfate reduction rates in the sulfate reduction zone. These conditions are often present within continental margin sediments that harbor gas hydrate. Under these conditions, sulfate and methane are coupled geochemical species because AMO occurring at the SMI involves the microbially mediated co-consumption of sulfate and methane. If anaerobic methane oxidation is complete, the stoichiometric ratio between sulfate and methane consumed by AMO is 1:1, and the flux of sulfate to the SMI is equivalent to the upward methane flux to the SMI. The determination of the magnitude of AMO will require careful modeling of diffusive fluxes. The SMI at Site NGHP-01-03 (~9 m) is much shallower than at Sites NGHP-01-10 and NGHP-01-12 (~17 mbsf), and is only somewhat shallower than the SMI depth at Site NGHP-01-05 (~12 mbsf), indicating the relative vertical methane flux in the upper 30 m of sediments is greatest at Site NGHP-01-03, and greater at Site NGHP-01-05 than at Sites NGHP-01-10 and NGHP-01-12. The difference in methane flux rates between these sites is very intriguing, because there are massive gas hydrates at Sites NGHP-01-10 and NGHP-01-12 though the methane flux is relatively low, whereas there are disseminated

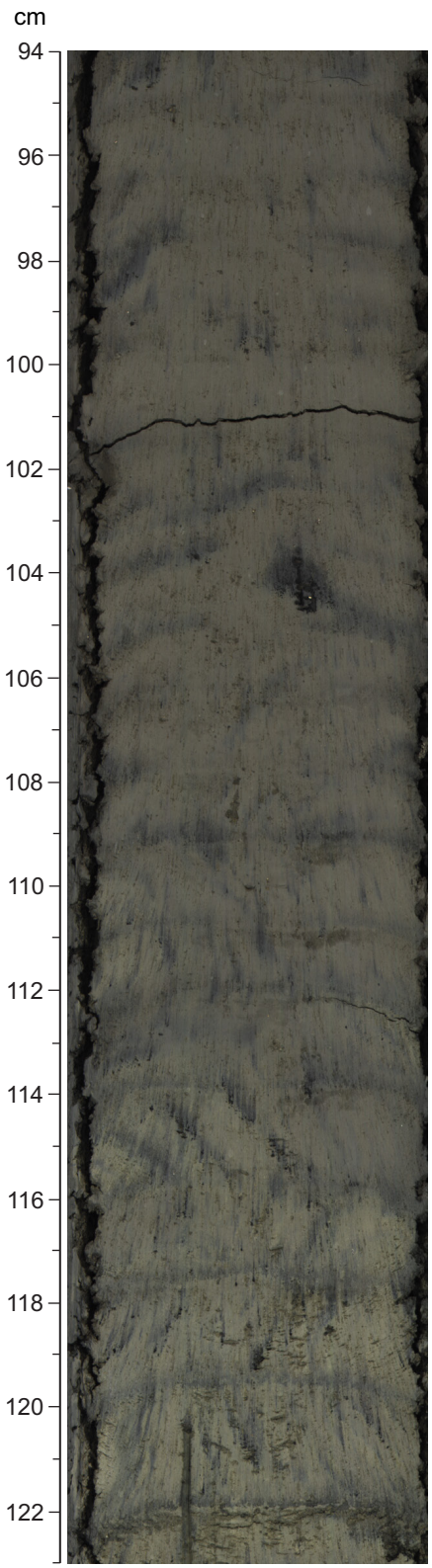

Figure 10. Iron monosulfides (dark black precipitates) and light and dark clays (boundary at 114 cm in this image) characteristic of Lithostratigraphic Unit II from Section NGHP-01-3B-36X-2, 94–123.5 cm. Biscuit and slurry texture (see "Lithostratigraphy" in the "Methods" chapter for more information) due to XCB coring is also seen throughout the image. [XCB, Extended Core Barrel]

gas hydrates at Site NGHP-01-03 coincident with a relatively high methane flux. The gas-hydrate distribution at Site NGHP-01-10 is mainly fracture controlled and the distribution at Sites NGHP-01-03 and NGHP-01-05 appears to be lithologically controlled. The difference in the stress state between these sites most likely plays a fundamental role in the subsurface hydrology and subsequent gas hydrate distribution.

Alkalinity and Bromide

The alkalinity concentration depth profile can be separated into three zones (fig. 11D). The first zone is from the seafloor to approximately 20 mbsf where concentrations increase from 10.2 to 33.7 mM (13 times seawater value), reflecting alkalinity production by oxidation of organic matter by sulfate reduction in the surface sediments and anaerobic oxidation of methane to about 10 m below the sulfate-methane interface. The elevated alkalinity below the present SMI is a result of alkalinity production in pore fluids previously at the depth of the SMI and subsequently buried and transported by diffusion. The second zone in the alkalinity depth profile is from 20 to 150 mbsf and is characterized by a progressive depletion in alkalinity from 34 mM to 7 mM with depth. The same decreasing trend in alkalinities within this depth interval was also observed at Sites NGHP-01-05 and NGHP-01-10. It is difficult to constrain the mechanism of alkalinity reduction between these depths without additional geochemical proxies but it could be a combination of authigenic carbonate formation driving down Ca^{+2} and alkalinity concentrations mixing with relict buried seawater, lower upward methane fluxes in the past resulting in decreased alkalinity production at the SMI, and(or) differing amounts of *in situ* methane production with depth controlling CO_2 concentrations, thus affecting carbonate dissolution/precipitation. The third zone is from 150 to 300 mbsf and is characterized by alkalinities varying from 8.3 to 23.7 mM. The alkalinity concentration depth profile in this interval exhibits three peaks and two troughs with similar amplitudes: one occurring above the BSR and two below the BSR. These variations in alkalinity could simply reflect changes in sedimentation rate with periods of higher sedimentation preserving relatively elevated alkalinity due to less diffusive exchange with seawater prior to burial. The relatively depleted intervals in this scenario would reflect lower sedimentation rates. The smoothness in the transitions between peaks and troughs reflects diffusion. The alkalinity variations may also represent varying degrees of methane and CO_2 production controlling carbonate precipitation/dissolution, and will be investigated as part of further shore-based studies.

Bromide concentrations are not typically measured shipboard during IODP/ODP cruises. During Leg 3 of NGHP Expedition 01, an ion chromatograph was utilized to measure both SO_4^{2-} and Br^-. Bromide concentrations in marine interstitial waters are sensitive to organic matter diagenesis, with concentrations higher than seawater reflecting marine organic matter decomposition. For this reason, Br^- profiles are similar to dissolved NH_4^+ profiles and to a lesser extent dissolved I profiles. Since gas hydrate was inferred to be

Table 5. Interstitial water data for Hole NGHP-01-03B.

["-", the value was not determined; bdl, below detection limit]

Core, section	Top	Bottom	Depth (mbsf)	Volume (mL)	pH	Alkalinity (mM)	Salinity	Cl^- (mM)*	Br^- (mM)	Br^-/Cl^-	SO_4^{2-} (mM)
NGHP-01-03B											
1H-2	140	150	2.9	34	7.6	19.92	33.0	556	0.87	0.00157	12.49
1H-3	140	150	4.4	30	7.5	25.08	33.5	554	0.91	0.00165	7.54
2H-1	140	150	6.8	30	7.7	30.17	34.5	554	0.88	0.00159	3.86
2H-2	140	150	8.3	29	7.7	32.24	32.0	555	0.88	0.00158	1.89
2H-3	140	150	9.8	30	7.6	-	32.5	555	0.91	0.00164	0.53
3H-3	140	150	19.3	2	7.5	33.66	32.5	554	0.92	0.00167	bdl
3H-5	140	150	22.3	29	7.4	31.43	33.5	553	0.89	0.00161	bdl
4H-3	140	150	28.8	21	7.4	28.39	34.0	554	0.96	0.00173	bdl
4H-5	140	150	31.8	-	7.3	30.78	33.0	567	1.00	0.00175	bdl
5H-3	140	150	38.3	30	7.7	23.87	32.5	572	0.99	0.00174	bdl
5H-5	140	150	41.3	26	7.8	25.75	34.0	563	1.01	0.00179	0.23
6H-3	140	150	47.8	22	7.6	21.71	34.5	560	1.06	0.00190	0.30
6H-5	140	150	50.8	21	7.6	20.64	33.5	559	1.06	0.00190	bdl
7H-3	140	150	57.3	20	7.6	16.74	33.5	561	1.10	0.00196	bdl
7H-5	140	150	60.3	13	7.6	-	32.5	551	1.09	0.00198	bdl
8X-3	130	150	66.7	5	-	-	-	554	1.18	-	bdl
8X-5	80	100	68.5	17	7.6	14.22	33.0	555	1.17	0.00212	0.16
9X-2	80	100	74.0	18	7.5	14.73	33.0	553	-	-	bdl
10X-1	51	71	81.8	14	7.6	10.08	32.5	552	-	-	0.23
11X-1	80	100	91.6	13	-	-	32.5	551	1.18	0.00214	bdl
12X-1	75	100	100.5	9	-	-	-	552	1.20	0.00216	bdl
13P-1	82	95	105.7	5	-	-	-	549	-	-	-
14X-1	120	150	107.1	11	-	-	32.5	551	1.22	0.00213	bdl
14X-2	120	150	108.6	15	7.5	11.04	-	548	1.15	0.00208	bdl
15X-3	120	150	119.7	20	7.4	8.18	32.5	555	1.15	0.00205	bdl
15X-5	120	150	122.7	20	7.7	-	-	558	1.22	0.00214	bdl
16X-2	120	150	127.1	23	7.7	8.07	32.0	558	-	-	bdl
16X-4	70	100	129.6	14	7.9	7.09	-	552	1.22	0.00220	bdl
17X-3	115	150	137.4	15	7.4	-	32.5	550	-	-	0.33
17X-4	115	150	138.9	17	7.6	9.59	32.0	549	1.24	0.00225	bdl
18X-3	115	150	146.1	18	7.8	8.54	32.0	562	1.25	0.00225	bdl
18X-5	115	150	149.1	18	8.0	8.31	31.5	556	1.36	0.00241	0.34
19X-3	115	150	155.9	24	8.0	10.92	32.0	557	1.22	0.00216	0.40
19X-4	44	76	156.6	26	7.7	10.39	32.5	559	1.34	0.00239	bdl
19X-5	65	100	157.6	23	7.9	11.38	31.5	557	1.27	0.00229	0.16
20X-2	65	100	163.5	20	7.9	17.48	33.5	552	1.18	0.00216	0.68
20X-3	60	80	164.4	30	8.0	17.50	30.5	517	1.15	0.00226	1.22
20X-5	115	150	167.3	21	7.7	17.98	33.0	555	1.27	0.00230	bdl
21X-1	115	150	172.2	25	-	19.59	33.0	551	1.30	0.00237	0.63
21X-3	115	150	175.2	21	7.9	21.17	32.5	554	-	-	0.75
24X-3	115	150	180.1	22	7.7	21.08	33.0	552	-	-	0.39
24X-5	100	130	183.0	20	7.8	19.91	-	552	1.11	0.00201	0.18
25X-3	115	150	189.5	20	8.0	15.18	33.0	561	-	-	bdl
25X-5	115	150	192.5	18	8.0	14.14	33.0	560	1.24	0.00225	0.20
26X-2	115	150	199.0	20	7.9	14.95	32.0	560	1.45	0.00260	0.21
27P-1	37	47	199.3	7	-	-	32.5	556	1.14	0.00212	4.88
29X-3	110	150	205.0	18	8.0	15.07	32.0	549	1.27	0.00229	0.66
29X-4	91	131	206.3	14	-	-	-	549	1.27	0.00234	0.20
30X-2	110	150	213.2	18	7.9	23.72	-	556	1.29	0.00232	0.32
30X-4	80	120	215.9	22	7.9	23.29	33.0	554	1.30	0.00237	0.32
31X-2	110	150	222.9	19	8.0	22.74	32.5	555	-	-	bdl
32X-3	110	150	233.8	24	8.1	19.25	33.5	554	1.29	0.00234	bdl
33X-3	110	150	242.2	13	8.1	15.30	32.0	554	1.32	0.00242	bdl
34X-3	110	150	252.7	21	8.0	13.11	34.5	554	1.28	0.00233	0.95
35X-3	110	150	260.8	23	8.1	11.47	32.0	554	1.44	0.00263	0.30
36X-3	110	150	271.8	14	8.1	12.00	32.0	559	1.36	0.00250	0.25
37X-3	110	150	280.3	19	8.0	15.61	31.5	551	1.26	0.00230	0.47
38X-3	110	150	290.3	17	8.0	23.06	33.0	551	1.33	0.00246	bdl
39X-3	110	150	299.9	12	8.2	25.15	33.5	554	-	-	-

*Cl^- analysis by titration (shorebased).

Table 6. Interstitial water data for Hole NGHP-01-03C.

["-", the value was not determined; bdl, below detection limit]

Core, section	Top	Bottom	Depth (mbsf)	Volume (mL)	pH	Alkalinity (mM)	Salinity	Cl^- (mM)*	Br^- (mM)	Br^-/Cl^-	SO_4^{2-} (mM)
						NGHP-01-03C					
1H-1	90	100	0.9	37	7.3	10.21	35.5	550	0.79	0.00144	21.15
1H-1	140	150	1.4	36	7.4	13.56	-	550	0.66	0.00121	19.32
1H-2	40	50	1.9	29	7.4	15.16	35.0	558	0.93	0.00167	19.67
1H-2	90	100	2.4	31	7.4	16.39	35.0	560	0.74	0.00131	16.54
1H-2	140	150	2.9	29	7.3	18.71	34.0	554	0.89	0.00161	13.46
1H-3	40	50	3.4	29	7.4	-	34.5	554	0.87	0.00157	9.67
1H-3	90	100	3.9	30	7.4	21.98	34.5	559	0.84	0.00150	11.04
1H-3	140	150	4.4	30	7.5	24.68	35.0	552	0.89	0.00161	8.32
1H-4	40	50	4.9	25	7.6	26.22	-	553	0.88	0.00160	6.85
1H-4	90	100	5.4	28	7.5	26.63	35.0	550	0.88	0.00161	5.46
1H-4	140	150	5.9	30	7.4	28.37	35.0	550	0.89	0.00163	4.30
1H-5	40	50	6.4	30	7.5	29.34	35.0	558	0.89	0.00160	3.34
1H-5	90	100	6.9	33	7.7	-	-	552	0.72	0.00130	2.88
1H-5	140	150	7.4	31	7.6	30.96	34.0	557	0.95	0.00171	2.40
1H-6	40	50	7.9	30	7.5	31.45	-	550	0.89	0.00162	1.35
1H-6	90	100	8.4	30	7.6	31.88	-	548	0.86	0.00157	0.93
1H-6	140	150	8.9	28	7.5	31.81	34.0	548	0.69	0.00127	0.41
2H-1	40	50	9.9	30	7.6	26.04	34.0	545	0.97	0.00177	-
2H-1	90	100	10.4	31	7.5	33.10	-	559	0.97	0.00173	bdl
2H-1	140	150	10.9	30	7.5	32.89	34.0	558	0.88	0.00158	bdl
2H-2	40	50	11.4	32	7.6	-	34.0	560	1.03	0.00184	bdl
2H-2	90	100	11.9	30	7.3	32.66	34.0	549	1.00	0.00182	bdl
2H-2	140	150	12.4	31	7.5	32.11	34.0	558	1.00	0.00180	bdl
2H-3	40	50	12.9	29	7.2	31.16	-	549	0.94	0.00171	bdl
2H-3	90	100	13.4	28	7.4	31.35	-	546	0.93	0.00171	bdl
2H-3	140	150	13.9	29	7.3	32.06	34.0	544	0.94	0.00173	bdl
2H-4	40	50	14.4	30	7.4	32.26	34.0	545	0.95	0.00174	bdl
2H-4	90	100	14.9	27	7.5	32.38	34.0	548	0.95	0.00173	bdl
2H-4	140	150	15.4	29	7.4	31.49	34.0	550	-	-	-
2H-5	40	50	15.9	29	7.4	31.99	33.5	558	0.99	0.00177	bdl
2H-5	90	100	16.4	30	7.4	32.73	34.0	552	-	-	-
2H-5	140	150	16.9	26	7.5	32.44	34.0	554	1.10	0.00198	bdl
2H-6	40	50	17.4	30	7.5	32.54	34.5	559	0.81	0.00146	bdl
2H-6	90	100	17.9	32	7.5	32.05	33.5	548	0.98	0.00179	bdl
2H-6	140	150	18.4	28	7.5	32.37	34.0	559	0.75	0.00134	bdl
2H-7	60	70	19.1	29	7.5	32.18	-	558	0.96	0.00172	bdl
3H-1	40	50	19.4	27	7.5	26.79	34.5	554	0.00	0.00000	bdl
3H-1	140	150	20.4	31	7.5	30.61	34.5	554	1.00	0.00180	1.16
3H-2	90	100	21.4	30	7.7	-	33.5	554	-	-	-
3H-4	90	100	24.4	22	7.6	26.30	33.0	552	0.97	0.00176	bdl
3H-6	90	100	27.4	29	7.3	-	33.0	556	1.01	0.00182	0.45
7P-1	35	47	184.35	21	8.0	17.08	31	544	1.20	0.00221	1.34

*Cl^- analysis by titration (shipboard).

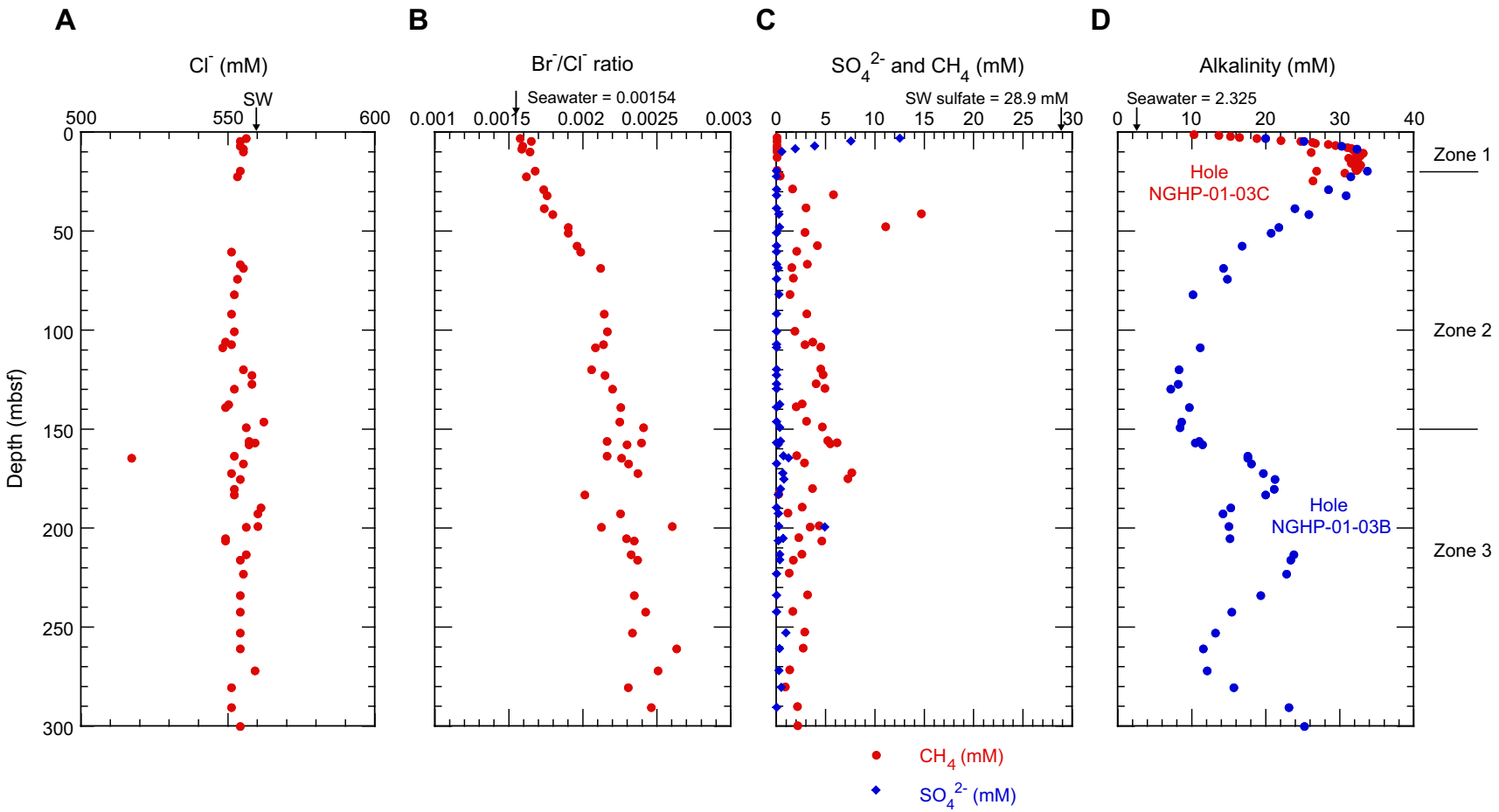

Figure 11. Concentration depth profiles of: A, Hole NGHP-01-03B chloride by titration (shore-based) (errors are smaller than the symbols); B, Hole NGHP-01-03B Br^-/Cl^- ratio; C, Hole NGHP-01-03B sulfate and methane; and D, Holes NGHP-01-03B and NGHP-01-03C alkalinity; blue circles are Hole NGHP-01-03B and red circles are Hole NGHP-01-03C alkalinity. PR indicates pressure core whole-round (or sample) [sw, seawater concentration]

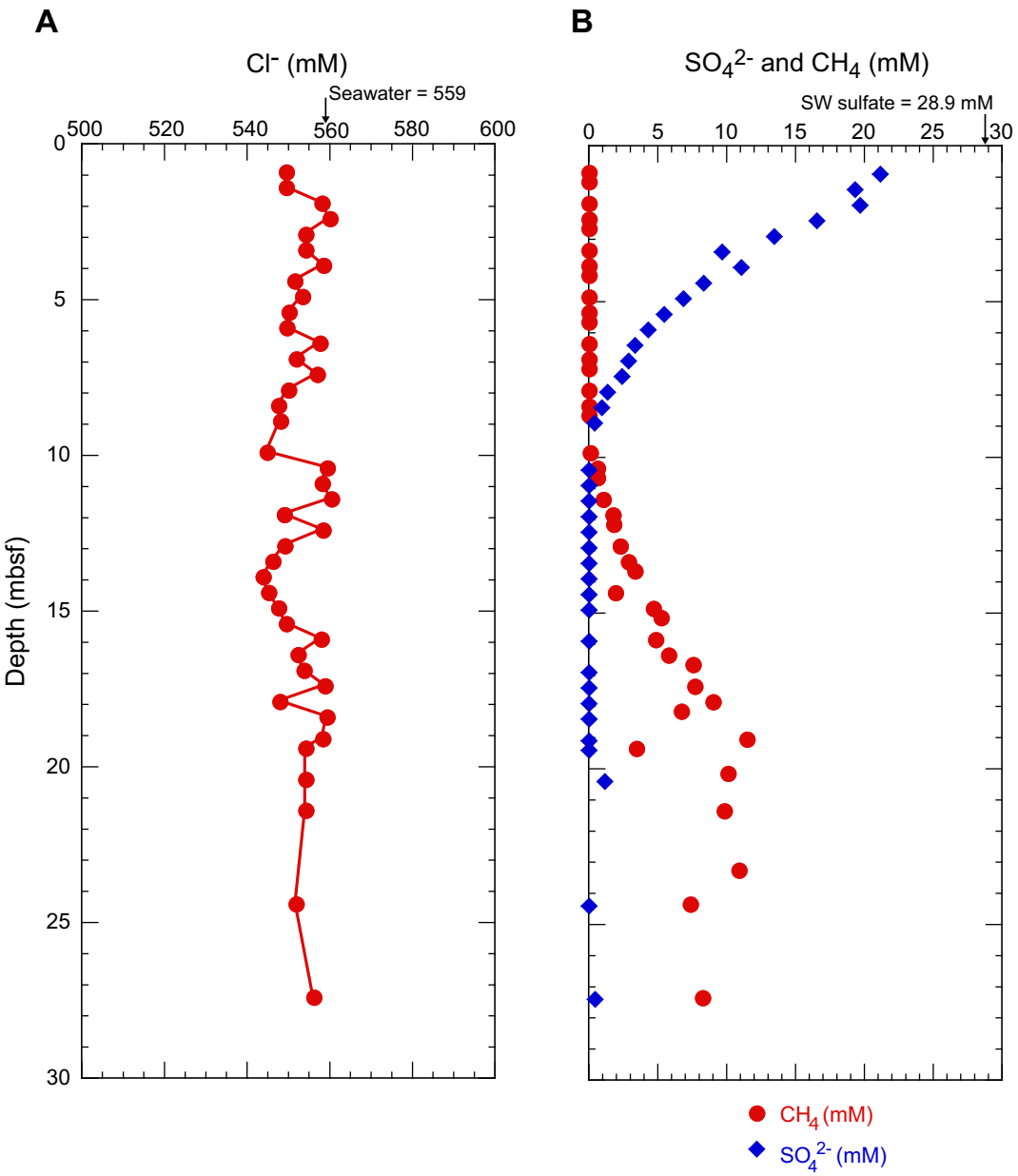

Figure 12. Concentration depth profiles of A, Hole NGHP-01-03C chloride by titration (shipboard) (errors are smaller than the symbols); B, Hole NGHP-01-03C sulfate and methane. [sw, seawater concentration]

present in a substantial amount of the samples at this site, Br^- concentrations have been normalized to chloride to dampen the influence of gas-hydrate dissociation on the Br^- concentration depth profile (fig. 11B). In Hole NGHP-01-03B, Br^-/Cl^- increases relatively sharply from values slightly higher than seawater (0.00154) at the seafloor to approximately 1.6 times the seawater value at 70 mbsf. From 70 mbsf to the bottom of the hole (~300 mbsf), Br^-/Cl^- ratios are more variable and increase slightly to a value of 0.00263 at 261 mbsf (~70 percent greater than seawater value). The Br^- concentration profile at this site reflects decomposition of marine organic matter with a greater rate of change in the decomposition rate occurring above approximately 70 mbsf, and more uniform values below this depth. The variability of the Br^-/Cl^- ratio in the middle and lower portion of the profile may be an artifact of gas-hydrate dissociation or may be impacted by varying amounts of terrestrial organic matter which does not contribute a significant amount of Br^- to the pore fluids during organic matter diagenesis compared with marine organic matter.

Organic Geochemistry

Organic geochemical studies at Site NGHP-01-03 (KGGH-05) included analysis of the composition of volatile hydrocarbons including methane, ethane, and propane (C_1–C_3) and fixed natural gases (that is, O_2, CO_2, and N_2+Ar) from headspace, void gas, and pressure-core sampler (PCS) degassing experiments. In general, these analyses indicate that methane and carbon dioxide are the predominant gases found in the cores at this site. However, ethane was present in low level concentrations in void gas and pressure-core degassing experiment samples. The samples overlying the sulfate-methane interface (SMI) were dominated by carbon dioxide, while methane was enriched below the SMI and above the seismically-inferred bottom simulating reflector (BSR). Specific details of the shipboard gas chemistry results for Site NGHP-01-03, Holes B and C are provided in the following discussion.

Headspace gas analyses were performed on 59 samples from Hole NGHP-01-03B and 43 samples from Hole NGHP-01-03C ranging in depth from 0.9 to 299.5 meters below seafloor (mbsf). The concentrations given here represent minimum proxy measurements of the actual concentrations due to limitations of the gas headspace method (Kvenvolden and Lorenson, 2000). The sediment pore water contained methane at concentrations ranging from non-detectable near the surface to 6.96 mM at ~41 mbsf (table 7). Theoretical methane saturation in pore water under site-specific physical conditions, calculated using the Duan and others (1992) and Xu (2002, 2004) methodologies, ranges from 60.4 mM at the seafloor to 128.9 mM at 200 mbsf, then declines to 124.8 mM near the borehole completion depth of 300 mbsf. No C_2 or C_3 hydrocarbon gases were detected in headspace samples, suggesting a microbial source of methane. Methane concentrations increase strongly from nondetectable to 3.8 mM at ~12 mbsf likely denoting the sulfate-methane interface (SMI) (fig. 13). The slight increase in methane concentration at ~40 mbsf (fig. 13) may be associated with the presence of free gas or gas hydrate; however, other gas-hydrate proxy measurements indicated that gas hydrate was not present (see "Inorganic geochemistry" and "Downhole logging"). The methane concentration peak at the SMI was confirmed in Hole NGHP-01-03C, however was offset ~3 m in this borehole occurs at ~9 mbsf (fig. 13). Methane concentration decreases below the bottom simulating reflector (BSR). The methane concentrations were generally at levels below saturation throughout the length of the borehole.

Carbon dioxide (CO_2) concentrations ranged from 0.1 to 22.5 mM in pore water contained within the sediment. An equivalent concentration expression of gas volume to sediment volume ranges from ~1,000 to nearly 350,000 microliters CO_2/liter wet sediment (table 7). There is no consistent, fine-scale trend in the CO_2 concentration with depth; however, the results can be roughly divided into two zones based on gas concentration. The highest concentrations are found near the SMI at depths ranging from 5 to 15 mbsf (fig. 14). No apparent change in lithology could be inferred at or near this interval (see "Lithostratigraphy"). More intermediate concentrations were found in the entire interval below the SMI; however, they are probably not associated with gas hydrate as inferred from the methane concentrations. The methane to carbon dioxide ratio for headspace also reflects these two zones, indicating that methane is preferentially concentrated between the SMI and BSR (fig. 15). The air gases (N_2+Ar), and O_2 were the balance gases; however, the $(N_2+Ar)/O_2$ ratios were typically greater than air, reflecting the high ratio in pore fluids or indicating that some air was trapped in the headspace samples and some oxygen has likely dissolved preferentially compared to N_2. Air gases are present in all samples as the core plugs were degassed in an air headspace.

Void gas samples were collected from sixteen different intervals ranging in depth from 54.4 to 282.4 mbsf. The void gas samples contained methane above 930,000 ppmv at all intervals except the uppermost, as noted in table 8. Methane concentration within voids averaged nearly 882,000 ppmv (±175,000 or 88.2 percent ± 17.5 percent); however, higher molecular weight hydrocarbon gases were not detected. Carbon dioxide concentrations ranged from 3,530 to 17,300 ppmv and are tabulated with other gas data in table 8. The methane to carbon dioxide ratios are higher in the depths between the SMI and continue below the BSR, indicating that any existing gas hydrate may have concentrated the methane relative to carbon dioxide (fig. 15). This trend occurs in headspace gas samples although the magnitude of the ratios is typically 2 orders less due to the preferential loss of volatile methane by the headspace sample method. The air gases (N_2+Ar), and O_2 composed the balance gases; however, the $(N_2+Ar)/O_2$ ratios showed a decreasing trend with depth in the core, indicating that there is less air contamination of the core with depth.

Table 7. Headspace (HS) gas composition for Site NGHP-01-03.

Sample	Site	Hole	Core	Section	Interval (cm)	Sed wt. (g)	Sample depth (mbsf)	CO_2	C_1	C_2	C_3
								(ppm-v)			
3B-1H2-95-100	3	B	1	2	95–100	8.7	2.5	33,100	nd	nd	nd
3B-1H3-135-140	3	B	1	3	135–140	10.9	4.4	37,500	nd	nd	nd
3B-2H1-135-140	3	B	2	1	135–140	7.2	6.8	9,100	nd	nd	nd
3B-2H2-135-140	3	B	2	2	135–140	7.6	8.3	13,400	nd	nd	nd
3B-2H3-105-110	3	B	2	3	105–110	9.7	9.5	9,000	nd	nd	nd
3B-2H5-105-110	3	B	2	5	105–110	6.1	12.5	15,600	100	nd	nd
3B-3H3-105-110	3	B	3	3	105–110	6.5	19.0	13,400	1,400	nd	nd
3B-3H5-95-100	3	B	3	5	95–100	8.7	21.9	4,800	800	nd	nd
3B-4H3-95-100	3	B	4	3	105–110	11.4	28.5	12,200	6,000	nd	nd
3B-4H5-95-100	3	B	4	5	95–100	13.9	31.4	91,200	27,900	nd	nd
3B-5H3-105-110	3	B	5	3	105–110	12.7	38.0	5,300	12,700	nd	nd
3B-5H5-95-100	3	B	5	5	95–110	13.6	40.9	51,400	69,000	nd	nd
3B-6H3-105-110	3	B	6	3	105–110	14.0	47.5	92,500	53,900	nd	nd
3B-6H5-95-100	3	B	6	5	95–100	11.4	50.4	16,200	10,600	nd	nd
3B-7H3-105-110	3	B	7	3	105–110	13.2	57.0	26,100	18,500	nd	nd
3B-7H5-95-100	3	B	7	5	95–100	13.1	59.9	13,400	9,000	nd	nd
3B-8X3-95-100	3	B	8	3	95–100	10.9	66.4	17,300	9,100	nd	nd
3B-8X5-35-40	3	B	8	5	35–40	14.0	68.1	17,100	6,100	nd	nd
3B-9X2-30-35	3	B	9	2	30–35	12.1	73.5	11,200	5,600	nd	nd
3B-10X1-46-51	3	B	10	1	46–51	8.1	81.8	5,300	2,800	nd	nd
3B-11X1-65-70	3	B	11	1	65–70	8.8	91.5	12,100	6,900	nd	nd
3B-12X1-60-65	3	B	12	1	60–65	9.3	100.3	11,000	4,400	nd	nd
3B-13P-80-82	3	B	13	P	80–82	9.3	105.7	30,400	8,900	nd	nd
3B-14X1-115-120	3	B	14	1	115–120	10.0	107.1	14,700	7,500	nd	nd
3B-14X2-75-80	3	B	14	1	75–80	7.8	108.2	31,700	8,800	nd	nd
3B-15X3-85-90	3	B	15	3	85–90	9.7	119.4	16,300	9,100	nd	nd
3B-15X5-75-80	3	B	15	5	75–80	11.9	122.3	23,700	12,300	nd	nd
3B-16X2-85-90	3	B	16	2	85–90	8.9	126.8	12,800	7,400	nd	nd
3B-16X4-25-30	3	B	16	4	25–30	9.2	129.2	14,800	9,300	nd	nd
3B-17X3-80-85	3	B	17	3	80–85	9.5	137.0	10,000	5,100	nd	nd
3B-17X4-70-75	3	B	17	4	70–75	7.1	138.4	8,200	2,800	nd	nd
3B-18X3-80-85	3	B	18	3	80–85	9.7	145.7	3,800	6,100	nd	nd
3B-18X4-70-75	3	B	18	4	70–75	9.6	148.6	8,600	9,300	nd	nd
3B-19X3-80-85	3	B	19	3	80–85	9.5	155.5	19,600	10,300	nd	nd
3B-19X4-39-44	3	B	19	4	39–44	11.3	156.6	26,300	15,100	nd	nd
3B-19X5-20-25	3	B	19	5	20–25	10.1	157.2	17,700	11,600	nd	nd
3B-20X5-70-75	3	B	20	5	70–75	8.9	163.1	15,900	3,700	nd	nd
3B-20X2-30-35	3	B	20	2	30–35	7.7	166.8	13,500	4,400	nd	nd
3B-21X1-80-85	3	B	21	1	80–85	9.1	171.8	44,400	14,400	nd	nd
3B-21X3-70-75	3	B	21	3	70–75	6.8	174.7	44,800	9,700	nd	nd
3B-24X3-80-85	3	B	24	3	80–85	7.9	179.8	19,900	5,800	nd	nd
3B-24X5-55-60	3	B	24	5	55–60	7.8	182.5	300	300	nd	nd
3B-25X3-80-85	3	B	25	3	80–85	10.2	189.2	19,400	8,400	nd	nd
3B-25X5-70-75	3	B	25	5	70–75	9.4	192.1	17,000	3,300	nd	nd
3B-26X2-70-75	3	B	26	2	70–75	8.7	198.5	18,300	11,600	nd	nd
3B-27P-47-52	3	B	27	P	47–52	7.8	199.2	29,700	8,000	nd	nd
3B-29X3-65-70	3	B	29	3	65–70	9.7	204.6	15,100	6,800	nd	nd
3B-29X4-86-91	3	B	29	4	86–91	10.1	206.3	17,300	14,700	nd	nd
3B-30X2-75-80	3	B	30	2	75–80	6.6	212.9	11,000	5,000	nd	nd
3B-30X4-75-80	3	B	30	4	75–80	9.2	215.9	12,100	4,800	nd	nd
3B-31X2-65-70	3	B	31	2	65–70	9.6	222.5	12,600	3,800	nd	nd
3B-32X3-65-70	3	B	32	3	65–70	8.8	233.4	22,900	8,500	nd	nd
3B-33X3-65-70	3	B	33	3	65–70	9.7	241.7	8,100	4,900	nd	nd
3B-34X3-65-70	3	B	34	3	65–70	10.2	252.3	13,800	9,200	nd	nd
3B-35X3-65-70	3	B	35	3	65–65	10.2	260.3	30,700	8,700	nd	nd
3B-36X3-65-70	3	B	36	3	65–70	8.4	271.4	12,600	3,300	nd	nd
3B-37X3-65-70	3	B	37	3	65–70	7.8	279.9	2,200	2,000	nd	nd

Table 7. Headspace (HS) gas composition for Site NGHP-01-03.—Continued

Sample	O_2	N_2+Ar	H_2S	C_1	C_1	CO_2	CO_2	C_1/CO_2
		(ppm-v)		(mL/L WS)	(mM PW)	(mL/L WS)	(mM PW)	
3B-1H2-95-100	176,400	752,100	nd	nd	nd	86,700	4.5	-
3B-1H3-135-140	17,000	732,000	nd	nd	nd	70,900	4.0	-
3B-2H1-135-140	242,200	777,900	nd	nd	nd	30,600	1.8	-
3B-2H2-135-140	245,600	773,900	nd	nd	nd	42,100	2.6	-
3B-2H3-105-110	246,800	777,100	nd	nd	nd	20,200	1.3	-
3B-2H5-105-110	184,700	732,900	nd	500	0.0	64,700	4.1	0.0
3B-3H3-105-110	247,100	776,900	nd	5,400	0.4	51,600	3.5	0.1
3B-3H5-95-100	252,600	788,300	nd	2,200	0.1	12,600	0.9	0.2
3B-4H3-95-100	250,900	783,100	nd	10,500	0.8	21,400	1.5	0.5
3B-4H5-95-100	138,000	701,200	nd	35,300	2.6	115,500	8.6	0.3
3B-5H3-105-110	248,000	790,000	nd	18,800	1.4	7,800	0.6	2.4
3B-5H5-95-100	13,800	717,600	nd	90,800	7.0	67,600	5.2	1.3
3B-6H3-105-110	113,600	733,600	nd	67,400	5.3	115,600	9.1	0.6
3B-6H5-95-100	149,300	763,100	nd	18,800	1.5	28,500	2.2	0.7
3B-7H3-105-110	171,700	760,600	nd	25,700	2.1	36,200	2.9	0.7
3B-7H5-95-100	177,300	748,100	nd	12,600	1.0	18,800	1.5	0.7
3B-8X3-95-100	177,500	763,500	nd	17,200	1.4	32,700	2.6	0.5
3B-8X5-35-40	185,700	787,400	nd	7,600	0.6	21,400	1.8	0.4
3B-9X2-30-35	180,600	759,300	nd	9,000	0.7	17,900	1.5	0.5
3B-10X1-46-51	189,800	750,900	nd	8,000	0.6	15,300	1.2	0.5
3B-11X1-65-70	177,400	772,700	nd	17,800	1.5	31,300	2.6	0.6
3B-12X1-60-65	191,000	794,200	nd	10,600	0.9	26,100	2.2	0.4
3B-13P-80-82	140,600	776,200	nd	21,200	1.8	72,500	6.1	0.3
3B-14X1-115-120	181,200	743,700	nd	16,200	1.4	31,700	2.7	0.5
3B-14X2-75-80	174,300	773,600	nd	26,800	2.2	96,300	8.0	0.3
3B-15X3-85-90	173,700	783,500	nd	20,500	1.8	36,600	3.1	0.6
3B-15X5-75-80	153,400	782,900	nd	20,300	1.8	39,100	3.4	0.5
3B-16X2-85-90	173,900	775,000	nd	18,700	1.6	32,500	2.8	0.6
3B-16X4-25-30	171,400	766,400	nd	22,600	2.0	35,900	3.1	0.6
3B-17X3-80-85	172,200	786,700	nd	11,800	1.0	23,300	2.0	0.5
3B-17X4-70-75	190,400	779,600	nd	9,500	0.8	28,100	2.4	0.3
3B-18X3-80-85	193,300	849,800	nd	13,800	1.2	8,600	0.8	1.6
3B-18X4-70-75	171,300	832,900	nd	21,200	1.9	19,600	1.7	1.1
3B-19X3-80-85	162,400	700,400	nd	23,800	2.1	45,400	4.0	0.5
3B-19X4-39-44	152,700	781,400	nd	26,900	2.4	47,100	4.2	0.6
3B-19X5-20-25	154,800	79,000	nd	24,700	2.2	37,400	3.3	0.7
3B-20X5-70-75	170,800	757,100	nd	9,500	0.8	40,300	3.6	0.2
3B-20X2-30-35	152,100	768,800	nd	13,500	1.2	41,600	3.7	0.3
3B-21X1-80-85	123,300	765,400	nd	35,500	3.2	109,300	9.8	0.3
3B-21X3-70-75	151,300	748,300	nd	35,400	3.1	162,700	14.3	0.2
3B-24X3-80-85	160,000	756,100	nd	17,300	1.5	59,300	5.3	0.3
3B-24X5-55-60	194,600	748,000	nd	900	0.1	1,000	0.1	1.0
3B-25X3-80-85	162,500	764,700	nd	17,500	1.6	40,400	3.7	0.4
3B-25X5-70-75	172,700	752,000	nd	7,700	0.7	39,900	3.6	0.2
3B-26X2-70-75	143,200	829,200	nd	30,300	2.7	47,900	4.3	0.6
3B-27P-47-52	156,600	763,400	nd	24,200	2.2	90,100	8.1	0.3
3B-29X3-65-70	177,300	748,400	nd	15,200	1.4	33,800	3.1	0.5
3B-29X4-86-91	170,900	746,200	nd	31,200	2.9	36,600	3.4	0.8
3B-30X2-75-80	188,300	746,600	nd	18,700	1.7	41,500	3.7	0.5
3B-30X4-75-80	181,300	750,600	nd	11,600	1.1	29,300	2.7	0.4
3B-31X2-65-70	175,800	766,100	nd	8,700	0.8	28,700	2.7	0.3
3B-32X3-65-70	175,300	755,800	nd	21,900	2.0	58,900	5.5	0.4
3B-33X3-65-70	184,600	747,300	nd	11,100	1.0	18,200	1.7	0.6
3B-34X3-65-70	151,300	777,900	nd	19,200	1.8	28,700	2.7	0.7
3B-35X3-65-70	121,300	807,100	nd	18,100	1.7	64,100	6.1	0.3
3B-36X3-65-70	162,600	764,700	nd	9,200	0.9	34,600	3.3	0.3
3B-37X3-65-70	182,900	731,500	nd	6,100	0.6	6,800	0.6	0.9

Table 7. Headspace (HS) gas composition for Site NGHP-01-03.—Continued

Sample	Site	Hole	Core	Section	Interval (cm)	Sed wt. (g)	Sample depth (mbsf)	CO_2	C_1	C_2	C_3
									(ppm-v)		
3B-38X3-65-70	3	B	38	3	65–70	8.1	289.9	14,400	5,200	nd	nd
3B-39X3-65-70	3	B	39	3	65–70	10.8	299.5	22,600	6,200	nd	nd
3C-1H1-85-90	3	C	1	1	85–90	6.2	0.9	16,700	nd	nd	nd
3C-1H1-115-120	3	C	1	1	115–120	6.7	1.2	23,000	nd	nd	nd
3C-1H2-35-40	3	C	1	2	35–40	5.5	1.9	33,500	nd	nd	nd
3C-1H2-85-90	3	C	1	2	85–90	6.2	2.4	39,600	nd	nd	nd
3C-1H2-115-120	3	C	1	2	115–120	6.3	2.7	42,200	nd	nd	nd
3C-1H3-35-40	3	C	1	3	35–40	6.8	3.4	53,800	nd	nd	nd
3C-1H3-85-90	3	C	1	3	85–90	5.9	3.9	58,800	nd	nd	nd
3C-1H3-115-120	3	C	1	3	115–120	6.1	4.2	23,000	nd	nd	nd
3C-1H4-35-40	3	C	1	4	35–40	6.6	4.9	50,800	nd	nd	nd
3C-1H4-85-90	3	C	1	4	85–90	6.4	5.4	57,700	nd	nd	nd
3C-1H4-115-120	3	C	1	4	115–120	6.1	5.7	67,800	nd	nd	nd
3C-1H5-35-40	3	C	1	5	35–40	6.6	6.4	74,700	nd	nd	nd
3C-1H5-85-90	3	C	1	5	85–90	6.3	6.9	77,400	nd	nd	nd
3C-1H5-115-120	3	C	1	5	115–120	7.3	7.2	82,100	nd	nd	nd
3C-1H6-35-40	3	C	1	6	35–40	6.7	7.9	79,200	nd	nd	nd
3C-1H6-85-90	3	C	1	6	85–90	6.7	8.4	72,300	nd	nd	nd
3C-1H6-115-120	3	C	1	6	115–120	7.2	8.7	15,700	nd	nd	nd
3C-2H1-35-40	3	C	2	1	35–40	6.9	9.9	52,800	200	nd	nd
3C-2H1-85-90	3	C	2	1	85–90	6.1	10.4	56,600	900	nd	nd
3C-2H1-115-120	3	C	2	1	115–120	6.5	10.7	63,200	1,000	nd	nd
3C-2H2-35-40	3	C	2	2	35–40	7.9	11.4	63,100	2,100	nd	nd
3C-2H2-85-90	3	C	2	2	85–90	6.9	11.9	56,100	3,000	nd	nd
3C-2H2-115-120	3	C	2	2	115–120	6.5	12.2	59,300	2,900	nd	nd
3C-2H3-35-40	3	C	2	3	35–40	6.4	12.9	83,400	3,600	nd	nd
3C-2H3-85-90	3	C	2	3	85–90	7.0	13.4	93,100	5,000	nd	nd
3C-2H3-115-120	3	C	2	3	115–120	6.4	13.7	88,900	5,300	nd	nd
3C-2H4-35-40	3	C	2	4	35–40	7.8	14.4	14,300	3,800	nd	nd
3C-2H4-85-90	3	C	2	4	85–90	7.3	14.9	76,800	8,600	nd	nd
3C-2H4-115-120	3	C	2	4	115–120	7.2	15.2	86,700	9,500	nd	nd
3C-2H5-35-40	3	C	2	5	35–40	7.6	15.9	73,800	9,300	nd	nd
3C-2H5-85-90	3	C	2	5	85–90	6.7	16.4	72,600	9,600	nd	nd
3C-2H5-115-120	3	C	2	5	115–120	6.2	16.7	80,700	11,500	nd	nd
3C-2H6-35-40	3	C	2	6	35–40	5.9	17.4	70,500	11,100	nd	nd
3C-2H6-85-90	3	C	2	6	85–90	5.9	17.9	70,800	13,000	nd	nd
3C-2H6-115-120	3	C	2	6	115–120	5.9	18.2	17,300	9,700	nd	nd
3C-2H7-55-60	3	C	2	7	55–60	5.9	19.1	67,800	16,500	nd	nd
3C-3H1-35-40	3	C	3	1	35–40	13.4	19.4	21,900	13,200	nd	nd
3C-3H1-115-120	3	C	3	1	115–120	5.9	20.2	48,200	14,600	nd	nd
3C-3H2-85-90	3	C	3	2	85–90	7.5	21.4	47,800	18,600	nd	nd
3C-3H3-125-130	3	C	3	3	125–130	6.2	23.3	35,500	16,600	nd	nd
3C-3H4-85-90	3	C	3	4	85–90	8.7	24.4	43,300	16,600	nd	nd
3C-3H6-85-90	3	C	3	6	85–90	7.8	27.4	42,000	16,300	nd	nd
3C-7P-30-35	3	C	7	P	30–35	7.8	184.3	40,500	9,400	nd	nd

Table 7. Headspace (HS) gas composition for Site NGHP-01-03.—Continued

Sample	O_2	N_2+Ar	H_2S	C_1	C_1	CO_2	CO_2	C_1/CO_2
		(ppm-v)		(mL/L WS)	(mM PW)	(mL/L WS)	(mM PW)	
3B-38X3-65-70	177,900	710,400	nd	14,900	1.4	41,500	3.9	0.4
3B-39X3-65-70	165,200	751,400	nd	11,800	1.2	43,400	4.2	0.3
3C-1H1-85-90	183,000	767,600	nd	nd	nd	68,200	3.2	-
3C-1H1-115-120	170,700	751,400	nd	nd	nd	85,300	4.1	-
3C-1H2-35-40	175,200	751,500	nd	nd	nd	158,400	8.1	-
3C-1H2-85-90	172,900	751,100	nd	nd	nd	161,400	8.4	-
3C-1H2-115-120	173,200	741,400	nd	nd	nd	168,600	8.9	-
3C-1H3-35-40	167,600	741,300	nd	nd	nd	195,200	10.6	-
3C-1H3-85-90	164,100	734,500	nd	nd	nd	255,000	14.1	-
3C-1H3-115-120	183,300	744,800	nd	nd	nd	95,900	5.4	-
3C-1H4-35-40	166,700	742,000	nd	nd	nd	191,800	10.9	-
3C-1H4-85-90	161,700	745,000	nd	nd	nd	226,200	13.0	-
3C-1H4-115-120	159,400	730,600	nd	nd	nd	282,500	16.4	-
3C-1H5-35-40	158,300	728,100	nd	nd	nd	282,000	16.6	-
3C-1H5-85-90	160,800	734,000	nd	nd	nd	309,600	18.4	-
3C-1H5-115-120	156,800	724,300	nd	nd	nd	272,200	16.3	-
3C-1H6-35-40	158,600	720,200	nd	nd	nd	293,000	17.7	-
3C-1H6-85-90	160,400	728,700	nd	nd	nd	267,500	16.3	-
3C-1H6-115-120	180,700	729,600	nd	nd	nd	52,900	3.2	-
3C-2H1-35-40	162,000	737,300	nd	600	0.0	188,200	11.7	0.0
3C-2H1-85-90	173,900	739,900	nd	3,800	0.2	235,800	14.7	0.0
3C-2H1-115-120	166,200	722,700	nd	3,900	0.2	243,200	15.2	0.0
3C-2H2-35-40	165,500	742,200	nd	6,200	0.4	188,400	11.9	0.0
3C-2H2-85-90	166,000	748,700	nd	10,700	0.7	199,800	12.7	0.1
3C-2H2-115-120	161,800	733,000	nd	11,200	0.7	227,900	14.5	0.0
3C-2H3-35-40	157,200	715,500	nd	14,100	0.9	327,200	21.0	0.0
3C-2H3-85-90	147,200	713,600	nd	17,500	1.1	325,700	21.0	0.1
3C-2H3-115-120	151,600	718,500	nd	20,700	1.3	348,600	22.5	0.1
3C-2H4-35-40	185,400	745,900	nd	11,600	0.8	43,400	2.8	0.3
3C-2H4-85-90	151,000	713,300	nd	28,500	1.9	254,600	16.6	0.1
3C-2H4-115-120	146,300	711,900	nd	31,900	2.1	292,600	19.2	0.1
3C-2H5-35-40	152,600	720,900	nd	29,300	1.9	232,100	15.3	0.1
3C-2H5-85-90	150,200	724,700	nd	35,600	2.3	268,500	17.7	0.1
3C-2H5-115-120	148,800	734,200	nd	47,000	3.1	329,300	21.8	0.1
3C-2H6-35-40	147,400	730,900	nd	48,000	3.2	305,900	20.3	0.2
3C-2H6-85-90	148,000	738,900	nd	56,300	3.7	307,200	20.4	0.2
3C-2H6-115-120	184,500	734,500	nd	42,000	2.8	74,800	5.0	0.6
3C-2H7-55-60	145,500	732,600	nd	71,700	4.8	294,200	19.7	0.2
3C-3H1-35-40	150,200	768,000	nd	17,900	1.2	29,600	2.0	0.6
3C-3H1-115-120	157,300	730,500	nd	63,100	4.3	209,100	14.1	0.3
3C-3H2-85-90	148,700	741,500	nd	59,400	4.1	152,800	10.4	0.4
3C-3H3-125-130	145,700	765,400	nd	67,700	4.7	144,700	9.9	0.5
3C-3H4-85-90	151,100	739,600	nd	43,500	3.0	113,400	7.9	0.4
3C-3H6-85-90	156,500	742,300	nd	49,600	3.5	127,600	9.0	0.4
3C-7P-30-35	134,900	794,700	nd	28,500	2.5	122,900	11.0	0.2

Notes: nd = not detected. WS = Wet sediment. PW = porewater. Approximate detection limits are about 15 ppmv for methane, 30 ppmv for ethane, 50 ppmv for propane, and 20 ppmv for hydrogen sulfide.

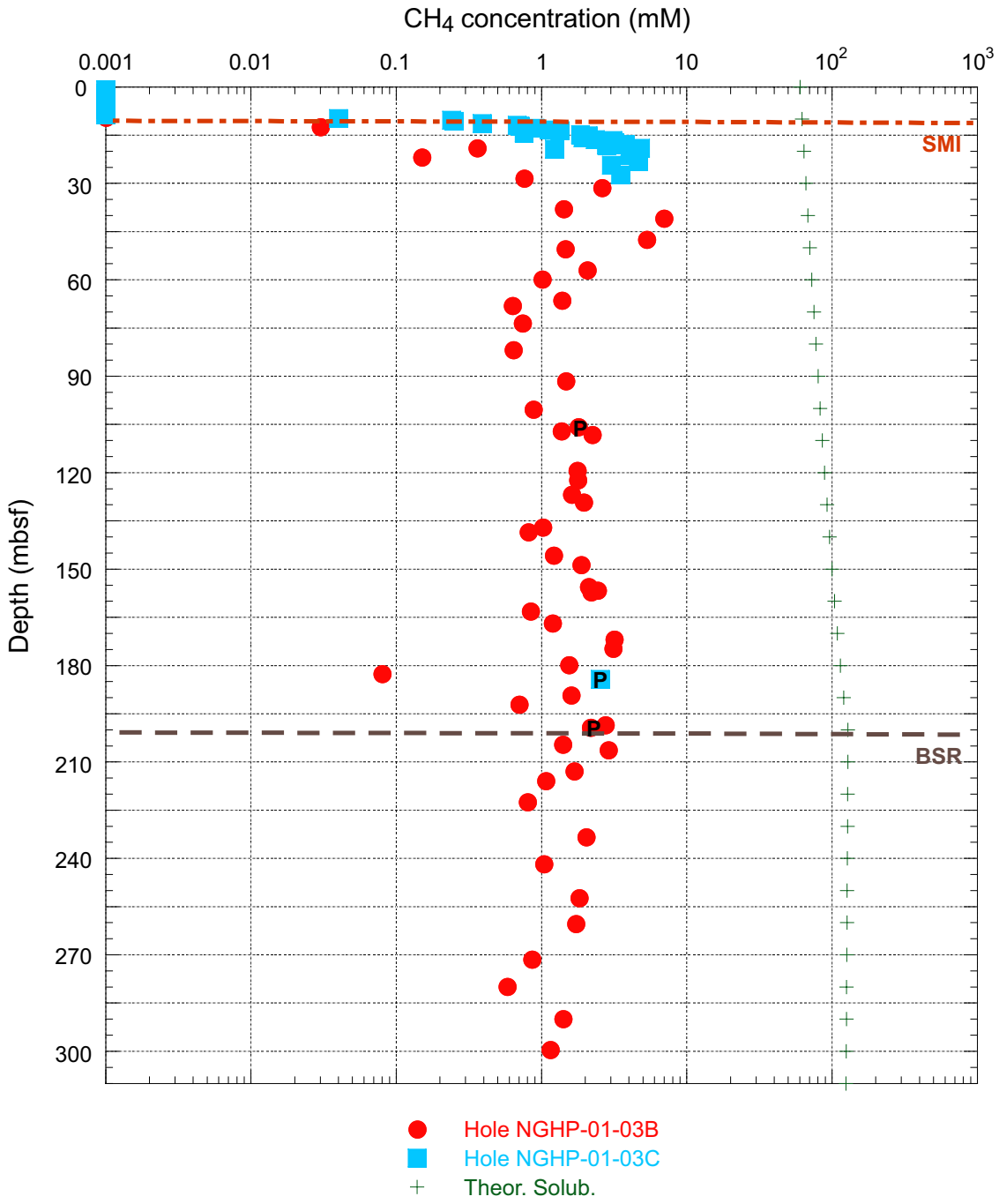

Figure 13. Plot of headspace methane gas concentration (mM) with depth for Site NGHP-01-03, Holes B and C. Note the methane gradient at ~10 mbsf denoting the SMI. Values less than 0.003 mM are below instrument detection limits, but plotted for reference. Text inside a symbol denotes special coring tool (E, HRC; P, PCS; Y, FPC). Theoretical solubility of methane calculated using the Duan and others (1992) and Xu (2002, 2004) methodologies. Hole NGHP-01-03C was not sampled continuously, thus resulting in the random data collection intervals at depth.

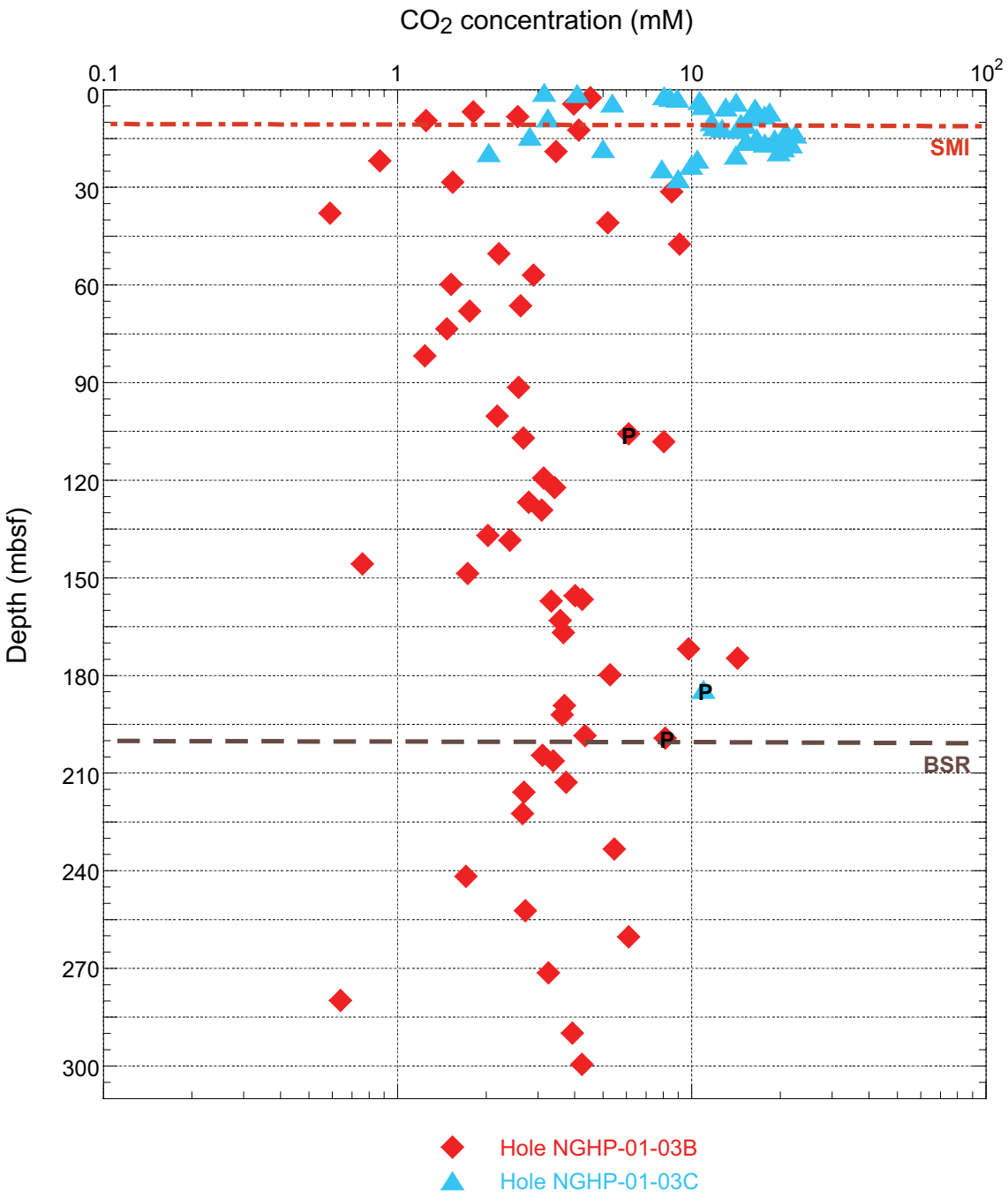

Figure 14. Plot of headspace carbon dioxide gas concentration (mM) with depth for Site NGHP-01-03, Holes B and C. Text inside a symbol denotes special coring tool (E, HRC; P, PCS; Y, FPC). Hole NGHP-01-03C was not sampled continuously, thus resulting in the random data collection intervals at depth, and as such could not confirm the elevated concentration at depth.

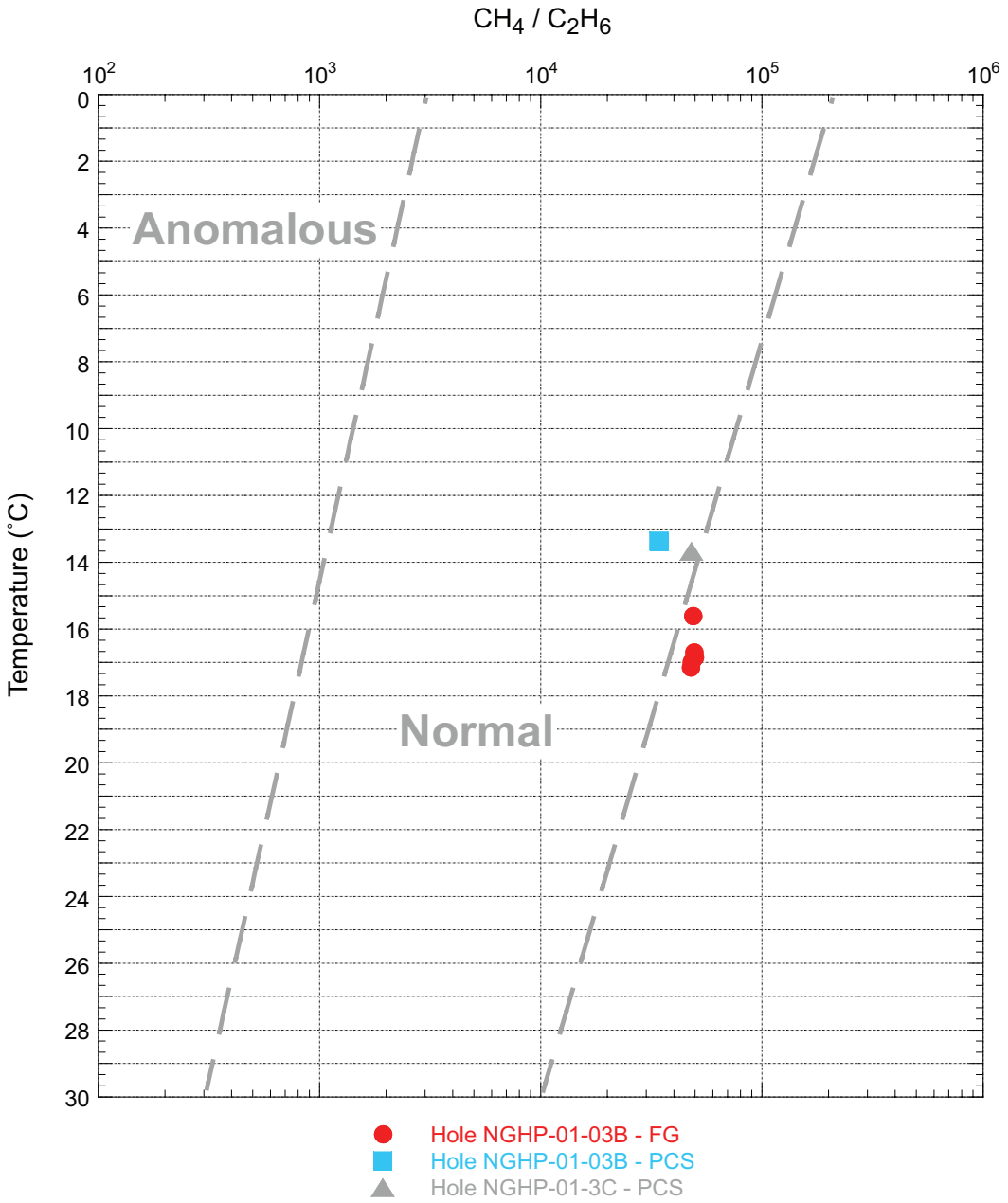

Figure 15. Plot of methane to carbon dioxide gas ratio with depth for headspace, free/void gas, and PCS gas for Site NGHP-01-03, Holes B and C. Note the spikes in methane concentration, perhaps indicating the presence of free gas or gas hydrate. Hole NGHP-01-03C was not sampled continuously and free gas samples are rarely obtained after XCB coring begins (~80 mbsf at this site), thus resulting in the random data collection intervals at depth. [PCS, pressure core sampler]

Table 8. Void gas (FG) composition for Site NGHP-01-03.

Sample	Site	Hole	Core	Section	Interval (cm)	Sample depth (mbsf)	CO_2	C_1	C_2	C_3	O_2	N_2+Ar	H_2S	C_1/CO_2	$C1/C_2$
							(ppmv) normalized to nitrogen+argon								
3B-7H1-147	3	B	7	1	147	54.37	17,200	484,600	nd	nd	110,400	387,700	nd	30	-
3B-20X1-101	3	B	20	1	101	162.31	12,400	952,100	nd	nd	10,500	25,000	nd	80	-
3B-25X	3	B	25	0	nr	nr	17,300	936,200	nd	nd	13,000	33,500	nd	50	-
3B-30X3-1	3	B	30	3	1	213.61	14,400	941,600	nd	nd	12,900	31,100	nd	70	-
3B-32X3-69	3	B	32	3	69	233.39	7,600	976,600	20	nd	4,700	11,100	nd	130	48,800
3B-32X5-18	3	B	32	5	18	235.88	7,600	938,500	nd	nd	14,800	39,100	nd	120	-
3B-33X3-56	3	B	33	3	56	241.64	7,700	944,500	nd	nd	13,000	34,800	nd	120	-
3B-34X5-20	3	B	34	5	20	254.8	5,300	985,400	nd	nd	2,600	6,600	nd	190	-
3B-35X5-23	3	B	35	5	23	262.88	3,500	991,300	nd	nd	1,300	3,800	nd	280	-
3B-35X6-97	3	B	35	6	97	265.12	3,700	992,300	20	nd	1,100	3,000	nd	270	49,600
3B-35X4-1	3	B	35	4	1	261.15	6,400	987,300	20	nd	2,000	4,300	nd	150	49,400
3B-36X1-83	3	B	36	1	83	265.12	5,400	988,100	nd	nd	1,700	4,700	nd	180	-
3B-36X2-124	3	B	36	2	124	268.53	8,000	960,700	20	nd	9,600	21,700	nd	120	48,000
3B-36X4-55	3	B	36	4	55	270.44	7,200	970,100	nd	nd	7,100	15,600	nd	130	-
3B-37X2-0	3	B	37	2	0	272.75	16,500	951,500	20	nd	9,600	22,300	nd	60	47,600
3B-37X5-12	3	B	37	5	12	282.35	6,300	960,700	nd	nd	9,700	23,400	nd	150	-

Notes: nd = not detected. nr = not recorded. Approximate detection limits are about 15 ppmv for methane, 30 ppmv for ethane, 50 ppmv for propane, and 20 ppmv for hydrogen sulfide.

Gas was collected from three pressure-core sampler (PCS) cores: two in Hole NGHP-01-03B and one in Hole NGHP-01-03C. The PCS gas concentration results are very similar to the void gas results (tables 8 and 9); however, CO_2 concentrations were 10 or greater fold lower, as exhibited by C_1/CO_2 ratio (fig. 15). The decrease in CO_2 concentration is likely due to the sampling method whereby the exsolved gas is bubbled through a large volume of seawater resulting in the stripping out of soluble gases like CO_2 relative to insoluble gas like methane. PCS core gases did indicate the presence of low level C_2 concentrations, ranging from non-detectable to ~20 ppmv. Ratio values for C_1 to C_2 gases ranged from ~20,000 to ~48,000 and showed no apparent trend with depth (fig. 16). The ratios are focused in the center of the "normal" occurrence interval as depicted in the graph. These high methane concentrations versus low concentrations of ethane are strong evidence of a microbially-dominated hydrocarbon gas source.

Microbiology

Hole NGHP-01-03B

Analysis of all microbiological samples will be shore-based. Thirty-four samples were collected for cell enumeration (CEL), 30 for hydrogenase activity analysis (SPH), one 30 cm section identified as anomalous on the IR scan of the core (MAF, MAG, MAR) for detailed microbiological studies and one 30 cm background section (MBF, MBG, MBR) (table 10). The 30 cm sections were split into three subsections as described in the "Methods" chapter. Additional microbiological samples were taken (Lab code JUD, 47 samples; Lab code JAN, 31 samples).

Hole NGHP-01-03C

Ten samples with Lab code JAN were collected (table 10).

Physical Properties

Infrared (IR) imaging of whole-round cores at Site NGHP-01-03 was performed on the catwalk to determine the location of temperature anomalies on the surface of core liners and enable sections containing potential gas hydrate to be quickly removed, preserved, and studied. After IR imaging was finished, nondestructive measurements were conducted on temperature-equilibrated whole-round core sections with the MSCL. Thermal conductivity measurements were also conducted on whole-round cores. Various tests were performed on split cores including: electrical resistivity by use of a Wenner array, *P*-wave velocity by inserted spades, and shear strength by mini-vane, Torvane, and Pocket Penetrometer. Core subsamples were placed in 10-mL beakers and dried at 105 °C to determine water content. Subsequently, the dried samples were analyzed for grain density using gas pycnometers and other sediment relations were then calculated. See the "Physical properties" section of the "Methods" chapter for more details.

The physical properties program at Site NGHP-01-03 was focused primarily on Hole NGHP-01-03B drilled in the Krishna-Godavari Basin in about 1,076 m of water and continuously cored to about 300 mbsf. However, perhaps because of gas-hydrate dissociation, overall core recovery was 85 percent, and was less than 50 percent in Cores NGHP-01-03B-09X to NGHP-01-03B-14X (about 72 to 115 mbsf). No physical gas-hydrate samples were recovered at Site NGHP-01-03.

Table 9. Pressure-Core Sampler (PCS) gas composition for Site NGHP-01-03.

Sample	Site	Hole	Core	Section	Sample depth (mbsf)	Time	Gas vol. (ml)	CO_2	C_1	C_2	C_3	O_2	N_2+Ar	H_2S	C_1/CO_2	C_1/C_2
								(ppmv) normalized to nitrogen+argon								
3B-13P-t1	3	B	13	P	105	1	-	1,000	788,900	nd	nd	21,000	189,200	nd	800	-
3B-23Y-t1	3	B	23	Y	176	1	-	500	987,900	20	nd	4,100	7,400	nd	2,000	49,400
3B-23Y-t2	3	B	23	Y	176	2	-	3,700	957,100	20	nd	27,800	11,400	nd	300	47,900
3C-7P-t1	3	C	7	P	184	1	-	300	996,900	20	nd	2,800	nd	nd	3,300	49,800
3C-7P-t2	3	C	7	P	184	2	-	2,300	984,400	nd	nd	2,800	10,400	nd	400	-

Notes: nd = not detected. Approximate detection limits are about 15 ppmv for methane, 30 ppmv for ethane, 50 ppmv for propane, and 20 ppmv for hydrogen sulfide.

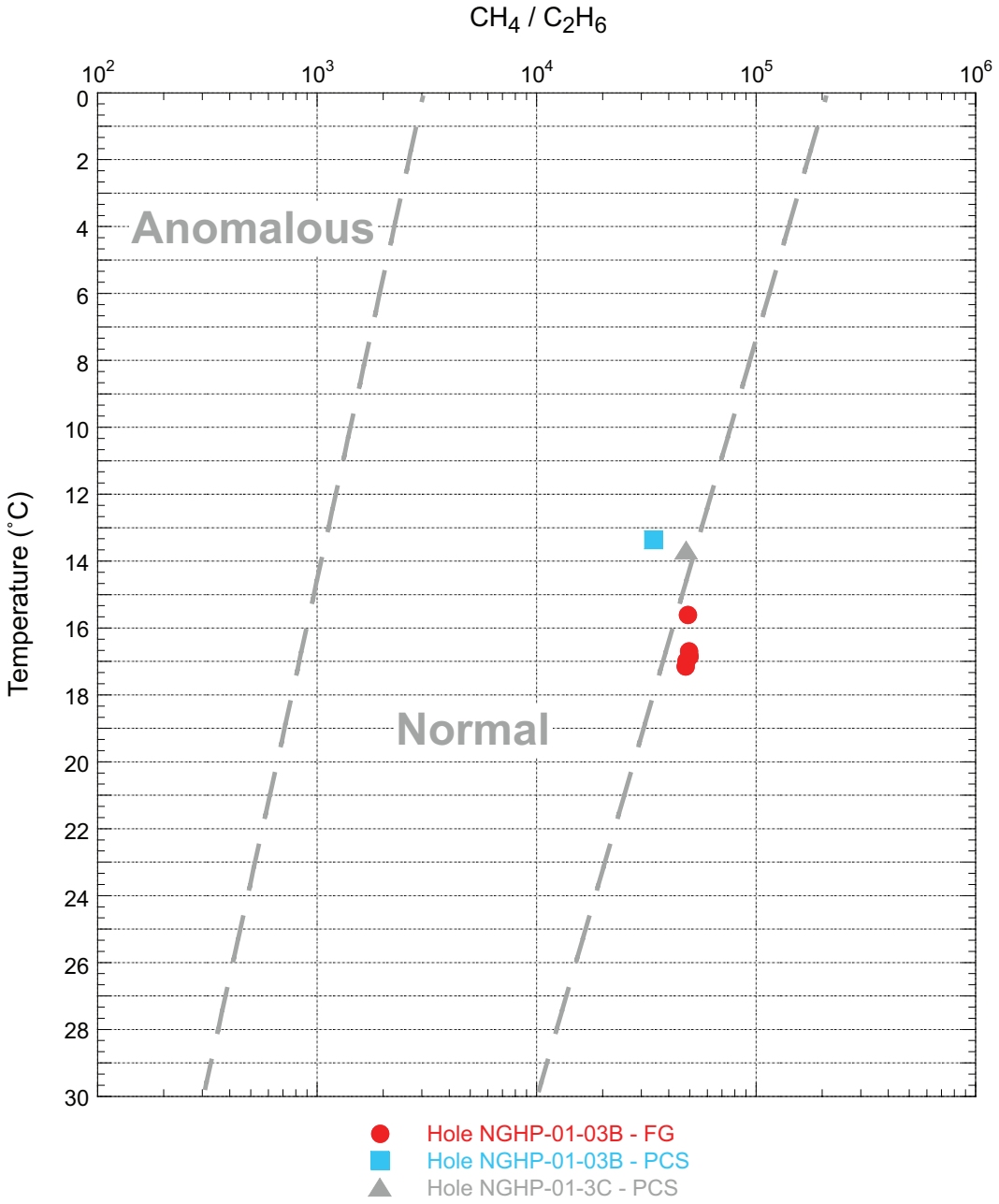

Figure 16. Plot of PCS methane to ethane gas ratio with depth for Site NGHP-01-03, Holes B and C. Ethane levels were below detection limits for all headspace samples (table 7). Note that the hydrocarbon gas occurrences fall into the typical range. [PCS, pressure core sampler]

Table 10. List of microbiological samples taken for Site NGHP-01-03.

Core, section, interval (cm)	Sample code	Depth (mbsf)	Volume (cc)	Comment	Core, section, interval (cm)	Sample code	Depth (mbsf)	Volume (cc)	Comment
NGHP-01-03B									
1H-2,95-100	CEL	2.45	5		33X-3,75-80	JAN	241.83	187	
2H-5,105-110	CEL	12.45	5		34X-3,75-80	JAN	252.35	187	
3H-5,95-100	CEL	21.85	5		35X-3,75-80	JAN	260.4	187	
4H-5,95-100	CEL	31.35	5		36X-3,75-80	JAN	271.45	187	
5H-5,95-100	CEL	40.85	5		37X-3,75-80	JAN	279.98	187	
6H-5,95-100	CEL	50.35	5		38X-3,75-80	JAN	289.95	187	
7H-5,95-100	CEL	59.85	5		39X-3,75-80	JAN	299.55	187	
8X-5,35-40	CEL	68.05	5		1H-2,120-130	JUD	2.7	374	
9X-2,30-35	CEL	73.5	5		2H-3,120-130	JUD	9.6	374	
10X-1,46-51	CEL	81.76	5		2H-5,130-140	JUD	12.7	374	
11X-1,65-70	CEL	91.45	5		3H-3,120-130	JUD	19.1	374	
12X-1,60-65	CEL	100.3	5		3H-5,120-130	JUD	22.1	374	
14X-2,75-80	CEL	108.15	5		4H-3,120-130	JUD	28.6	374	
15X-5,75-80	CEL	122.25	5		4H-5,120-130	JUD	31.6	374	
16X-4,25-30	CEL	129.15	5		5H-3,120-130	JUD	38.1	374	
17X-4,70-75	CEL	138.4	5		5H-5,120-130	JUD	41.1	374	
18X-5,70-75	CEL	148.6	5		6H-3,120-130	JUD	47.6	374	
19X-5,20-25	CEL	157.16	5		6H-5,120-130	JUD	50.6	374	
20X-5,70-75	CEL	166.8	5		7H-3,120-130	JUD	57.1	374	
21X-3,70-75	CEL	174.7	5		7H-5,120-130	JUD	60.1	374	
24X-5,55-60	CEL	182.54	5		8X-3,110-120	JUD	66.5	374	
25X-5,70-75	CEL	192.08	5		8X-5,60-70	JUD	68.3	374	
26X-2,70-75	CEL	198.5	5		9X-2,60-70	JUD	73.8	374	
29X-3,65-70	CEL	204.55	5		14X-2,100-110	JUD	108.4	374	
30X-2,75-80	CEL	212.85	5		15X-3,100-110	JUD	119.5	374	
31X-2,65-70	CEL	222.45	5		15X-5,100-110	JUD	122.5	374	
32X-3,65-70	CEL	233.35	5		16X-2,100-110	JUD	126.9	374	
33X-3,65-70	CEL	241.73	5		16X-4,50-60	JUD	129.4	374	
34X-3,65-70	CEL	252.25	5		17X-3,95-105	JUD	137.15	374	
35X-3,65-70	CEL	260.3	5		17X-4,95-105	JUD	138.65	374	
36X-3,65-70	CEL	271.35	5		18X-3,95-105	JUD	145.85	374	
37X-3,65-70	CEL	279.88	5		18X-5,95-105	JUD	148.85	374	
38X-3,65-70	CEL	289.85	5		19X-3,95-105	JUD	155.65	374	
39X-3,65-70	CEL	299.45	5		19X-5,45-55	JUD	157.41	374	
1H-2,105-110	JAN	2.55	187		20X-2,45-55	JUD	163.25	374	
2H-5,115-120	JAN	12.55	187	BIO ANOMALY	20X-5,95-105	JUD	167.05	374	
3H-5,105-110	JAN	21.95	187	BIO ANOMALY	21X-1,95-105	JUD	171.95	374	
4H-5,105-110	JAN	31.45	187	BIO ANOMALY	21X-3,95-105	JUD	174.95	374	
5H-5,105-110	JAN	40.95	187		24X-3,95-105	JUD	179.94	374	
6H-5,105-110	JAN	50.45	187	MBIO BACKGROUND	24X-5,80-90	JUD	182.79	374	
7H-5,105-110	JAN	59.95	187	MBIO BACKGROUND	25X-3,95-105	JUD	189.33	374	
8X-5,45-50	JAN	68.15	187	MBIO BACKGROUND	25X-5,95-105	JUD	192.33	374	
9X-2,40-50	JAN	73.6	374		26X-2,95-105	JUD	198.75	374	
13P-1,70-75	JAN	105.6	187		29X-3,90-100	JUD	204.8	374	
14X-2,85-90	JAN	108.25	187		30X-2,90-100	JUD	213	374	
15X-5,85-90	JAN	122.35	187		31X-2,90-100	JUD	222.7	374	
16X-4,35-40	JAN	129.25	187		32X-3,90-100	JUD	233.6	374	
17X-4,80-85	JAN	138.5	187		33X-3,90-100	JUD	241.98	374	
18X-5,80-85	JAN	148.7	187		34X-3,90-100	JUD	252.5	374	
19X-5,30-35	JAN	157.26	187		35X-3,90-100	JUD	260.55	374	
20X-5,80-85	JAN	166.9	187		36X-3,90-100	JUD	271.6	374	
21X-3,80-85	JAN	174.8	187		37X-3,90-100	JUD	280.13	374	
24X-5,65-70	JAN	182.64	187		38X-3,90-100	JUD	290.1	374	
25X-5,80-85	JAN	192.18	187		39X-3,90-100	JUD	299.7	374	
26X-2,80-85	JAN	198.6	187		20X-3,40-50	MAF	164.2	374	
29X-3,75-80	JAN	204.65	187		20X-3,50-60	MAG	164.3	374	
31X-2,75-80	JAN	222.55	187		20X-3,30-40	MAR	164.1	374	
32X-3,75-80	JAN	233.45	187		20X-1,130-140	MBF	162.6	187	

Table 10. List of microbiological samples taken for Site NGHP-01-03.—Continued

Core, section, interval (cm)	Sample code	Depth (mbsf)	Volume (cc)	Comment
NGHP-01-03B—Continued				
20X-1,140-150	MBG	162.7	187	
20X-1,120-130	MBR	162.5	187	
1H-2,100-105	SPH	2.5	187	
2H-5,110-115	SPH	12.5	187	
3H-5,100-105	SPH	21.9	187	
4H-5,100-105	SPH	31.4	187	
5H-5,100-105	SPH	40.9	187	
6H-5,100-105	SPH	50.4	187	
7H-5,100-105	SPH	59.9	187	
8X-5,40-45	SPH	68.1	187	
9X-2,35-40	SPH	73.55	187	
14X-2,80-85	SPH	108.2	187	
15X-5,80-85	SPH	122.3	187	
16X-4,30-35	SPH	129.2	187	
17X-4,75-80	SPH	138.45	187	
18X-5,75-80	SPH	148.65	187	
19X-5,25-30	SPH	157.21	187	
20X-5,75-80	SPH	166.85	187	
21X-3,75-80	SPH	174.75	187	
24X-5,60-65	SPH	182.59	187	
25X-5,75-80	SPH	192.13	187	
26X-2,75-80	SPH	198.55	187	
29X-3,70-75	SPH	204.6	187	
31X-2,70-75	SPH	222.5	187	
32X-3,70-75	SPH	233.4	187	
33X-3,70-75	SPH	241.78	187	
34X-3,70-75	SPH	252.3	187	
35X-3,70-75	SPH	260.35	187	
36X-3,70-75	SPH	271.4	187	
37X-3,70-75	SPH	279.93	187	
38X-3,70-75	SPH	289.9	187	
39X-3,70-75	SPH	299.5	187	
NGHP-01-03C				
1H-2,100-110	JAN	2.5	374	
1H-4,100-110	JAN	5.5	374	
1H-6,100-110	JAN	8.5	374	
2H-2,100-110	JAN	12	374	
2H-4,100-110	JAN	15	374	
2H-6,100-110	JAN	18	374	
3H-2,100-110	JAN	21.5	374	
3H-4,100-110	JAN	24.5	374	
3H-6,100-110	JAN	27.5	374	
7P-1,52-57	JAN	184.52	150	

Infrared (IR) Imaging

Environmental Conditions

Catwalk environment was monitored during the entire drilling operation at Site NGHP-01-03. Temperature on the catwalk remained relatively constant averaging about 30 °C, and ranging from 28.2 to 31.0 °C during the drilling operation, as shown in figure 17. Relative humidity averaged 79 percent and ranged from 67 to 92 percent (fig. 17), consistent with a marine environment setting in the Indian Ocean. No adverse environmental conditions such as thunderstorms, rough seas, lightening, or high winds, persisted during drilling operations at this site. Also presented in figure 17 are the relative times at which each core was transferred onto the catwalk from the drill floor. The last core (NGHP-01-03B-39X) arrived on the catwalk over 51.4 hours after the first core (NGHP-01-03B-01H).

IR Images

All APC and XCB cores from Site NGHP-01-03 were systematically scanned upon arrival on the catwalk using the track-mounted IR camera described in the "Physical Properties" section of the "Methods" chapter. IR anomalies, commonly referred to as "cold spots," indicate gas-hydrate dissociation during core recovery, which subsequently provides guidance to catwalk sampling. Summary digital maps of the scans of all cores are available in the supplemental data files section of this report (see tables 11, 12, and 13 for listings of the scans). Temperature arrays in text-formatted files (comma-separated value or CSV) were exported from the IR camera software and then concatenated for each core. The arrays were then further concatenated for all cores available in a given borehole and down core temperatures were averaged for each pixel row in the array, excluding pixels ~1 cm from the edge of the image and 2 cm along the midline of the image. Exclusion of these pixels minimized the effects caused by major thermal artifacts in the images. This processing enabled us to measure the average amplitude of the cold anomalies and separate warm anomalies due to voids from the background temperature field.

Infrared track imaging at Hole NGHP-01-03B consisted of 34 scans for a total scanned core length of 255 m. The complete set of IR images collected for borehole NGHP-01-03B is presented in figure 18 along with the corresponding down core temperatures. The median core temperature extracted from the IR images for Hole NGHP-01-03B ranged from a high of 25.8 °C (Core NGHP-01-03B-26X, 196.24 mbsf), to a low of 21.5 °C (Core NGHP-01-03B-02H). The lowest temperature (19.7 °C) measured by the IR imaging track on the 34 cores was also in Core NGHP-01-03B-02H. As shown in figure 18, the measured down core temperature log generated from the IR imaging shows that sediment is initially cooler in the first two cores, but becomes relatively uniform down to the bottom of the hole at 300 mbsf. No significant IR anomalies were reported at this site. The three IR scans taken at Hole NGHP-01-03C, for a total imaged length of 28.6 m (fig. 19) were similar to the temperature in the top of Hole NGHP-01-03B.

IR images of the cut ends of core sections were acquired with a hand-held IR camera on the catwalk during sampling activities when possible. Twenty-five core-end IR images were collected from Hole NGHP-01-03B. Figure 20 shows a typical section-end IR image from Section NGHP-01-03B-34X-4 (top).

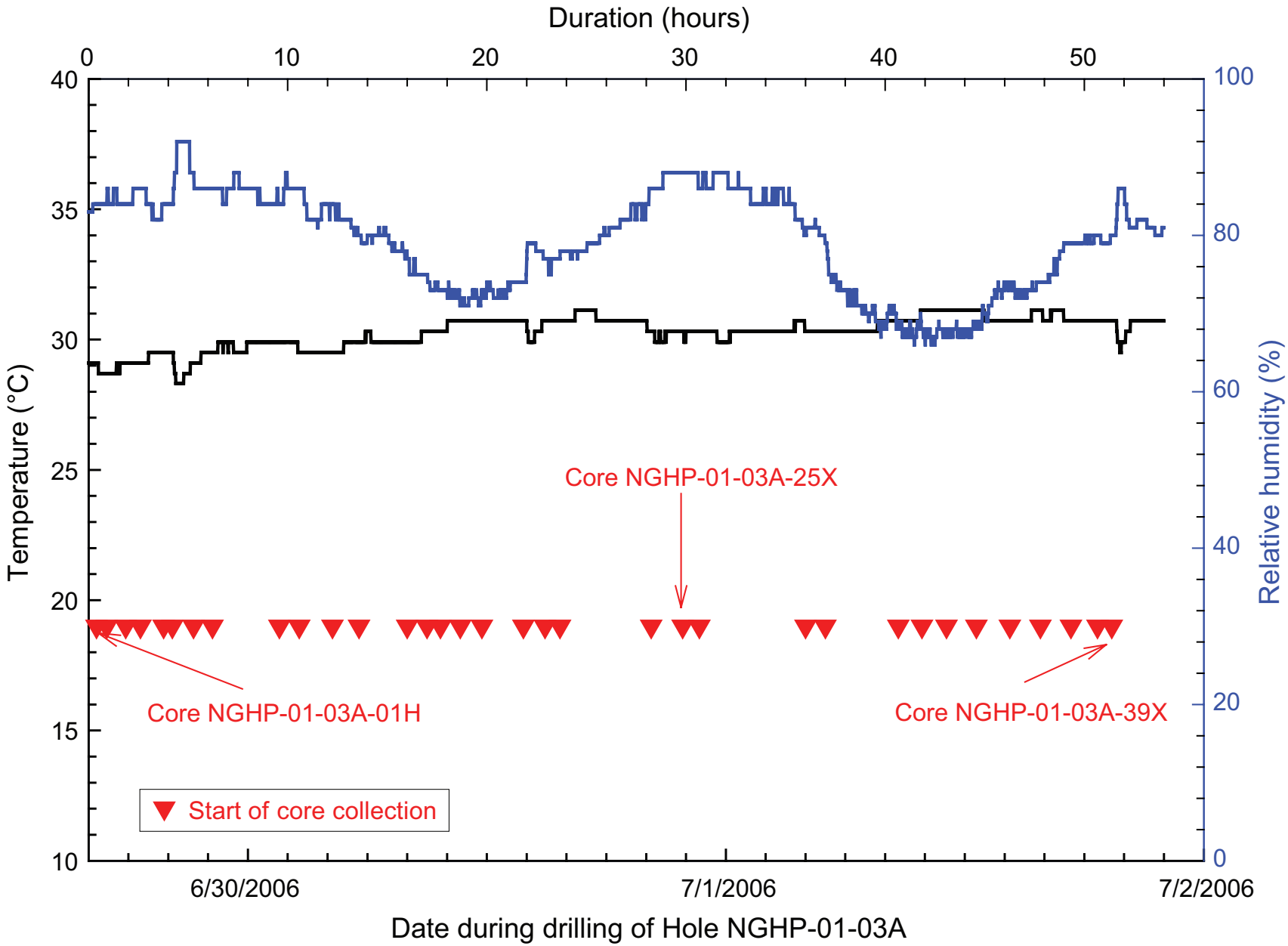

Figure 17. Catwalk temperature and humidity during drilling operations at Site NGHP-01-03.

Table 11. List of infrared image files collected on the catwalk from Hole NGHP-01-03B.

Core	Imaging length (cm)	First run	Date	Start time	Temperature (start/end) (˚C)	File ID	Screen image saved	Comments*
1H	510	x	6/29	16:24	29.1/29.1	NGHP-03-B-1	Yes	15–25 °C
2H	960	x	6/29	16:55	28.7/28.7	NGHP-03-B-2	Yes	15–30 °C
3H	960	x	6/29	17:52	29.9/29.9	NGHP-03-B-3	Yes	15–30 °C
4H	930	x	6/29	18:36	29.1/29.1	NGHP-03-B-4	Yes	15–30 °C
5H	970	x	6/29	19:46	29.1/29.1	NGHP-03-B-5	Yes	15–30 °C
6H	890	x	6/29	20:12	29.1/29.1	NGHP-03-B-6	Yes	15–30 °C
7H	860	x	6/29	21:16	29.1/29.1	NGHP-03-B-7	Yes	15–30 °C
8H	700	x	6/29	22:13	29.5/29.5	NGHP-03-B-8	Yes	15–30 °C
9X	340	x	6/30	1:35	29.5/29.5	NGHP-03-B-9	Yes	15–30 °C
10X	80	x	6/30	2:35	29.5/29.5	NGHP-03-B-10	Yes	15–30 °C
11X	190	x	6/30	4:15	29.1/29.1	NGHP-03-B-11	Yes	15–30 °C
12X	150	x	6/30	5:35	29.9/29.9	NGHP-03-B-12	Yes	15–30 °C
14X	400	x	6/30	8:00	29.9/29.9	NGHP-03-B-14	Yes	15–30 °C
15X	840	x	6/30	9:00	29.9/29.9	NGHP-03-B-15	Yes	15–30 °C
16X	610	x	6/30	9:40	30.3/30.3	NGHP-03-B-16	Yes	15–30 °C
17X	860	x	6/30	10:40	30.3/30.3	NGHP-03-B-17	Yes	15–30 °C
18X	950	x	6/30	11:45	30.7/30.7	NGHP-03-B-18	Yes	15–30 °C
19X	815	x	6/30	13:50	30.3/30.3	NGHP-03-B-19	Yes	15–30 °C
20X	860	x	6/30	14:55	30.7/30.7	NGHP-03-B-20	Yes	15–30 °C
21X	510	x	6/30	15:40	30.7/30.7	NGHP-03-B-21	Yes	15–30 °C
24X	825	x	6/30	20:15	30.3/30.3	NGHP-03-B-24	Yes	15–30 °C
25X	880	x	6/30	21:50	29.9/29.9	NGHP-03-B-25	Yes	15–30 °C
26X	530	x	6/30	22:40	29.9/29.9	NGHP-03-B-26	Yes	15–30 °C
29X	890	x	6/30	4:00	30.3/30.3	NGHP-03-B-29	Yes	15–30 °C
30X	840	x	7/1	5:00	30.3/30.3	NGHP-03-B-30	Yes	15–30 °C
31X	940	x	7/1	8:40	30.3/30.3	NGHP-03-B-31	Yes	15–30 °C
32X	950	x	7/1	9:57	30.7/30.7	NGHP-03-B-32	Yes	15–30 °C
33X	740	x	7/1	11:05	31.1/31.1	NGHP-03-B-33	Yes	15–30 °C
34X	940	x	7/1	12:35	31.1/31.1	NGHP-03-B-34	Yes	15–30 °C
35X	970	x	7/1	14:16	30.3/30.3	NGHP-03-B-35	Yes	15–30 °C
36X	950	x	7/1	15:48	30.7/30.7	NGHP-03-B-36	Yes	15–30 °C
37X	960	x	7/1	17:20	30.3/30.3	NGHP-03-B-37	Yes	15–30 °C
38X	960	x	7/1	18:40	30.3/30.3	NGHP-03-B-38	Yes	15–30 °C
39X	720	x	7/1	19:23	30.3/30.3	NGHP-03-B-39	Yes	15–30 °C

*Temperature range for images displayed during core collection.

The image has been processed and the calculated temperature profile with a scale ranging from 30–10 °C has been superimposed onto the IR image. The outside of the core end has a temperature of 26 °C and is evenly represented by the color red. The coldest portion of the core-end image is represented by the dark blue to black colors and can be seen as the dominant colors in the image. Notice that the inside temperature is about 20 °C for most of the interior section. This IR section-end image is representative of the images typically collected from this site and shows no evidence of thermal anomalies or interior core temperatures indicative of gas hydrate.

Core-End Temperature Readings

Core-end temperature readings were taken on all cores immediately following the IR track imaging. Typically four temperature probes were inserted approximately 8 cm into the end of each core and allowed to remain there until the core was completely processed and removed from the catwalk. A summary of the core-end temperature results (center position only) for Hole NGHP-01-03B is presented in figure 21. The coldest section of Hole NGHP-01-03B is positioned at the top, in Cores NGHP-01-03B-01H and NGHP-01-03B-02H, with temperatures measuring between 12 °C and 14 °C. The core-end temperatures gradually increase a few degrees with depth. No temperatures below 12 °C were measured on cores collected from Hole NGHP-01-03B.

Index Properties

Based on composite profiles of MAD, MSCL, and other test programs (figs. 22 and 23), three physical-property-behavior units are present at Site NGHP-01-03 (table 14). The upper section, 0–30 mbsf, is influenced by its proximity to the seafloor and is similar to other sites in that water content and porosity decrease while bulk density, grain density, and shear strength increase typically at higher rates than lower in the core. A middle unit, 30–205 mbsf, has uniform properties, whereas the lower unit has changing properties (table 14).

Water content (related to solids) varies from a high of 133 percent to a low of 36 percent (table 15) and rapidly decreases to a subbottom depth of 30 mbsf. Porosity varies from 77 percent to 49 percent downhole and decreases nearly linearly in the middle physical properties unit. This overall

Table 12. List of infrared section-end image files collected from Hole NGHP-01-03B.

Core	Section	Top	Bottom	Date	Time	Image #	Comments
1	4	x		6/29	16:36	G0629-01	IMG file
1	4	x		6/29	16:36	G0629-02	Core end, BMP
2	3	x		6/29	17:09	G0629-03	IMG file
2	3	x		6/29	17:09	G0629-04	Core end, BMP
3	4	x		6/29	18:23	G0629-05	IMG file
3	4	x		6/29	18:23	G0629-06	Core end, BMP
4	3	x		6/29	18:50	G0629-07	IMG file
4	3	x		6/29	18:50	G0629-08	Core end, BMP
5	4	x		6/29	20:00	G0629-09	IMG file
5	4	x		6/29	20:00	G0629-10	Core end, BMP
6	3	x		6/29	20:33	G0629-11	IMG file
6	3	x		6/29	20:33	G0629-12	IMG file
7	3	x		6/29	21:42	G0629-13	Core end, BMP
7	3	x		6/29	21:42	G0629-14	IMG file
8	?	x		6/29	23:22	G0629-15	Core end, BMP
8	?	x		6/29	23:22	G0629-16	IMG file
8	3	x		6/29	23:33	G0629-17	Core end, BMP
8	3	x		6/29	23:33	G0629-18	IMG file
9	2	x		6/30	1:50	G0630-01	Core end, BMP
9	2	x		6/30	1:50	G0630-02	IMG file
14	3	x		6/30	8:25	G0630-03	Core end, BMP
14	3	x		6/30	8:25	G0630-04	IMG file
14	3	x		6/30	8:25	G0630-05	IMG file
14	3	x		6/30	8:25	G0630-06	Core end, BMP
15	2	x		6/30	9:23	G0630-07	IMG file
15	2	x		6/30	9:23	G0630-08	Core end, BMP
16	3	x		6/30	9:57	G0630-09	IMG file
16	3	x		6/30	9:57	G0630-10	Core end, BMP
17	2	x		6/30	11:03	G0630-11	IMG file
17	2	x		6/30	11:03	G0630-12	Core end, BMP
18	3	x		6/30	12:02	G0630-13	IMG file
18	3	x		6/30	12:02	G0630-14	Core end, BMP
29	3	x		7/1	4:20	G0701-01	IMG file
29	3	x		7/1	4:20	G0701-02	Core end, BMP
30	3	x		7/1	5:15	G0701-03	IMG file
30	3	x		7/1	5:15	G0701-04	Core end, BMP
31	4	x		7/1	8:45	G0701-05	IMG file
31	4	x		7/1	8:45	G0701-06	Core end, BMP
32	4	x		7/1	10:15	G0701-07	IMG file
32	4	x		7/1	10:15	G0701-08	Core end, BMP
34	3	x		7/1	13:04	G0701-09	IMG file
34	3	x		7/1	13:04	G0701-10	Core end, BMP
35	3	x		7/1	14:39	G0701-11	IMG file
35	3	x		7/1	14:39	G0701-12	Core end, BMP
36	2	x		7/1	16:07	G0701-13	IMG file
36	2	x		7/1	16:07	G0701-14	Core end, BMP
37	2	x		7/1	17:47	G0701-15	IMG file
37	2	x		7/1	17:47	G0701-16	Core end, BMP
38	2	x		7/1	20:04	G0701-17	IMG file
38	2	x		7/1	20:04	G0701-18	Core end, BMP
39	2	x		7/1	21:40	G0701-19	IMG file
39	2	x		7/1	21:40	G0701-20	Core end, BMP

Table 13. List of infrared image files collected on the catwalk from Hole NGHP-01-03C.

Core	Imaging length (cm)	First run	Date	Start time	Temperature (start/end) (°C)	File ID	Screen image saved	Comments
1H	920	x	7/2	0:45	29.1/29.1	NGHP-03-C-1	Yes	15–25 °C
2H	970	x	7/2	2:13	28.3/28.3	NGHP-03-C-2	Yes	15–30 °C
3H	970	x	7/3	3:25	28.7/28.7	NGHP-03-C-3	Yes	15–30 °C

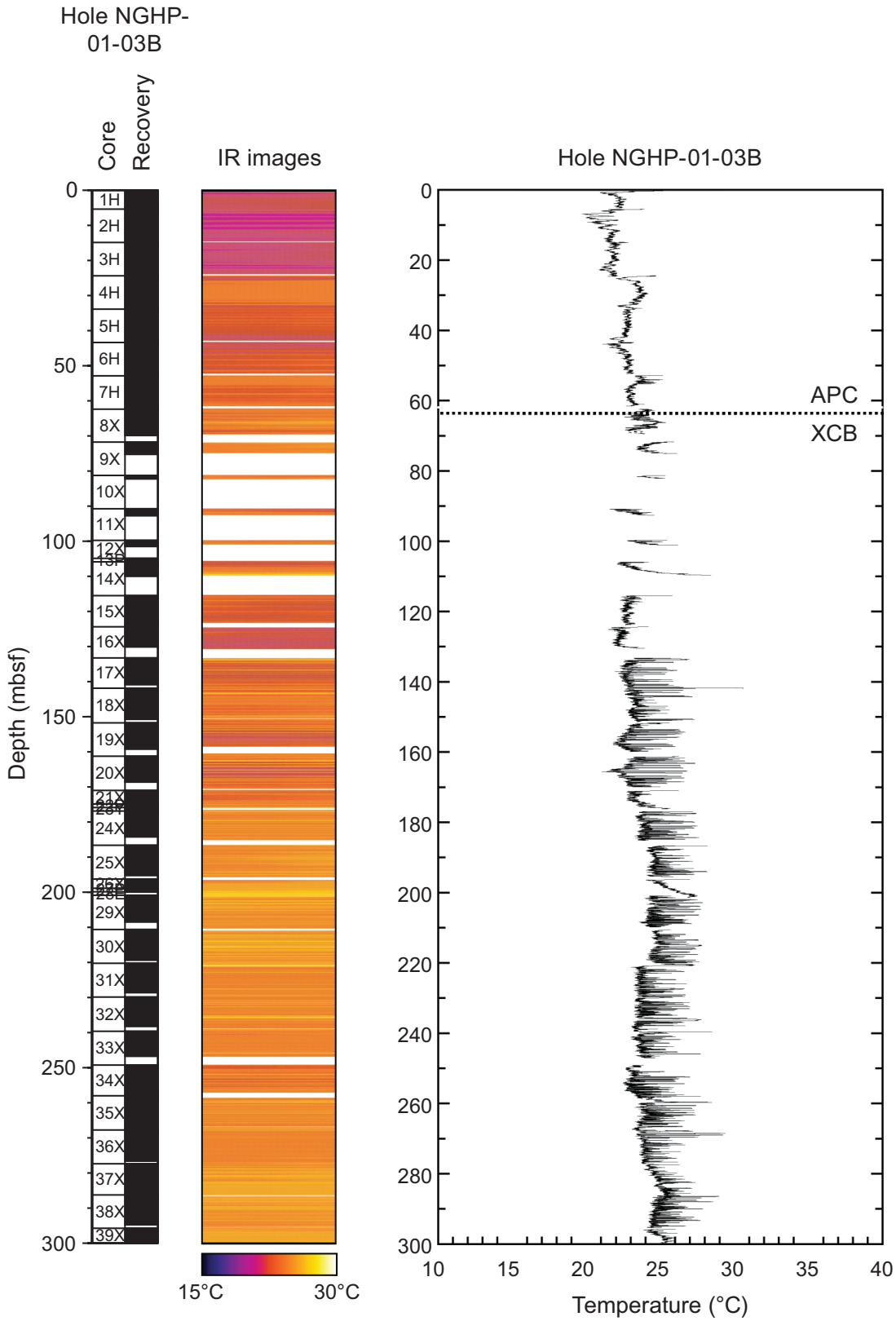

Figure 18. IR imaging and the derived downhole temperature profile for Hole NGHP-01-03B. [IR, infrared]

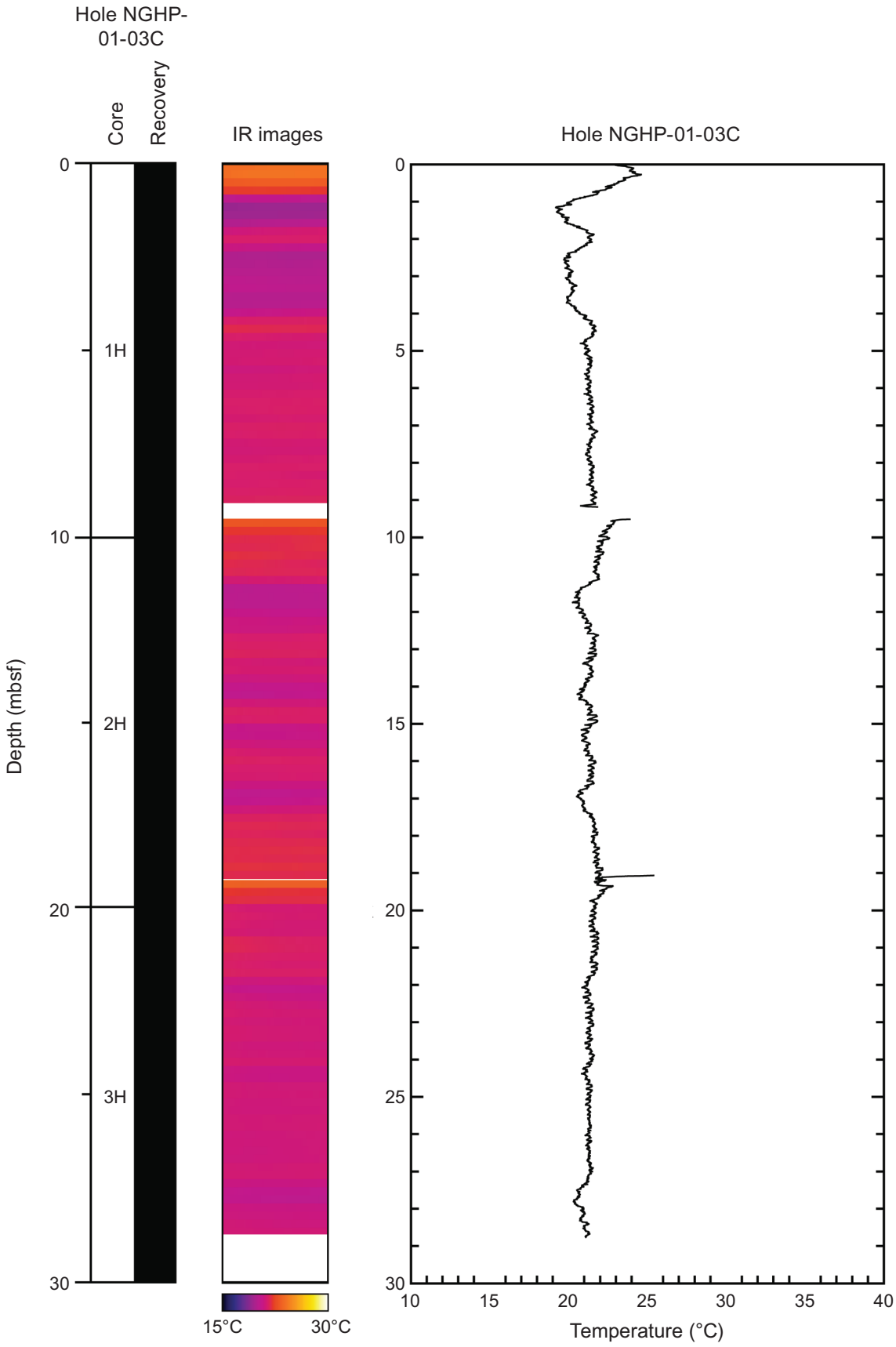

Figure 19. IR imaging and the derived downhole temperature profile for Hole NGHP-01-03C. [IR, infrared]

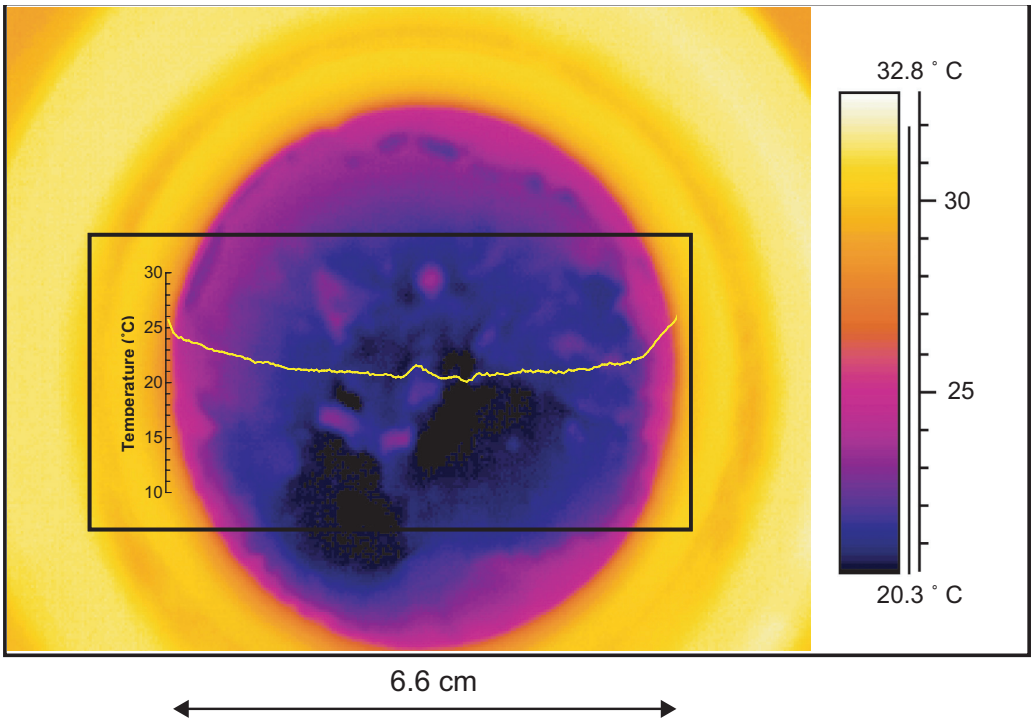

Figure 20. Core end IR image of Section NGPH-01-03B-16X-3, top, with the corresponding reference temperature scale. [IR, infrared]

trend is similar to the LWD data in slope, however an offset of as much as 12 percentage points exists between the MAD derived and LWD porosity. The MAD and LWD porosity values are uniform across the BSR located at about 209 mbsf.

Bulk density from MAD and MSCL measurements in Hole NGHP-01-3B are in close agreement except for an offset in the upper 30 m of core. The LWD values agree except for an offset below the BSR (fig. 22). Grain density varies from 2.53 to 2.80 g/cm^3 with an average value of 2.69 g/cm^3. Some of this variation is a result of performing mass measurements at sea on small sediment samples after the water has been removed by drying. This result is most pronounced in the upper sections of the hole where water contents are highest. Grain densities are lower in the upper part of the hole, possibly the result of increased marine organic content (see "Lithostratigraphy"). The pycnometers often had difficulty measuring volume of samples from the top of the hole. Higher grain densities may be related to the presence of carbonate which has a slightly higher grain density (2.73 g/cm^3) than the average.

Strength

Shear strength increased with depth to the APC – XCB boundary when using all three different methods (tables 16, 17, and 18; fig. 22). Below that depth, more variation exists, illustrating the effect of disturbance caused by rotary coring on sediment. Although testing was to be restricted to intact biscuits, it was occasionally difficult to differentiate between biscuits and adjacent disturbed sediment.

The measured shear strengths were normalized to the effective vertical stress, σ'_v (fig. 24), to provide qualitative information on the stress history of the sediment. The strength/effective vertical stress ranges from approximately 0.5 at the top of the hole (with one outlier at 1.26) to 0.05 near the bottom of the hole. These values are in overall agreement with a number of other normally consolidated clays (Holtz and Kovacs, 1981), although the values below 0.1 are probably an artifact of the more deeply recovered sediment from this hole compared to most engineering-type projects from which the published comparison samples were taken. Hunt (1984) states that the strength/effective vertical stress ratio typically is between 0.4 and 0.16. The wide scatter in the results at the top of the hole reflects the dependency of this ratio on the stress path as well as the test method (Bjerrum, 1972; Ladd and others, 1977). Because almost all of the values are below 0.4, the implication is that these sediments are currently in a depositional environment and have not been overconsolidated by erosional or other geologic processes.

Although the peak (Sv) and remolded (Srem) vane shear strengths increase with depth, the sensitivity (St), which equals Sv/Srem, remained essentially constant with depth (fig. 25). Sensitivity values represent the amount of strength loss after remolding and in extreme examples can reach values of 500 (Lambe and Whitman, 1969). Sensitivity values (approximately 3) downhole classify this sediment as low sensitivity (Holtz and Kovacs, 1981). High values of sensitivity are indicative of good quality core recovery because the sediment has not been highly disturbed.

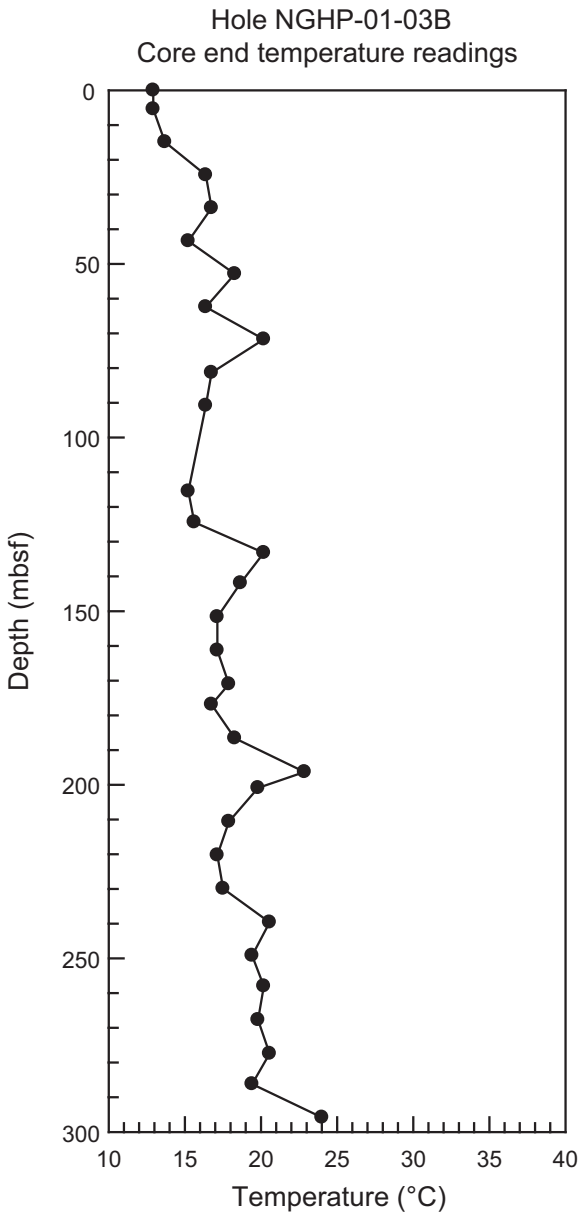

Figure 21. Core end temperature measurements for Hole NGHP-01-03B.

Electrical Resistivity

Logging-While-Drilling (LWD) conducted previously in Hole NGHP-01-03A indicates that resistivity values are fairly low and uniform downhole in overall agreement with the MSCL data. Unlike other holes, for example, Hole NGHP-01-10B, the Resistivity-At-Bit (RAB) image does not indicate that zones of high resistivity (and gas hydrate) are present in Hole NGHP-01-03A. The resistivities determined using the Wenner array on split cores are also uniform (table 19); however, they are offset below both the MSCL and LWD values (fig. 23). This may in part be due to Wenner measurements being conducted on intact core material, rather than a wider portion of core that may contain voids or small expansion cracks. Lower MSCL values are more representative of undisturbed sediment as they are less impacted by the presence of micro voids caused by gas expansion.

The apparent formation factor is the ratio of the resistivity of a saturated sediment to the resistivity of the pore fluid and provides an indication of the relationships between sediment structure, void space, tortuosity, and other factors, and the ability of fluid to flow through the formation. Because pore water salinity typically varies a small amount from that of seawater in the recovered sediment (see "Inorganic Geochemistry"), we have normalized the measured Wenner resistivity values to that of seawater (approximately 0.2 ohm-m) (table 19). Values range from about 1.5 at the top of the core to 3.5 at the bottom, with a spike at 142 mbsf (fig. 26). Other equations and methods exist for calculating formation factor; however, they require the use of empirical constants that have not yet been determined for these particular sediments.

P-Wave Velocity

P-wave velocity (V_P) measured with the MSCL increased slightly from 1.48 km/s in the top of the hole (fig. 23) to 1.55 km/s at a subbottom depth of 37 m, which represents the depth where gas and voids present in the sediment prevented further valid measurements from being logged. The contact V_P values of 1.47 to 1.48 km/s (table 20) are in agreement with the MSCL values at the top of the hole. Valid contact V_P measurements could not be determined below 11.5 mbsf which is consistent with a SMI located at about 10 mbsf. Methane, which is typically produced below the SMI, may come out of solution if present in enough quantity and attenuate acoustic signals.

Magnetic Susceptibility

Wide excursions exist in the magnetic susceptibility data indicating that primary and secondary magnetic minerals are present in alternating non-uniform high and low frequency layers (fig. 23; see "Lithostratigraphy"). A low frequency layer at the Unit II to III physical property boundary is present at 205 mbsf which is near the BSR and a lithostratigraphic boundary between nannofossil bearing clay and foraminifera bearing clay (see "Lithostratigraphy").

Thermal Conductivity

Thermal conductivities vary between 0.630 and 1.023 W/(m×K) and increase slightly with subbottom depth (table 21 and fig. 23). Such values are well within the range of marine sediments (for example, Novosel and others, 2007), although they are all lower than values determined by Davis and others (1990) for sediment from Cascadia and the Nankai Trough.

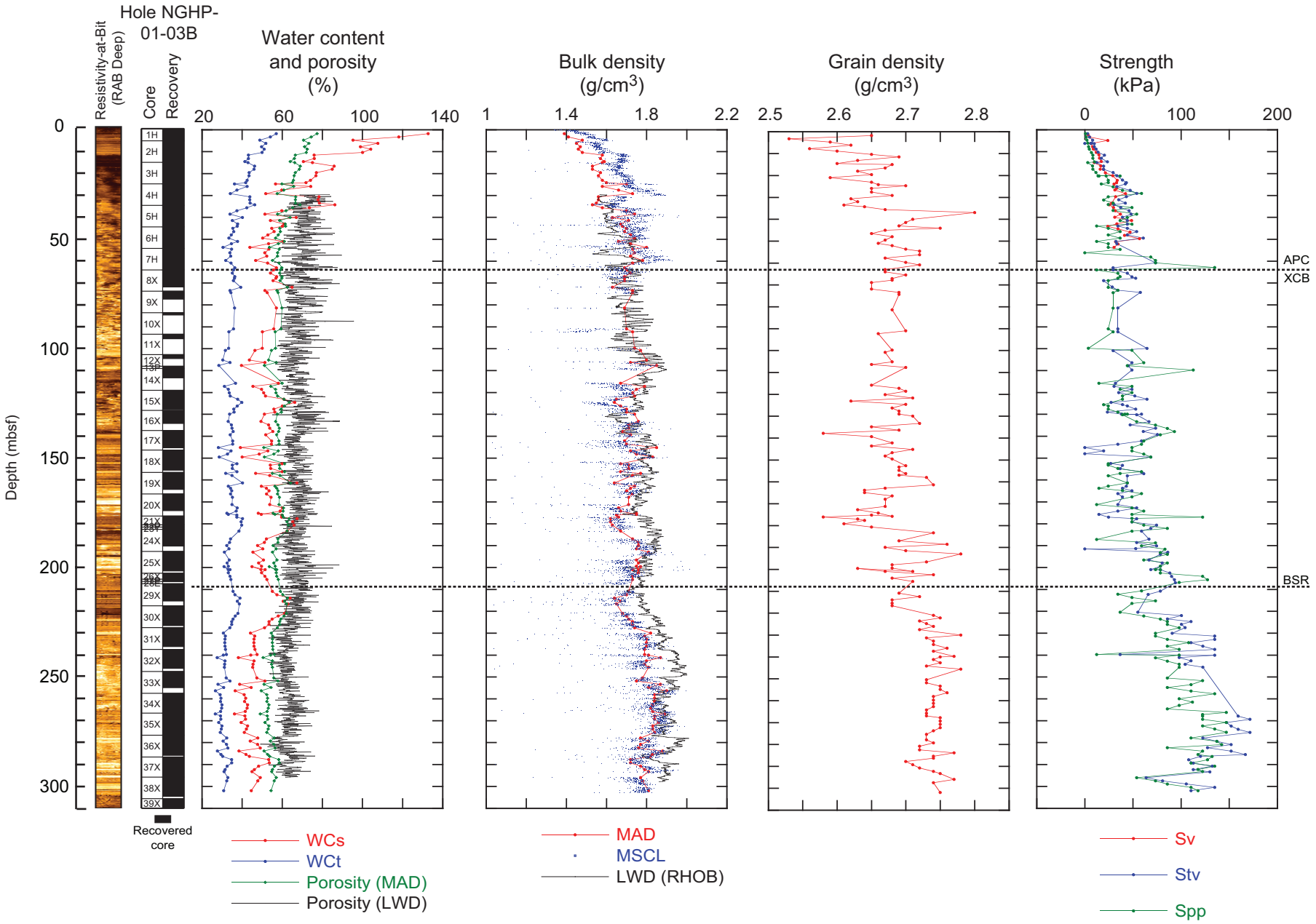

Figure 22. Profiles of LWD Resistivity-At-Bit (RAB), core recovery, index and strength properties for Hole NGHP-01-03B. [LWD, logging-while-drilling]

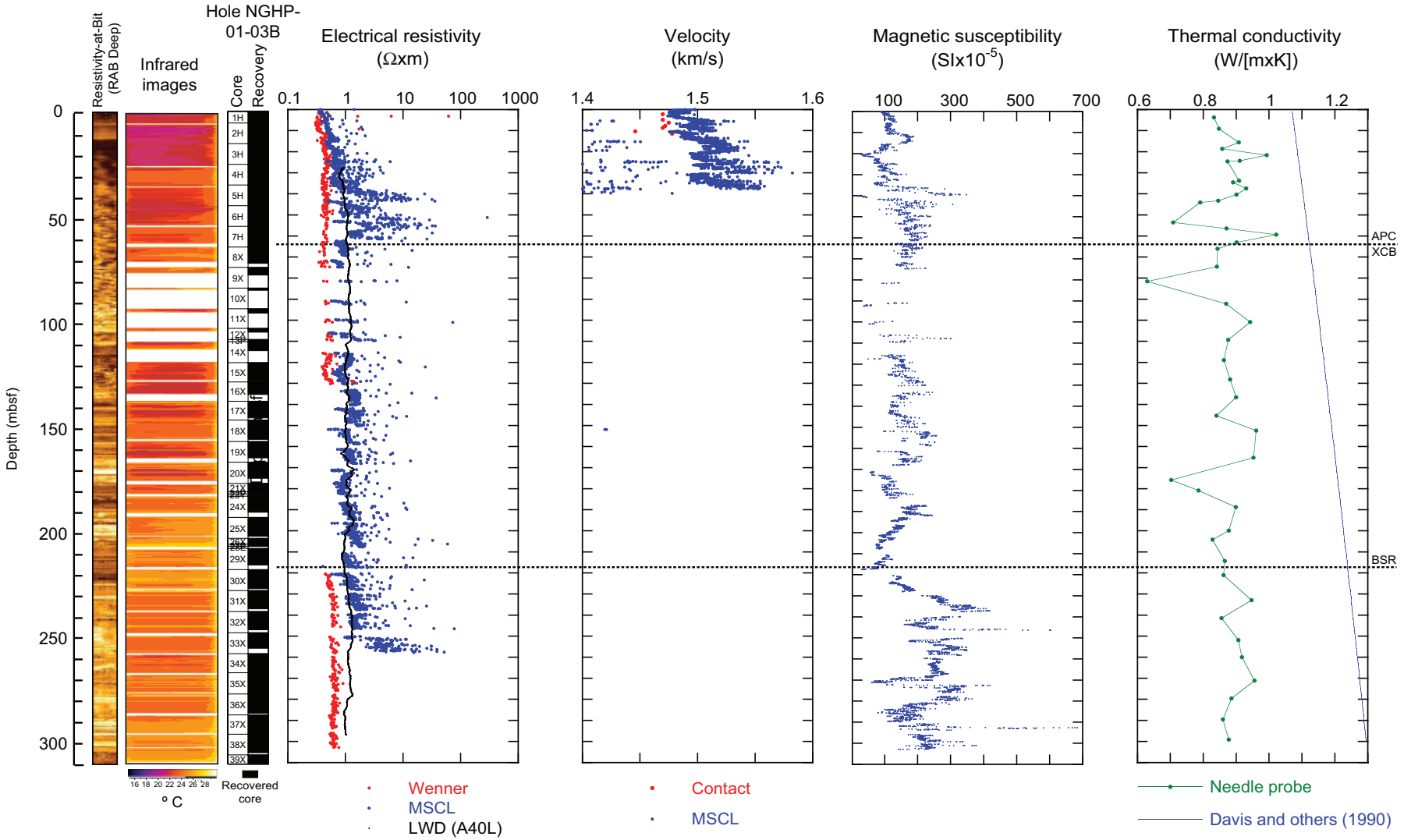

Figure 23. Profiles of LWD Resistivity-At-Bit (RAB), infrared images, core recovery, electrical resistivity, acoustic P-wave velocity, magnetic susceptibility, and thermal conductivity for Hole NGHP-01-03B. [LWD, logging-while-drilling]

Table 14. Physical property behavior units for Hole NGHP-01-03C.

Depth (mbsf)	Water content	Porosity	Bulk density	Grain density	Strength	Magnetic susceptibility
0–30	Decreases	Decreases	Increases	Increases	Increases	Less scatter
30–205	Uniform	Uniform	Uniform	Uniform	Uniform	Uniform
205–300	Bulge	Bulge	Bulge	Increases	Increases	Increases

Table 15. Moisture and density (MAD) physical properties for Hole NGHP-01-03B.

Core, section, interval (cm)	Sample code	Depth (mbsf)	WCt (%)	WCs (%)	Grain density (g/cm³)	Bulk density (g/cm³)	Dry bulk density (g/cm³)	Porosity (%)	Void ratio	Unit weight (kN/m³)
NGHP-01-03B										
1H-2,26-28	MAD	1.76	57.05	132.84	2.65	1.39	0.6	77.44	3.43	13.65
1H-3,26-28	MAD	3.26	54.15	118.12	2.53	1.41	0.65	74.48	2.92	13.83
1H-4,26-28	MAD	4.76	48.8	95.3	2.59	1.48	0.76	70.64	2.41	14.55
2H-1,77-79	MAD	6.17	51.85	107.68	2.62	1.45	0.7	73.34	2.75	14.22
2H-2,91-93	MAD	7.81	49.74	98.98	2.56	1.47	0.74	71.21	2.47	14.39
2H-3,50-52	MAD	8.9	51.03	104.21	2.6	1.46	0.71	72.54	2.64	14.29
2H-4,46-48	MAD	10.36	50.01	100.05	2.65	1.48	0.74	72.09	2.58	14.49
2H-5,19-21	MAD	11.59	43.16	75.92	2.69	1.58	0.9	66.57	1.99	15.51
2H-6,24-26	MAD	13.14	43.19	76.02	2.63	1.57	0.89	66.1	1.95	15.39
2H-7,18-20	MAD	14.58	41.38	70.59	2.6	1.59	0.93	64.05	1.78	15.56
3H-1,13-15	MAD	15.03	42.91	75.16	2.68	1.58	0.9	66.23	1.96	15.52
3H-2,18-20	MAD	16.58	46.22	85.93	2.67	1.53	0.82	69.08	2.23	15.03
3H-3,14-16	MAD	18.04	45.94	84.98	2.63	1.53	0.83	68.57	2.18	15.01
3H-4,20-22	MAD	19.6	43.52	77.06	2.65	1.57	0.89	66.55	1.99	15.37
3H-5,15-17	MAD	21.05	43.46	76.85	2.59	1.56	0.88	66.02	1.94	15.27
3H-6,68-70	MAD	23.08	42.57	74.13	2.65	1.58	0.91	65.67	1.91	15.51
3H-7,32-34	MAD	24.22	41.82	71.89	2.66	1.6	0.93	65.14	1.87	15.66
4H-1,33-35	MAD	24.73	36.19	56.71	2.7	1.7	1.08	59.89	1.49	16.64
4H-2,7-9	MAD	25.97	42.62	74.27	2.65	1.58	0.91	65.78	1.92	15.52
4H-3,22-24	MAD	27.62	37.45	59.87	2.65	1.66	1.04	60.78	1.55	16.32
4H-4,28-30	MAD	29.18	34.13	51.83	2.68	1.73	1.14	57.52	1.35	16.94
4H-5,23-25	MAD	30.63	43.93	78.34	2.62	1.56	0.87	66.71	2	15.27
4H-6,12-14	MAD	32.02	43.79	77.91	2.63	1.56	0.88	66.64	2	15.3
4H-7,8-10	MAD	33.48	43.97	78.49	2.61	1.55	0.87	66.64	2	15.24
5H-1,39-41	MAD	34.29	46.33	86.34	2.64	1.53	0.82	68.96	2.22	14.96
5H-2,22-24	MAD	35.62	42.4	73.62	2.67	1.58	0.91	65.16	1.87	15.45
5H-3,8-10	MAD	36.98	37.44	59.83	2.8	1.7	1.06	62.01	1.63	16.65
5H-5,18-20	MAD	40.08	40.13	67.03	2.71	1.63	0.98	63.92	1.77	16.01
5H-6,5-7	MAD	41.45	35.16	54.22	2.7	1.71	1.11	58.8	1.43	16.82
5H-7,15-17	MAD	43.05	37.84	60.87	2.69	1.67	1.04	61.52	1.6	16.35
6H-1,68-70	MAD	44.08	37.55	60.13	2.75	1.68	1.05	61.69	1.61	16.52
6H-2,13-15	MAD	45.03	35.43	54.87	2.67	1.7	1.1	58.87	1.43	16.71
6H-3,13-15	MAD	46.53	35.89	55.99	2.65	1.69	1.08	59.14	1.45	16.56
6H-4,13-15	MAD	48.03	34.6	52.9	2.68	1.72	1.13	58.06	1.38	16.87
6H-5,13-15	MAD	49.53	33.45	50.26	2.67	1.74	1.16	56.72	1.31	17.05
6H-6,13-15	MAD	51.03	37.71	60.55	2.66	1.66	1.03	61.08	1.57	16.28
6H-7,13-15	MAD	52.03	34.73	53.21	2.68	1.72	1.12	58.11	1.39	16.82
7H-1,85-87	MAD	53.75	30.51	43.92	2.7	1.8	1.25	53.63	1.16	17.67
7H-2,22-24	MAD	54.62	34.8	53.37	2.72	1.73	1.13	58.61	1.42	16.94
7H-3,33-35	MAD	56.23	33.93	51.36	2.72	1.74	1.15	57.66	1.36	17.09
7H-4,38-40	MAD	57.78	34.36	52.34	2.67	1.72	1.13	57.72	1.36	16.89
7H-5,83-85	MAD	59.73	31.88	46.8	2.7	1.78	1.21	55.23	1.23	17.42
7H-6,47-49	MAD	60.87	34.55	52.78	2.72	1.73	1.13	58.37	1.4	16.98
8X-1,63-65	MAD	63.03	36.38	57.18	2.67	1.69	1.07	59.86	1.49	16.54
8X-2,16-18	MAD	64.06	35.77	55.69	2.67	1.7	1.09	59.23	1.45	16.65
8X-3,12-14	MAD	65.52	35.14	54.18	2.7	1.72	1.11	58.8	1.43	16.82
8X-4,26-28	MAD	67.16	36.41	57.25	2.68	1.69	1.07	59.95	1.5	16.55

Table 15. Moisture and density (MAD) physical properties for Hole NGHP-01-03B.—Continued

Core, section, interval (cm)	Sample code	Depth (mbsf)	WCt (%)	WCs (%)	Grain density (g/cm³)	Bulk density (g/cm³)	Dry bulk density (g/cm³)	Porosity (%)	Void ratio	Unit weight (kN/m³)
NGHP-01-03B—Continued										
8X-5,12-14	MAD	67.82	36.27	56.91	2.68	1.69	1.08	59.8	1.49	16.58
8X-6,25-27	MAD	68.95	35.69	55.49	2.65	1.69	1.09	58.97	1.44	16.61
9X-1,23-25	MAD	71.93	39.35	64.89	2.65	1.63	0.99	62.65	1.68	16
9X-2,23-25	MAD	73.43	33.96	51.41	2.69	1.73	1.14	57.38	1.35	16.99
9X-3,23-25	MAD	74.43	34.43	52.51	2.69	1.73	1.13	57.96	1.38	16.93
10X-1,13-15	MAD	81.43	36.36	57.14	2.68	1.69	1.07	59.91	1.49	16.56
11X-1,17-19	MAD	90.97	35.81	55.79	2.7	1.7	1.09	59.46	1.47	16.69
11X-2,55-57	MAD	92.35	33.43	50.21	2.66	1.73	1.15	56.57	1.3	17.01
12X-1,13-15	MAD	99.83	33.36	50.07	2.68	1.74	1.16	56.69	1.31	17.08
12X-2,13-15	MAD	100.83	31.7	46.41	2.67	1.77	1.21	54.69	1.21	17.35
13P-1,29-31	MAD	105.19	30.38	43.63	2.68	1.8	1.25	53.26	1.14	17.63
14X-1,51-53	MAD	106.41	33.96	51.43	2.65	1.72	1.14	57.1	1.33	16.9
14X-2,34-36	MAD	107.74	28.41	39.68	2.7	1.85	1.32	51.15	1.05	18.1
15X-1,32-34	MAD	115.82	36.78	58.17	2.65	1.67	1.06	60.02	1.5	16.41
15X-2,23-25	MAD	117.23	31.23	45.41	2.69	1.79	1.23	54.4	1.19	17.51
15X-3,7-9	MAD	118.57	33.22	49.74	2.7	1.75	1.17	56.7	1.31	17.16
15X-4,17-19	MAD	120.17	33.67	50.77	2.67	1.73	1.15	56.97	1.32	17.01
15X-5,17-19	MAD	121.67	34.09	51.72	2.71	1.74	1.14	57.73	1.37	17.03
15X-6,12-14	MAD	123.12	37.83	60.86	2.62	1.65	1.03	60.91	1.56	16.19
16X-1,24-26	MAD	124.64	39.86	66.27	2.7	1.64	0.98	63.57	1.75	16.04
16X-2,33-35	MAD	126.23	37.53	60.07	2.68	1.67	1.04	61.07	1.57	16.36
16X-3,32-34	MAD	127.72	35.87	55.94	2.69	1.7	1.09	59.44	1.47	16.66
16X-4,10-12	MAD	129	36.03	56.32	2.69	1.7	1.09	59.63	1.48	16.64
16X-5,6-8	MAD	129.96	33.84	51.14	2.71	1.74	1.15	57.5	1.35	17.08
17X-1,13-15	MAD	133.33	33.1	49.48	2.72	1.76	1.18	56.78	1.31	17.25
17X-2,15-17	MAD	134.85	34.73	53.22	2.65	1.71	1.12	57.9	1.38	16.76
17X-3,14-16	MAD	136.34	35.01	53.88	2.69	1.71	1.11	58.56	1.41	16.82
17X-4,17-19	MAD	137.87	35.64	55.37	2.58	1.68	1.08	58.25	1.4	16.43
17X-5,18-20	MAD	139.38	34.12	51.8	2.65	1.72	1.13	57.23	1.34	16.86
18X-1,29-31	MAD	142.19	35.38	54.76	2.68	1.69	1.09	58.44	1.41	16.6
18X-2,27-29	MAD	143.67	35.34	54.65	2.65	1.7	1.1	58.52	1.41	16.65
18X-3,31-33	MAD	145.21	28.16	39.2	2.71	1.85	1.33	50.85	1.03	18.15
18X-4,30-32	MAD	146.7	34.57	52.84	2.68	1.72	1.13	58.02	1.38	16.87
18X-5,30-32	MAD	148.2	32.71	48.61	2.67	1.75	1.18	55.89	1.27	17.18
18X-6,16-18	MAD	149.56	28.59	40.04	2.68	1.83	1.31	51.17	1.05	17.99
19X-1,92-94	MAD	152.62	37.51	60.02	2.7	1.67	1.05	61.25	1.58	16.42
19X-2,6-8	MAD	153.26	35.13	54.15	2.69	1.71	1.11	58.68	1.42	16.79
19X-3,6-8	MAD	154.76	35.2	54.33	2.69	1.71	1.11	58.74	1.42	16.77
19X-4,6-8	MAD	156.26	37.52	60.04	2.7	1.67	1.05	61.23	1.58	16.41
19X-5,4-6	MAD	157	31.88	46.79	2.69	1.77	1.21	55.14	1.23	17.39
19X-6,7-9	MAD	158.03	35	53.84	2.73	1.73	1.12	58.93	1.44	16.93
20X-1,13-15	MAD	161.43	40.24	67.34	2.74	1.64	0.98	64.26	1.8	16.05
20X-2,13-15	MAD	162.93	33.18	49.66	2.67	1.74	1.16	56.43	1.3	17.1
20X-3,8-10	MAD	163.88	34.26	52.11	2.64	1.72	1.13	57.33	1.34	16.83
20X-4,31-33	MAD	164.91	34.85	53.49	2.64	1.7	1.11	57.94	1.38	16.72
20X-5,31-33	MAD	166.41	34.3	52.2	2.68	1.73	1.13	57.73	1.37	16.92
20X-6,31-33	MAD	167.91	35.25	54.44	2.67	1.71	1.1	58.67	1.42	16.73
21X-1,30-32	MAD	171.3	35.01	53.87	2.67	1.71	1.11	58.42	1.4	16.78
21X-2,30-32	MAD	172.8	37.56	60.15	2.63	1.66	1.03	60.67	1.54	16.24
21X-3,30-32	MAD	174.3	37.12	59.02	2.66	1.67	1.05	60.48	1.53	16.38
21X-4,30-32	MAD	175.8	33.15	49.59	2.68	1.75	1.17	56.46	1.3	17.12
22P-1,32-34	MAD	175.22	32.5	48.15	2.65	1.75	1.18	55.42	1.24	17.14
23Y-1,14-16	MAD	176.04	37.43	59.82	2.58	1.65	1.03	60.12	1.51	16.15
24X-1,10-12	MAD	177	37.41	59.76	2.63	1.66	1.04	60.53	1.53	16.27
24X-2,15-17	MAD	177.64	40.28	67.44	2.64	1.62	0.97	63.49	1.74	15.85
24X-3,14-16	MAD	179.13	39.51	65.31	2.61	1.62	0.98	62.41	1.66	15.88
24X-4,14-16	MAD	180.63	39.77	66.04	2.65	1.63	0.98	63.07	1.71	15.94
24X-6,7-9	MAD	183.36	38.48	62.56	2.74	1.67	1.02	62.54	1.67	16.34

Table 15. Moisture and density (MAD) physical properties for Hole NGHP-01-03B.—Continued

Core, section, interval (cm)	Sample code	Depth (mbsf)	WCt (%)	WCs (%)	Grain density (g/cm³)	Bulk density (g/cm³)	Dry bulk density (g/cm³)	Porosity (%)	Void ratio	Unit weight (kN/m³)
NGHP-01-03B—Continued										
25X-2,10-12	MAD	186.98	34.28	52.17	2.69	1.73	1.14	57.83	1.37	16.96
25X-3,14-16	MAD	188.52	33.85	51.16	2.76	1.76	1.16	57.94	1.38	17.21
25X-4,13-15	MAD	190.01	32.34	47.8	2.67	1.76	1.19	55.48	1.25	17.25
25X-5,9-11	MAD	191.47	33.51	50.4	2.7	1.75	1.16	57.07	1.33	17.12
25X-6,9-11	MAD	192.97	31.25	45.44	2.78	1.81	1.24	55.17	1.23	17.75
26X-1,30-32	MAD	196.6	33.64	50.69	2.73	1.75	1.16	57.44	1.35	17.17
26X-2,18-20	MAD	197.98	32.56	48.27	2.68	1.76	1.18	55.77	1.26	17.22
26X-3,17-19	MAD	199.47	33.22	49.74	2.68	1.75	1.17	56.56	1.3	17.12
26X-4,12-14	MAD	200.92	33.11	49.49	2.71	1.76	1.17	56.71	1.31	17.22
27P-1,74-76	MAD	199.64	31.03	45	2.63	1.77	1.22	53.57	1.15	17.35
29X-1,7-9	MAD	200.97	34.01	51.53	2.67	1.73	1.14	57.34	1.34	16.95
29X-2,8-10	MAD	202.48	33.23	49.77	2.74	1.76	1.18	57.05	1.33	17.26
29X-3,15-17	MAD	204.05	33.95	51.4	2.68	1.73	1.14	57.3	1.34	16.97
29X-4,14-16	MAD	205.54	34.4	52.45	2.71	1.73	1.14	58.08	1.39	16.97
30X-1,30-32	MAD	210.9	35.53	55.11	2.69	1.71	1.1	59.14	1.45	16.74
30X-2,33-35	MAD	212.43	36.48	57.44	2.72	1.7	1.08	60.35	1.52	16.63
30X-3,35-37	MAD	213.95	39.01	63.97	2.68	1.64	1	62.57	1.67	16.12
30X-4,34-36	MAD	215.44	37.67	60.45	2.68	1.67	1.04	61.2	1.58	16.33
30X-5,34-36	MAD	216.64	38.62	62.92	2.68	1.65	1.01	62.23	1.65	16.2
31X-1,66-68	MAD	220.96	37.95	61.15	2.74	1.68	1.04	62.03	1.63	16.43
31X-2,37-39	MAD	222.17	36.72	58.03	2.75	1.7	1.08	60.89	1.56	16.67
31X-3,27-29	MAD	223.57	35.48	55	2.72	1.71	1.11	59.35	1.46	16.82
31X-4,17-19	MAD	224.75	34.86	53.5	2.73	1.73	1.13	58.72	1.42	16.94
31X-5,17-19	MAD	226.05	34.85	53.49	2.74	1.73	1.13	58.85	1.43	16.98
31X-6,16-18	MAD	227.54	33.88	51.23	2.72	1.74	1.15	57.64	1.36	17.11
32X-1,10-12	MAD	230	30.65	44.19	2.78	1.82	1.27	54.55	1.2	17.89
32X-2,11-13	MAD	231.31	31.67	46.35	2.73	1.79	1.22	55.26	1.24	17.54
32X-3,8-10	MAD	232.78	31.51	46.01	2.74	1.8	1.23	55.19	1.23	17.61
32X-4,17-19	MAD	234.37	31.44	45.85	2.74	1.8	1.23	55.09	1.23	17.62
32X-5,31-33	MAD	236.01	31.5	45.98	2.76	1.8	1.23	55.28	1.24	17.64
32X-6,69-71	MAD	237.39	31.72	46.45	2.74	1.79	1.22	55.38	1.24	17.55
33X-1,15-17	MAD	239.75	32.2	47.49	2.77	1.79	1.21	56.2	1.28	17.55
33X-2,15-17	MAD	239.98	30.71	44.33	2.75	1.81	1.26	54.32	1.19	17.78
33X-3,12-14	MAD	241.2	27.66	38.24	2.74	1.87	1.36	50.56	1.02	18.38
33X-4,12-14	MAD	242.7	31.49	45.96	2.75	1.8	1.23	55.21	1.23	17.63
33X-5,10-12	MAD	244.18	31.29	45.53	2.73	1.79	1.23	54.78	1.21	17.6
33X-6,14-16	MAD	245.6	31.21	45.37	2.78	1.81	1.25	55.17	1.23	17.77
34X-2,35-37	MAD	250.45	32.16	47.41	2.73	1.78	1.21	55.82	1.26	17.45
34X-3,28-30	MAD	251.88	33.96	51.43	2.73	1.75	1.15	57.84	1.37	17.12
34X-4,28-30	MAD	253.38	27.98	38.85	2.75	1.87	1.35	50.99	1.04	18.32
34X-5,28-30	MAD	254.88	30.84	44.59	2.75	1.81	1.25	54.43	1.19	17.74
34X-6,26-28	MAD	256.36	26.76	36.55	2.76	1.9	1.39	49.56	0.98	18.62
34X-7,46-48	MAD	258.06	29.12	41.09	2.74	1.84	1.31	52.35	1.1	18.07
35X-3,8-10	MAD	259.73	29.49	41.82	2.74	1.84	1.29	52.8	1.12	18
35X-4,8-10	MAD	261.23	29.22	41.28	2.74	1.84	1.3	52.44	1.1	18.04
35X-5,8-10	MAD	262.73	29.96	42.78	2.74	1.83	1.28	53.37	1.14	17.91
35X-6,12-14	MAD	264.27	29.84	42.54	2.73	1.82	1.28	53.12	1.13	17.89
35X-7,10-12	MAD	265.75	29.37	41.58	2.73	1.83	1.3	52.54	1.11	17.98
35X-8,30-32	MAD	266.95	26.62	36.27	2.73	1.89	1.39	49.14	0.97	18.56
36X-1,13-15	MAD	267.83	29.29	41.42	2.75	1.84	1.3	52.6	1.11	18.05
36X-2,10-12	MAD	269.3	29.46	41.77	2.75	1.84	1.3	52.85	1.12	18.03
36X-3,10-12	MAD	270.8	28.33	39.52	2.75	1.86	1.33	51.46	1.06	18.27
36X-4,19-21	MAD	272.39	29.93	42.72	2.75	1.83	1.28	53.38	1.15	17.93
36X-5,14-16	MAD	273.84	29.68	42.21	2.74	1.83	1.29	53.03	1.13	17.96
36X-6,17-19	MAD	275.37	29.15	41.14	2.73	1.84	1.3	52.3	1.1	18.04
37X-2,15-17	MAD	277.88	32.38	47.88	2.73	1.77	1.2	56.05	1.28	17.41
37X-3,14-16	MAD	279.37	30.62	44.13	2.74	1.81	1.26	54.09	1.18	17.76
37X-4,13-15	MAD	280.86	32.31	47.73	2.72	1.77	1.2	55.88	1.27	17.39

Table 15. Moisture and density (MAD) physical properties for Hole NGHP-01-03B.—Continued

Core, section, interval (cm)	Sample code	Depth (mbsf)	WCt (%)	WCs (%)	Grain density (g/cm³)	Bulk density (g/cm³)	Dry bulk density (g/cm³)	Porosity (%)	Void ratio	Unit weight (kN/m³)
NGHP-01-03B—Continued										
37X-5,23-25	MAD	282.46	32.92	49.07	2.72	1.76	1.18	56.53	1.3	17.26
37X-6,14-16	MAD	283.87	27.76	38.43	2.77	1.88	1.36	50.94	1.04	18.45
37X-7,20-22	MAD	285.43	29.53	41.91	2.74	1.83	1.29	52.79	1.12	17.97
38X-1,9-11	MAD	286.29	30.37	43.62	2.74	1.82	1.26	53.79	1.16	17.8
38X-2,8-10	MAD	287.78	34.76	53.28	2.7	1.72	1.12	58.35	1.4	16.88
38X-3,9-11	MAD	289.29	34.87	53.54	2.71	1.72	1.12	58.61	1.42	16.9
38X-4,9-11	MAD	290.79	32.57	48.29	2.72	1.77	1.19	56.16	1.28	17.34
38X-5,19-21	MAD	292.35	31.56	46.12	2.74	1.79	1.23	55.22	1.23	17.59
38X-6,15-17	MAD	293.31	31.05	45.03	2.75	1.81	1.25	54.71	1.21	17.72
39X-1,21-23	MAD	296.01	32.95	49.15	2.77	1.77	1.19	57.03	1.33	17.4
39X-2,15-17	MAD	297.45	32.37	47.86	2.74	1.78	1.2	56.08	1.28	17.42
39X-5,16-18	MAD	301.96	30.85	44.62	2.75	1.81	1.25	54.46	1.2	17.75

Table 16. Vane shear strength results for Hole NGHP-01-03B.

Core, section	Sample	Top (cm)	Depth (mbsf)	Sv (kPa)	Sres (kPa)	Srem (kPa)	St
NGHP-01-03B							
1H-2	VS	75	2.25	3.3	1.6	0.7	5.0
1H-3	VS	34	3.34	5.1	2.5	0.8	6.2
1H-4	VS	40	4.9	23.9	16.5	1.1	22.3
2H-1	VS	90	6.3	6.2	3.3	1.6	3.8
2H-2	VS	90	7.8	8.2	2.9	2.9	2.9
2H-3	VS	40	8.8	9.1	5.6	2.5	3.7
2H-4	VS	50	10.4	11.9	9.5	4.9	2.4
2H-5	VS	10	11.5	14.6	9.9	5.2	2.8
2H-6	VS	10	13	15.3	10.3	5.8	2.7
2H-7	VS	10	14.5	17.1	12.3	7.4	2.3
3H-1	VS	10	15	10.0	8.1	3.3	3.0
3H-2	VS	10	16.5	16.6	9.5	5.3	3.1
3H-3	VS	10	18	16.0	14.4	0.0	0.0
3H-3	VS	20	18.1	19.4	10.3	7.0	2.8
3H-4	VS	30	19.7	21.4	13.2	6.6	3.3
3H-5	VS	10	21	29.1	18.1	9.1	3.2
3H-6	VS	70	23.1	33.7	16.5	11.5	2.9
3H-7	VS	30	24.2	32.9	18.9	9.9	3.3
4H-1	VS	40	24.8	30.4	19.7	12.3	2.5
4H-2	VS	85	26.75	32.9	20.6	9.9	3.3
4H-3	VS	15	27.55	31.3	19.7	11.5	2.7
4H-4	VS	23	29.13	42.4	27.2	14.6	2.9
4H-5	VS	17	30.57	32.1	18.9	12.3	2.6
4H-7	VS	15	33.55	28.0	18.1	9.9	2.8
5H-1	VS	38	34.28	25.5	11.5	8.9	2.9
5H-2	VS	15	35.55	29.8	19.7	9.5	3.1
5H-3	VS	9	36.99	31.8	20.6	11.5	2.8
5H-4	VS	15	38.55	37.0	20.6	11.5	3.2
5H-5	VS	9	39.99	31.1	19.7	7.8	4.0
5H-6	VS	5	41.45	48.6	19.7	16.5	3.0
5H-7	VS	9	42.99	33.3	21.4	9.9	3.4
6H-1	VS	77	44.17	23.9	0.0	0.0	0.0
6H-2	VS	38	45.28	34.6	17.3	13.2	2.6
6H-3	VS	35	46.75	46.9	19.7	14.8	3.2
6H-4	VS	35	48.25	41.1	21.4	16.5	2.5
6H-5	VS	35	49.75	56.8	29.6	24.7	2.3
6H-6	VS	30	51.2	32.1	16.5	13.2	2.4
6H-7	VS	35	52.25	34.6	18.1	13.2	2.6
7H-1	VS	82	53.72	30.4	15.6	6.6	4.6

Table 17. Torvane strength results for Hole NGHP-01-03B.

Core, section, interval (cm)	Sample	Depth (mbsf)	Stv (kPa)	Core, section, interval (cm)	Sample	Depth (mbsf)	Stv (kPa)
NGHP-01-03B							
1H-2,30-32	TV	1.8	2.9	15X-3,9-11	TV	118.59	49.0
1H-3,30-32	TV	3.3	4.9	15X-4,14-16	TV	120.14	35.3
1H-4,30-32	TV	4.8	8.2	15X-5,14-16	TV	121.64	52.0
2H-1,75-77	TV	6.15	7.4	15X-6,14-16	TV	123.14	64.7
2H-1,79-81	TV	6.19	6.4	16X-1,22-24	TV	124.62	27.5
2H-1,95-97	TV	6.35	9.8	16X-1,119-121	TV	125.59	39.2
2H-2,87-89	TV	7.77	9.8	16X-2,29-31	TV	126.19	44.1
2H-3,42-44	TV	8.82	11.8	16X-3,29-31	TV	127.69	53.0
2H-4,42-44	TV	10.32	13.7	16X-4,13-15	TV	129.03	23.5
2H-5,22-24	TV	11.62	20.6	16X-5,7-9	TV	129.97	38.2
2H-6,17-19	TV	13.07	17.2	16X-5,10-12	TV	130	58.8
2H-7,28-30	TV	14.68	23.5	16X-5,29-31	TV	130.19	53.9
3H-1,9-11	TV	14.99	12.3	17X-1,16-18	TV	133.36	66.7
3H-2,21-23	TV	16.61	19.6	17X-2,17-19	TV	134.87	47.1
3H-3,18-20	TV	18.08	19.6	17X-3,17-19	TV	136.37	73.5
3H-4,12-14	TV	19.52	29.4	17X-4,18-20	TV	137.88	60.8
3H-5,12-14	TV	21.02	33.3	17X-5,13-15	TV	139.33	75.5
3H-6,65-67	TV	23.05	39.2	18X-1,35-37	TV	142.25	58.8
3H-7,26-28	TV	24.16	43.1	18X-2,35-37	TV	143.75	34.3
4H-1,36-38	TV	24.76	42.2	18X-4,35-37	TV	146.75	19.6
4H-2,13-15	TV	26.03	33.3	18X-6,13-15	TV	149.53	68.6
4H-3,28-30	TV	27.68	47.1	19X-1,80-82	TV	152.5	27.0
4H-4,17-19	TV	29.07	53.9	19X-2,14-16	TV	153.34	39.2
4H-5,19-21	TV	30.59	43.1	19X-3,14-16	TV	154.84	36.8
4H-6,8-10	TV	31.98	35.3	19X-4,14-16	TV	156.34	58.8
4H-7,10-12	TV	33.5	42.2	19X-5,14-16	TV	157.1	61.3
5H-1,33-35	TV	34.23	30.4	19X-6,16-18	TV	158.12	44.1
5H-2,18-20	TV	35.58	37.3	20X-1,8-10	TV	161.38	44.1
5H-3,5-7	TV	36.95	46.1	20X-2,10-12	TV	162.9	43.1
5H-4,18-20	TV	38.58	48.1	20X-3,8-10	TV	163.88	39.2
5H-5,9-11	TV	39.99	39.2	20X-4,34-36	TV	164.94	49.0
5H-6,8-10	TV	41.48	44.1	20X-5,16-18	TV	166.26	34.3
5H-7,22-24	TV	43.12	44.1	20X-6,16-18	TV	167.76	39.2
6H-1,64-66	TV	44.04	34.3	21X-1,26-28	TV	171.26	34.3
6H-2,16-18	TV	45.06	44.1	21X-2,26-28	TV	172.76	53.9
6H-3,16-18	TV	46.56	53.9	21X-3,26-28	TV	174.26	34.3
6H-4,16-18	TV	48.06	44.1	21X-4,26-28	TV	175.76	14.7
6H-5,16-18	TV	49.56	60.8	24X-1,14-16	TV	177.04	24.5
6H-6,16-18	TV	51.06	32.4	24X-2,21-23	TV	177.7	53.9
6H-7,16-18	TV	52.06	33.3	24X-3,21-23	TV	179.2	49.0
7H-6,42-44	TV	60.82	73.5	24X-4,18-20	TV	180.67	74.5
8X-1,60-62	TV	63	29.4	24X-5,16-18	TV	182.15	68.6
8X-2,16-18	TV	64.06	29.4	24X-6,14-16	TV	183.43	58.8
8X-3,16-18	TV	65.56	44.1	25X-2,15-17	TV	187.03	66.7
8X-4,29-31	TV	67.19	49.0	25X-3,22-24	TV	188.6	53.9
8X-5,15-17	TV	67.85	53.0	25X-4,22-24	TV	190.1	74.5
8X-6,28-30	TV	68.98	19.6	25X-5,5-7	TV	191.43	53.0
9X-1,17-19	TV	71.87	28.4	25X-6,17-19	TV	193.05	86.3
9X-2,13-15	TV	73.33	34.3	25X-7,14-16	TV	194.02	78.5
9X-3,15-17	TV	74.35	57.9	26X-1,32-34	TV	196.62	66.7
10X-1,14-16	TV	81.44	34.3	26X-2,16-18	TV	197.96	80.4
11X-1,21-23	TV	91.01	34.3	26X-3,18-20	TV	199.48	78.5
11X-2,51-53	TV	92.31	34.3	26X-4,15-17	TV	200.95	68.6
12X-1,23-25	TV	99.93	64.7	29X-1,9-11	TV	200.99	78.5
12X-2,24-26	TV	100.94	29.4	29X-2,10-12	TV	202.5	88.3
14X-1,54-56	TV	106.44	49.0	29X-3,18-20	TV	204.08	90.2
14X-2,37-39	TV	107.77	45.1	29X-4,18-20	TV	205.58	93.2
14X-3,83-85	TV	109.73	49.0	29X-5,21-23	TV	206.92	94.1
15X-1,34-36	TV	115.84	31.9	30X-1,18-20	TV	210.78	78.5
15X-2,25-27	TV	117.25	30.4	30X-2,18-20	TV	212.28	65.7

Table 17. Torvane strength results for Hole NGHP-01-03B.—Continued

Core, section, interval (cm)	Sample	Depth (mbsf)	Stv (kPa)	Core, section, interval (cm)	Sample	Depth (mbsf)	Stv (kPa)
NGHP-01-03B—Continued							
31X-1,17-19	TV	220.47	55.2	36X-4,23-25	TV	272.43	152.0
31X-2,13-15	TV	221.93	100.5	36X-5,24-26	TV	273.94	159.4
31X-3,23-25	TV	223.53	85.8	36X-6,21-23	TV	275.41	171.6
31X-4,11-13	TV	224.69	110.3	37X-2,19-21	TV	277.92	122.6
31X-5,12-14	TV	226	100.5	37X-3,17-19	TV	279.4	137.3
31X-6,12-14	TV	227.5	104.2	37X-4,18-20	TV	280.91	152.0
32X-1,14-16	TV	230.04	90.7	37X-5,13-15	TV	282.36	127.5
32X-2,14-16	TV	231.34	134.8	37X-6,18-20	TV	283.91	152.0
32X-3,14-16	TV	232.84	134.8	37X-7,25-27	TV	285.48	166.7
32X-4,14-16	TV	234.34	110.3	38X-1,6-8	TV	286.26	120.1
32X-5,27-29	TV	235.97	122.6	38X-2,12-14	TV	287.82	107.9
32X-6,74-76	TV	237.44	134.8	38X-3,12-14	TV	289.32	112.8
33X-1,17-19	TV	239.77	36.8	38X-4,11-13	TV	290.81	132.4
33X-2,30-32	TV	240.13	134.8	38X-5,18-20	TV	292.34	112.8
33X-3,7-9	TV	241.15	98.1	38X-6,20-22	TV	293.36	129.9
33X-4,7-9	TV	242.65	110.3	39X-1,25-27	TV	296.05	63.7
33X-5,18-20	TV	244.26	104.2	39X-2,17-19	TV	297.47	80.9
33X-6,7-9	TV	245.53	122.6	39X-3,14-16	TV	298.94	105.4
36X-1,17-19	TV	267.87	159.4	39X-4,15-17	TV	300.45	134.8
36X-2,18-20	TV	269.38	171.6	39X-5,21-23	TV	302.01	110.3
36X-3,12-14	TV	270.82	147.1				

Table 18. Pocket Penetrometer strength results for Hole NGHP-01-03B.

Core, section	Sample	Top (cm)	Depth (mbsf)	Spp (kPa)	Core, section	Sample	Top (cm)	Depth (mbsf)	Spp (kPa)
NGHP-01-03B									
1H-2	PP	24	1.74	0.8	5H-4	PP	20	38.6	53.9
1H-3	PP	36	3.36	1.5	5H-5	PP	13	40.03	44.1
1H-4	PP	26	4.76	2.3	5H-6	PP	7	41.47	36.8
2H-1	PP	72	6.12	3.1	5H-7	PP	25	43.15	49.0
2H-2	PP	91	7.81	4.0	6H-1	PP	62	44.02	12.3
2H-3	PP	51	8.91	4.6	6H-2	PP	14	45.04	24.5
2H-4	PP	54	10.44	7.0	6H-3	PP	14	46.54	36.8
2H-5	PP	25	11.65	8.4	6H-4	PP	14	48.04	24.5
2H-6	PP	20	13.1	8.4	6H-5	PP	14	49.54	36.8
2H-7	PP	32	14.72	10.1	6H-6	PP	14	51.04	12.3
3H-1	PP	16	15.06	3.1	6H-7	PP	14	52.04	24.5
3H-2	PP	13	16.53	8.0	7H-1	PP	79	53.69	24.5
3H-3	PP	10	18	8.4	7H-2	PP	24	54.64	36.8
3H-4	PP	16	19.56	11.5	7H-4	PP	75	58.15	68.6
3H-5	PP	19	21.09	13.8	7H-5	PP	82	59.72	73.5
3H-5	PP	19	21.09	14.7	7H-6	PP	45	60.85	73.5
3H-5	PP	22	21.12	36.8	8X-1	PP	57	62.97	134.8
3H-5	PP	23	21.13	14.7	8X-2	PP	13	64.03	12.3
3H-5	PP	23	21.13	14.7	8X-3	PP	13	65.53	34.3
3H-5	PP	24	21.14	22.1	8X-4	PP	27	67.17	36.8
3H-6	PP	69	23.09	24.5	8X-5	PP	14	67.84	34.3
3H-7	PP	25	24.15	24.5	8X-6	PP	26	68.96	24.5
4H-1	PP	34	24.74	17.2	9X-1	PP	30	72	24.5
4H-2	PP	17	26.07	29.4	9X-2	PP	16	73.36	34.3
4H-3	PP	26	27.66	39.2	9X-3	PP	30	74.5	29.4
4H-4	PP	20	29.1	58.8	10X-1	PP	21	81.51	29.4
4H-5	PP	24	30.64	24.5	11X-1	PP	18	90.98	24.5
4H-6	PP	17	32.07	19.6	11X-2	PP	50	92.3	29.4
4H-7	PP	8	33.48	29.4	12X-2	PP	3	100.73	49.0
5H-1	PP	31	34.21	24.5	14X-1	PP	57	106.47	61.3
5H-2	PP	16	35.56	49.0	14X-2	PP	36	107.76	44.1
5H-3	PP	4	36.94	29.4	14X-3	PP	84	109.74	112.7

Table 18. Pocket Penetrometer strength results for Hole NGHP-01-03B.—Continued

Core, section	Sample	Top (cm)	Depth (mbsf)	Spp (kPa)	Core, section	Sample	Top (cm)	Depth (mbsf)	Spp (kPa)
NGHP-01-03B—Continued									
15X-1	PP	38	115.88	14.7	29X-4	PP	17	205.57	127.4
15X-2	PP	23	117.23	49.0	29X-5	PP	19	206.9	98.0
15X-2	PP	25	117.25	49.0	30X-1	PP	14	210.74	58.8
15X-3	PP	8	118.58	36.8	30X-2	PP	15	212.25	34.3
15X-4	PP	13	120.13	49.0	30X-3	PP	15	213.75	49.0
15X-5	PP	13	121.63	39.2	30X-4	PP	15	215.25	73.5
15X-6	PP	12	123.12	39.2	30X-5	PP	15	216.45	49.0
16X-1	PP	123	125.63	19.6	31X-1	PP	16	220.46	36.8
16X-2	PP	28	126.18	24.5	31X-2	PP	37	222.17	61.3
16X-3	PP	30	127.7	24.5	31X-3	PP	27	223.57	78.4
16X-4	PP	11	129.01	34.3	31X-4	PP	14	224.72	85.8
16X-5	PP	7	129.97	44.1	31X-5	PP	14	226.02	85.8
16X-5	PP	9	129.99	41.7	31X-6	PP	15	227.53	98.0
16X-5	PP	30	130.2	39.2	32X-1	PP	17	230.07	73.5
17X-1	PP	15	133.35	53.9	32X-2	PP	10	231.3	73.5
17X-2	PP	21	134.91	73.5	32X-3	PP	12	232.82	85.8
17X-3	PP	21	136.41	85.8	32X-4	PP	12	234.32	107.8
17X-4	PP	21	137.91	93.1	32X-5	PP	30	236	85.8
17X-5	PP	17	139.37	78.4	32X-6	PP	74	237.44	98.0
18X-1	PP	30	142.2	61.3	33X-1	PP	15	239.75	12.3
18X-2	PP	28	143.68	58.8	33X-2	PP	18	240.01	98.0
18X-3	PP	32	145.22	49.0	33X-3	PP	17	241.25	73.5
18X-4	PP	30	146.7	49.0	33X-4	PP	17	242.75	85.8
18X-5	PP	30	148.2	61.3	33X-5	PP	16	244.24	98.0
18X-6	PP	17	149.57	68.6	33X-6	PP	17	245.63	98.0
19X-1	PP	92	152.62	24.5	34X-2	PP	40	250.5	85.8
19X-2	PP	8	153.28	24.5	34X-3	PP	10	251.7	122.5
19X-3	PP	10	154.8	34.3	34X-4	PP	42	253.52	110.3
19X-4	PP	10	156.3	58.8	34X-5	PP	27	254.87	85.8
19X-5	PP	7	157.03	36.8	34X-6	PP	35	256.45	110.3
19X-6	PP	10	158.06	24.5	34X-7	PP	10	257.7	134.8
20X-1	PP	6	161.36	44.1	35X-3	PP	35	260	98.0
20X-2	PP	4	162.84	24.5	35X-4	PP	34	261.49	111.7
20X-3	PP	6	163.86	14.7	35X-5	PP	31	262.96	98.0
20X-4	PP	23	164.83	39.2	35X-6	PP	49	264.64	85.8
20X-5	PP	20	166.3	58.8	35X-7	PP	54	266.19	147.0
20X-6	PP	8	167.68	49.0	35X-8	PP	53	267.18	122.5
21X-1	PP	25	171.25	12.3	36X-1	PP	15	267.85	122.5
21X-2	PP	25	172.75	49.0	36X-2	PP	17	269.37	122.5
21X-3	PP	25	174.25	61.3	36X-3	PP	9	270.79	147.0
21X-4	PP	25	175.75	49.0	36X-4	PP	22	272.42	122.5
24X-2	PP	8	177.57	49.0	36X-5	PP	12	273.82	134.8
24X-3	PP	16	179.15	49.0	36X-6	PP	10	275.3	147.0
24X-4	PP	17	180.66	61.3	37X-2	PP	17	277.9	110.3
24X-5	PP	15	182.14	85.8	37X-3	PP	15	279.38	137.2
24X-6	PP	12	183.41	49.0	37X-4	PP	16	280.89	142.1
25X-2	PP	31	187.19	12.3	37X-5	PP	11	282.34	85.8
25X-3	PP	41	188.79	73.5	37X-6	PP	17	283.9	122.5
25X-4	PP	22	190.1	58.8	37X-7	PP	24	285.47	117.6
25X-5	PP	22	191.6	83.3	38X-1	PP	17	286.37	132.3
25X-6	PP	29	193.17	78.4	38X-2	PP	16	287.86	127.4
25X-7	PP	9	193.97	85.8	38X-3	PP	17	289.37	110.3
26X-1	PP	31	196.61	61.3	38X-4	PP	8	290.78	134.8
26X-2	PP	14	197.94	85.8	38X-5	PP	8	292.24	117.6
26X-3	PP	18	199.48	78.4	38X-6	PP	10	293.26	122.5
26X-4	PP	18	200.98	73.5	39X-1	PP	24	296.04	53.9
29X-1	PP	10	201	78.4	39X-2	PP	20	297.5	73.5
29X-2	PP	9	202.49	78.4	39X-3	PP	17	298.97	85.8
29X-3	PP	16	204.06	122.5	39X-4	PP	18	300.48	110.3
					39X-5	PP	19	301.99	117.6

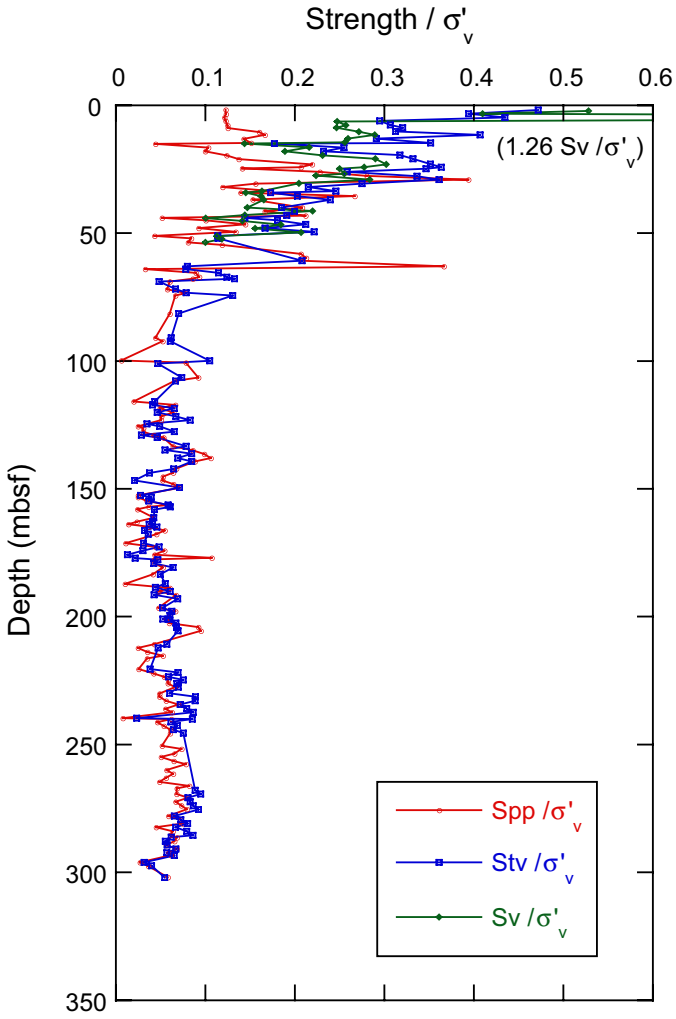

Figure 24. Shear strengths normalized by the effective vertical stress versus sub-bottom depth for Hole NGHP-01-03B.

Downhole Temperature Measurements

A number of different tools are available for determining downhole sediment temperature (see "Physical Properties" section of "Methods" chapter). Both APC3 and DVTP tools were used to measure temperatures at six subbottom depths in Site NGHP-01-03. Seafloor temperature was determined to be 6.5 ± 0.2 °C and the geothermal gradient was calculated as 39 ± 2 °C per km (table 22 and fig. 27). The intersection of the geothermal gradient with the gas-hydrate pressure (depth) – temperature stability field from Sloan (1998) provides an estimated depth to the BGHS of 203 mbsf. This is in close agreement with the depth of the BSR at 209 mbsf determined from well logging and seismic record interpretations.

Pressure Coring

The main objectives of pressure coring during NGHP Expedition 01 were to quantify natural gas composition and concentration in sediments and to determine the nature and distribution of gas hydrate and free gas within the sediment matrix. Secondary objectives were to obtain measurements of physical properties on gas-hydrate-bearing sediments under *in situ* conditions, which can be used to help interpret regional seismic data, and to obtain samples under full pressure for shorebased studies. To achieve these objectives, we conducted depressurization experiments and captured resultant gas to calculate gas hydrate quantity, made nondestructive measurements (X-ray imaging, *P*-wave velocity, gamma density) at *in situ* pressures and during depressurization to examine gas hydrate habit within sediments, and archived gas-hydrate-bearing sediments at *in situ* pressures for more comprehensive investigations on shore.

The BSR at Site NGHP-01-03, located in the Krishna-Godavari Basin, has an estimated depth of 209 mbsf, and high-amplitude reflections below the BSR to either side of the drill site were interpreted as possible indicators free gas. LWD data from Hole NGHP-01-03A showed thin (2–6 m thick) layers of

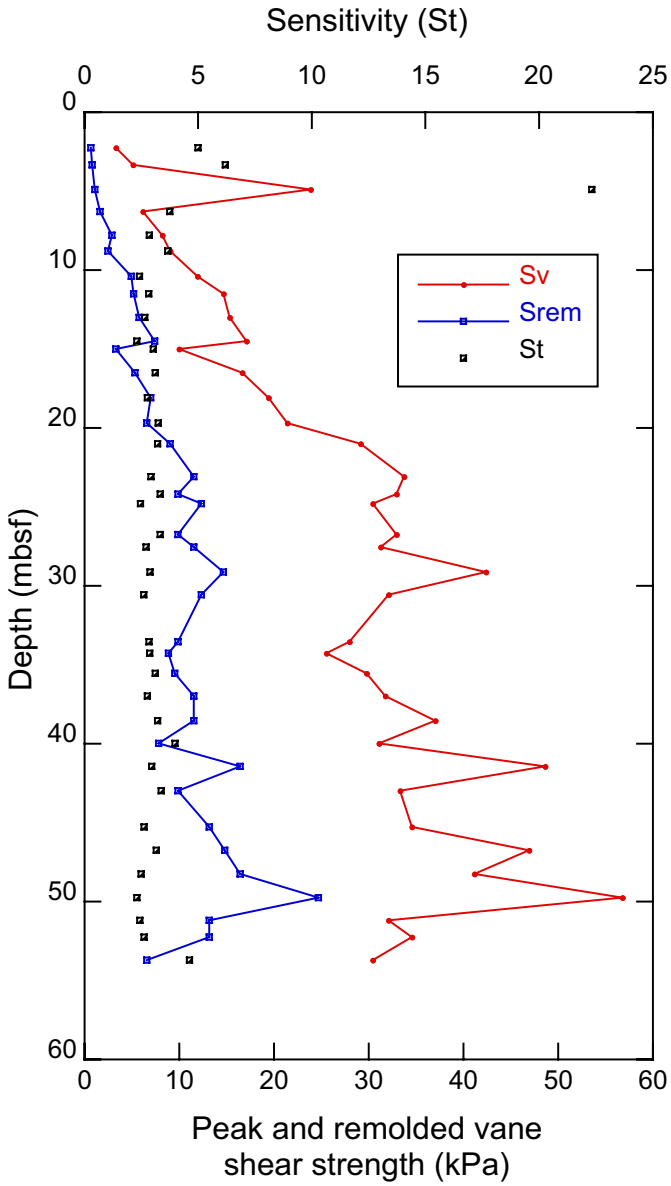

Figure 25. Peak and remolded vane shear strengths and sensitivity for Hole NGHP-01-03B.

Table 19. Wenner array electrical resistivity and formation factor results for Hole NGHP-01-03B. (To view the complete table, please see the ASCII files in the supplemental data files.)

Core, section	Sample	Top (cm)	Depth (mbsf)	Resistivity (W×m)	Apparent formation factor	Core, section	Sample	Top (cm)	Depth (mbsf)	Resistivity (W×m)	Apparent formation factor
NGHP-01-03B											
1H-2	ER	20	1.7	0.343	1.72	3H-2	ER	90	17.3	0.439	2.20
1H-2	ER	75	2.25	0.362	1.81	3H-2	ER	110	17.5	0.476	2.38
1H-3	ER	20	3.2	0.504	2.52	3H-2	ER	130	17.7	0.434	2.17
1H-3	ER	40	3.4	0.325	1.63	3H-3	ER	10	18	0.442	2.21
1H-3	ER	60	3.6	0.378	1.89	3H-3	ER	30	18.2	0.502	2.51
1H-3	ER	105	4.05	0.319	1.60	3H-3	ER	50	18.4	0.479	2.40
1H-4	ER	20	4.7	0.335	1.68	3H-3	ER	70	18.6	0.408	2.04
1H-4	ER	40	4.9	0.361	1.81	3H-3	ER	90	18.8	0.478	2.39
2H-1	ER	50	5.9	0.311	1.56	3H-4	ER	10	19.5	0.444	2.22
2H-1	ER	70	6.1	0.328	1.64	3H-4	ER	30	19.7	0.409	2.05
2H-1	ER	90	6.3	0.356	1.78	3H-4	ER	50	19.9	0.446	2.23
2H-1	ER	110	6.5	0.331	1.66	3H-4	ER	70	20.1	0.444	2.22
2H-1	ER	130	6.7	0.302	1.51	3H-4	ER	90	20.3	0.439	2.20
2H-2	ER	10	7	0.382	1.91	3H-4	ER	112	20.52	0.455	2.28
2H-2	ER	30	7.2	0.349	1.75	3H-4	ER	130	20.7	0.459	2.30
2H-2	ER	50	7.4	0.337	1.69	3H-5	ER	10	21	0.434	2.17
2H-2	ER	70	7.6	0.31	1.55	3H-5	ER	30	21.2	0.46	2.30
2H-2	ER	90	7.8	0.321	1.61	3H-5	ER	50	21.4	0.475	2.38
2H-2	ER	110	8	0.344	1.72	3H-5	ER	70	21.6	0.558	2.79
2H-2	ER	130	8.2	0.331	1.66	3H-5	ER	90	21.8	0.45	2.25
2H-3	ER	10	8.5	0.329	1.65	3H-6	ER	10	22.5	0.52	2.60
2H-3	ER	30	8.7	0.344	1.72	3H-6	ER	30	22.7	0.535	2.68
2H-3	ER	50	8.9	0.333	1.67	3H-6	ER	52	22.92	0.499	2.50
2H-3	ER	70	9.1	0.321	1.61	3H-6	ER	70	23.1	0.475	2.38
2H-3	ER	90	9.3	0.373	1.87	3H-6	ER	90	23.3	0.454	2.27
2H-4	ER	10	10	0.33	1.65	3H-6	ER	110	23.5	0.434	2.17
2H-4	ER	30	10.2	0.356	1.78	3H-6	ER	130	23.7	0.457	2.29
2H-4	ER	50	10.4	0.363	1.82	3H-7	ER	10	24	0.516	2.58
2H-4	ER	70	10.6	0.363	1.82	3H-7	ER	30	24.2	0.605	3.03
2H-4	ER	90	10.8	0.377	1.89	3H-7	ER	50	24.4	0.477	2.39
2H-4	ER	110	11	0.391	1.96	3H-7	ER	70	24.6	0.592	2.96
2H-4	ER	130	11.2	0.402	2.01	4H-1	ER	40	24.8	0.617	3.09
2H-5	ER	10	11.5	0.425	2.13	4H-1	ER	60	25	0.538	2.69
2H-5	ER	30	11.7	0.449	2.25	4H-1	ER	80	25.2	0.448	2.24
2H-5	ER	50	11.9	0.45	2.25	4H-1	ER	100	25.4	0.492	2.46
2H-5	ER	70	12.1	0.445	2.23	4H-1	ER	120	25.6	0.45	2.25
2H-5	ER	90	12.3	0.455	2.28	4H-2	ER	10	26	0.542	2.71
2H-6	ER	10	13	0.438	2.19	4H-2	ER	30	26.2	0.475	2.38
2H-6	ER	30	13.2	0.475	2.38	4H-2	ER	84	26.74	0.511	2.56
2H-6	ER	50	13.4	0.374	1.87	4H-2	ER	110	27	0.484	2.42
2H-6	ER	70	13.6	0.441	2.21	4H-2	ER	130	27.2	0.476	2.38
2H-6	ER	90	13.8	0.406	2.03	4H-3	ER	15	27.55	0.488	2.44
2H-6	ER	110	14	0.411	2.06	4H-3	ER	38	27.78	0.499	2.50
2H-6	ER	130	14.2	0.391	1.96	4H-3	ER	55	27.95	0.43	2.15
2H-7	ER	10	14.5	0.421	2.11	4H-3	ER	75	28.15	0.464	2.32
2H-7	ER	30	14.7	0.326	1.63	4H-3	ER	102	28.42	0.436	2.18
2H-7	ER	50	14.9	0.454	2.27	4H-4	ER	23	29.13	0.473	2.37
3H-1	ER	10	15	0.396	1.98	4H-4	ER	43	29.33	0.46	2.30
3H-1	ER	60	15.5	0.391	1.96	4H-4	ER	63	29.53	0.49	2.45
3H-1	ER	80	15.7	0.379	1.90	4H-4	ER	83	29.73	0.488	2.44
3H-1	ER	100	15.9	0.381	1.91	4H-4	ER	103	29.93	0.483	2.42
3H-1	ER	120	16.1	0.402	2.01	4H-4	ER	114	30.04	0.479	2.40
3H-1	ER	140	16.3	0.426	2.13	4H-5	ER	17	30.57	0.442	2.21
3H-2	ER	10	16.5	0.427	2.14	4H-5	ER	40	30.8	0.409	2.05
3H-2	ER	30	16.7	0.427	2.14	4H-5	ER	60	31	0.399	2.00
3H-2	ER	50	16.9	0.436	2.18	4H-5	ER	80	31.2	0.408	2.04
3H-2	ER	70	17.1	0.414	2.07	4H-5	ER	97	31.37	0.403	2.02

Table 19. Wenner array electrical resistivity and formation factor results for Hole NGHP-01-03B. (To view the complete table, please see the ASCII files in the supplemental data files.)—Continued

Core, section	Sample	Top (cm)	Depth (mbsf)	Resistivity (W×m)	Apparent formation factor	Core, section	Sample	Top (cm)	Depth (mbsf)	Resistivity (W×m)	Apparent formation factor
NGHP-01-03B—Continued											
4H-6	ER	15	32.05	0.434	2.17	6H-2	ER	75	45.65	0.469	2.35
4H-6	ER	35	32.25	0.44	2.20	6H-2	ER	95	45.85	0.461	2.31
4H-6	ER	55	32.45	0.416	2.08	6H-2	ER	115	46.05	0.405	2.03
4H-6	ER	75	32.65	0.405	2.03	6H-2	ER	135	46.25	0.452	2.26
4H-6	ER	95	32.85	0.493	2.47	6H-3	ER	20	46.6	0.48	2.40
4H-7	ER	15	33.55	0.566	2.83	6H-3	ER	30	46.7	0.482	2.41
4H-7	ER	35	33.75	0.395	1.98	6H-3	ER	35	46.75	0.418	2.09
4H-7	ER	55	33.95	0.421	2.11	6H-3	ER	60	47	0.459	2.30
4H-7	ER	75	34.15	0.401	2.01	6H-3	ER	80	47.2	0.462	2.31
5H-1	ER	38	34.28	0.417	2.09	6H-3	ER	100	47.4	0.408	2.04
5H-1	ER	58	34.48	0.478	2.39	6H-4	ER	15	48.05	0.608	3.04
5H-1	ER	78	34.68	0.422	2.11	6H-4	ER	35	48.25	0.481	2.41
5H-1	ER	98	34.88	0.437	2.19	6H-4	ER	55	48.45	0.533	2.67
5H-1	ER	118	35.08	0.391	1.96	6H-4	ER	75	48.65	0.424	2.12
5H-1	ER	138	35.28	0.422	2.11	6H-4	ER	95	48.85	0.497	2.49
5H-2	ER	15	35.55	0.439	2.20	6H-4	ER	115	49.05	0.438	2.19
5H-2	ER	45	35.85	0.471	2.36	6H-5	ER	15	49.55	0.595	2.98
5H-2	ER	65	36.05	0.463	2.32	6H-5	ER	35	49.75	0.474	2.37
5H-2	ER	85	36.25	0.546	2.73	6H-5	ER	55	49.95	0.452	2.26
5H-2	ER	102	36.42	0.444	2.22	6H-5	ER	80	50.2	0.38	1.90
5H-2	ER	122	36.62	0.466	2.33	6H-6	ER	15	51.05	0.42	2.10
5H-2	ER	142	36.82	0.417	2.09	6H-6	ER	50	51.4	0.48	2.40
5H-3	ER	6	36.96	0.399	2.00	6H-6	ER	75	51.65	0.496	2.48
5H-3	ER	26	37.16	0.407	2.04	6H-7	ER	15	52.05	0.495	2.48
5H-3	ER	46	37.36	0.392	1.96	6H-7	ER	35	52.25	0.473	2.37
5H-3	ER	66	37.56	0.436	2.18	7H-1	ER	80	53.7	0.469	2.35
5H-3	ER	86	37.76	0.467	2.34	7H-1	ER	135	54.25	0.46	2.30
5H-3	ER	105	37.95	0.395	1.98	7H-2	ER	22	54.62	0.469	2.35
5H-4	ER	8	38.48	0.57	2.85	7H-2	ER	55	54.95	0.454	2.27
5H-4	ER	45	38.85	0.43	2.15	7H-2	ER	75	55.15	0.484	2.42
5H-4	ER	98	39.38	0.429	2.15	7H-2	ER	115	55.55	0.478	2.39
5H-4	ER	136	39.76	0.492	2.46	7H-3	ER	83	56.73	0.467	2.34
5H-5	ER	8	39.98	0.46	2.30	7H-4	ER	39	57.79	0.425	2.13
5H-5	ER	18	40.08	0.466	2.33	7H-4	ER	78	58.18	0.423	2.12
5H-5	ER	41	40.31	0.41	2.05	7H-5	ER	23	59.13	0.419	2.10
5H-5	ER	58	40.48	0.527	2.64	7H-5	ER	82	59.72	0.458	2.29
5H-5	ER	79	40.69	0.436	2.18	7H-6	ER	43	60.83	0.447	2.24
5H-5	ER	95	40.85	0.476	2.38	7H-6	ER	100	61.4	0.475	2.38
5H-6	ER	5	41.45	0.468	2.34	8X-1	ER	40	62.8	0.482	2.41
5H-6	ER	26	41.66	0.477	2.39	8X-1	ER	60	63	0.401	2.01
5H-6	ER	44	41.84	0.493	2.47	8X-1	ER	90	63.3	0.44	2.20
5H-6	ER	67	42.07	0.465	2.33	8X-1	ER	123	63.63	0.421	2.11
5H-6	ER	85	42.25	0.484	2.42	8X-2	ER	17	64.07	0.389	1.95
5H-6	ER	105	42.45	0.467	2.34	8X-2	ER	60	64.5	0.413	2.07
5H-6	ER	143	42.83	0.436	2.18	8X-2	ER	103	64.93	0.413	2.07
5H-7	ER	9	42.99	0.524	2.62	8X-3	ER	17	65.57	0.42	2.10
5H-7	ER	33	43.23	0.43	2.15	8X-3	ER	43	65.83	0.431	2.16
5H-7	ER	50	43.4	0.471	2.36	8X-3	ER	80	66.2	0.434	2.17
5H-7	ER	78	43.68	0.468	2.34	8X-4	ER	30	67.2	0.425	2.13
6H-1	ER	46	43.86	0.59	2.95	8X-4	ER	60	67.5	0.357	1.79
6H-1	ER	66	44.06	0.492	2.46	8X-5	ER	16	67.86	0.432	2.16
6H-1	ER	86	44.26	0.442	2.21	8X-6	ER	29	68.99	0.432	2.16
6H-1	ER	106	44.46	0.507	2.54	8X-6	ER	56	69.26	0.43	2.15
6H-1	ER	126	44.66	0.472	2.36	9X-1	ER	17	71.87	0.466	2.33
6H-2	ER	15	45.05	0.486	2.43	9X-1	ER	37	72.07	0.43	2.15
6H-2	ER	35	45.25	0.475	2.38	9X-1	ER	57	72.27	0.376	1.88
6H-2	ER	55	45.45	0.415	2.08	9X-1	ER	77	72.47	0.487	2.44

Table 19. Wenner array electrical resistivity and formation factor results for Hole NGHP-01-03B. (To view the complete table, please see the ASCII files in the supplemental data files.)—Continued

Core, section	Sample	Top (cm)	Depth (mbsf)	Resistivity (W×m)	Apparent formation factor	Core, section	Sample	Top (cm)	Depth (mbsf)	Resistivity (W×m)	Apparent formation factor
NGHP-01-03B—Continued											
9X-1	ER	97	72.67	0.348	1.74	15X-5	ER	55	122.05	0.477	2.39
9X-1	ER	117	72.87	0.423	2.12	15X-5	ER	70	122.2	0.393	1.97
9X-1	ER	137	73.07	0.418	2.09	15X-6	ER	15	123.15	0.413	2.07
9X-2	ER	18	73.38	0.391	1.96	15X-6	ER	34	123.34	0.598	2.99
9X-3	ER	20	74.4	0.383	1.92	15X-6	ER	54	123.54	0.424	2.12
9X-3	ER	20	74.4	0.393	1.97	15X-6	ER	75	123.75	0.45	2.25
9X-3	ER	40	74.6	0.442	2.21	16X-1	ER	20	124.6	0.45	2.25
9X-3	ER	60	74.8	0.531	2.66	16X-1	ER	40	124.8	0.44	2.20
10X-1	ER	17	81.47	0.418	2.09	16X-1	ER	60	125	0.443	2.22
10X-1	ER	37	81.67	0.479	2.40	16X-1	ER	80	125.2	0.472	2.36
11X-1	ER	21	91.01	0.454	2.27	16X-1	ER	100	125.4	0.589	2.95
11X-1	ER	43	91.23	0.45	2.25	16X-1	ER	120	125.6	0.415	2.08
11X-2	ER	16	91.96	0.506	2.53	16X-1	ER	140	125.8	0.461	2.31
11X-2	ER	52	92.32	0.456	2.28	16X-2	ER	10	126	0.423	2.12
12X-1	ER	11	99.81	0.501	2.51	16X-2	ER	30	126.2	0.458	2.29
12X-1	ER	31	100.01	0.472	2.36	16X-2	ER	50	126.4	0.476	2.38
12X-1	ER	51	100.21	0.529	2.65	16X-2	ER	70	126.6	0.455	2.28
12X-2	ER	10	100.8	0.452	2.26	16X-3	ER	10	127.5	0.458	2.29
12X-2	ER	30	101	0.595	2.98	16X-3	ER	30	127.7	0.464	2.32
14X-1	ER	25	106.15	0.556	2.78	16X-3	ER	50	127.9	0.453	2.27
14X-1	ER	45	106.35	0.502	2.51	16X-3	ER	70	128.1	0.526	2.63
14X-1	ER	65	106.55	0.584	2.92	16X-3	ER	90	128.3	0.5	2.50
14X-1	ER	85	106.75	0.497	2.49	16X-3	ER	110	128.5	0.572	2.86
14X-2	ER	15	107.55	0.492	2.46	16X-3	ER	130	128.7	0.521	2.61
14X-2	ER	15	107.55	0.502	2.51	16X-4	ER	4	128.94	0.556	2.78
14X-2	ER	35	107.75	0.572	2.86	16X-4	ER	24	129.14	0.581	2.91
14X-2	ER	55	107.95	0.538	2.69	16X-5	ER	10	130	0.599	3.00
14X-3	ER	15	109.05	0.479	2.40	16X-5	ER	30	130.2	0.549	2.75
14X-3	ER	35	109.25	0.479	2.40	17X-1	ER	15	133.35	0.53	2.65
14X-3	ER	55	109.45	0.565	2.83	17X-1	ER	35	133.55	0.548	2.74
14X-3	ER	75	109.65	0.596	2.98	17X-1	ER	55	133.75	0.489	2.45
15X-1	ER	16	115.66	0.409	2.05	17X-1	ER	78	133.98	0.694	3.47
15X-1	ER	35	115.85	0.44	2.20	17X-1	ER	97	134.17	0.541	2.71
15X-1	ER	55	116.05	0.456	2.28	17X-1	ER	115	134.35	0.563	2.82
15X-1	ER	75	116.25	0.536	2.68	17X-1	ER	135	134.55	0.505	2.53
15X-1	ER	95	116.45	0.582	2.91	17X-2	ER	16	134.86	0.524	2.62
15X-1	ER	115	116.65	0.532	2.66	17X-2	ER	36	135.06	0.509	2.55
15X-1	ER	135	116.85	0.533	2.67	17X-2	ER	55	135.25	0.58	2.90
15X-2	ER	10	117.1	0.682	3.41	17X-2	ER	78	135.48	0.516	2.58
15X-2	ER	30	117.3	0.52	2.60	17X-2	ER	95	135.65	0.611	3.06
15X-2	ER	50	117.5	0.497	2.49	17X-2	ER	115	135.85	0.549	2.75
15X-2	ER	70	117.7	0.56	2.80	17X-3	ER	15	136.35	0.524	2.62
15X-2	ER	90	117.9	0.485	2.43	17X-3	ER	41	136.61	0.653	3.27
15X-2	ER	110	118.1	0.487	2.44	17X-3	ER	58	136.78	0.501	2.51
15X-2	ER	130	118.3	0.551	2.76	17X-3	ER	73	136.93	0.55	2.75
15X-3	ER	10	118.6	0.491	2.46	17X-4	ER	15	137.85	0.467	2.34
15X-3	ER	30	118.8	0.547	2.74	17X-4	ER	35	138.05	0.504	2.52
15X-3	ER	50	119	0.465	2.33	17X-4	ER	55	138.25	0.518	2.59
15X-3	ER	70	119.2	0.566	2.83	17X-5	ER	15	139.35	0.486	2.43
15X-4	ER	15	120.15	0.511	2.56	17X-5	ER	35	139.55	0.541	2.71
15X-4	ER	35	120.35	0.455	2.28	17X-5	ER	55	139.75	0.45	2.25
15X-4	ER	55	120.55	0.532	2.66	17X-5	ER	81	140.01	0.494	2.47
15X-4	ER	80	120.8	0.714	3.57	17X-5	ER	95	140.15	0.496	2.48
15X-4	ER	95	120.95	0.467	2.34	17X-5	ER	115	140.35	0.504	2.52
15X-4	ER	115	121.15	0.459	2.30	18X-1	ER	15	142.05	1.428	7.14
15X-5	ER	15	121.65	0.433	2.17	18X-1	ER	17	142.07	1.346	6.73
15X-5	ER	35	121.85	0.443	2.22	18X-1	ER	36	142.26	0.737	3.69

Table 19. Wenner array electrical resistivity and formation factor results for Hole NGHP-01-03B. (To view the complete table, please see the ASCII files in the supplemental data files.)—Continued

Core, section	Sample	Top (cm)	Depth (mbsf)	Resistivity (W×m)	Apparent formation factor	Core, section	Sample	Top (cm)	Depth (mbsf)	Resistivity (W×m)	Apparent formation factor
NGHP-01-03B—Continued											
18X-1	ER	55	142.45	0.932	4.66	20X-4	ER	120	165.8	0.568	2.84
18X-1	ER	75	142.65	1.237	6.19	20X-4	ER	140	166	0.643	3.22
18X-1	ER	97	142.87	1.161	5.81	20X-5	ER	10	166.2	0.628	3.14
18X-1	ER	115	143.05	1.332	6.66	20X-5	ER	30	166.4	0.536	2.68
18X-1	ER	135	143.25	1.391	6.96	20X-5	ER	53	166.63	0.681	3.41
18X-2	ER	15	143.55	0.867	4.34	20X-6	ER	6	167.66	0.668	3.34
18X-2	ER	40	143.8	1.005	5.03	20X-6	ER	32	167.92	0.577	2.89
18X-2	ER	60	144	1.03	5.15	21X-1	ER	25	171.25	0.62	3.10
18X-2	ER	75	144.15	0.906	4.53	21X-1	ER	50	171.5	0.543	2.72
18X-2	ER	100	144.4	1.309	6.55	21X-1	ER	70	171.7	0.611	3.06
18X-2	ER	125	144.65	0.817	4.09	21X-2	ER	24	172.74	0.692	3.46
18X-3	ER	20	145.1	0.87	4.35	21X-2	ER	44	172.94	0.601	3.01
18X-3	ER	50	145.4	0.874	4.37	21X-2	ER	65	173.15	0.607	3.04
18X-3	ER	75	145.65	0.982	4.91	21X-2	ER	85	173.35	0.571	2.86
18X-4	ER	15	146.55	0.736	3.68	21X-2	ER	105	173.55	0.588	2.94
18X-4	ER	35	146.75	0.777	3.89	21X-3	ER	15	174.15	0.555	2.78
18X-4	ER	55	146.95	0.851	4.26	21X-3	ER	34	174.34	0.537	2.69
18X-4	ER	75	147.15	0.655	3.28	21X-3	ER	61	174.61	0.565	2.83
18X-4	ER	95	147.35	0.864	4.32	21X-4	ER	12	175.62	0.536	2.68
18X-4	ER	115	147.55	0.913	4.57	21X-4	ER	32	175.82	0.546	2.73
18X-5	ER	41	148.31	0.622	3.11	21X-4	ER	48	175.98	0.675	3.38
18X-5	ER	60	148.5	0.634	3.17	24X-1	ER	13	177.03	0.556	2.78
18X-6	ER	15	149.55	0.651	3.26	24X-1	ER	42	177.32	0.488	2.44
18X-6	ER	45	149.85	0.651	3.26	24X-2	ER	15	177.64	0.523	2.62
18X-6	ER	75	150.15	0.699	3.50	24X-2	ER	35	177.84	0.548	2.74
19X-1	ER	52	152.22	0.602	3.01	24X-2	ER	55	178.04	0.545	2.73
19X-1	ER	70	152.4	0.593	2.97	24X-2	ER	65	178.14	0.538	2.69
19X-1	ER	90	152.6	0.615	3.08	24X-2	ER	88	178.37	0.547	2.74
19X-1	ER	110	152.8	0.596	2.98	24X-2	ER	105	178.54	0.568	2.84
19X-1	ER	130	153	0.572	2.86	24X-2	ER	125	178.74	0.553	2.77
19X-2	ER	15	153.35	0.582	2.91	24X-3	ER	15	179.14	0.486	2.43
19X-2	ER	35	153.55	0.592	2.96	24X-3	ER	35	179.34	0.475	2.38
19X-2	ER	60	153.8	0.556	2.78	24X-3	ER	55	179.54	0.437	2.19
19X-2	ER	80	154	0.586	2.93	24X-3	ER	75	179.74	0.631	3.16
19X-2	ER	107	154.27	0.54	2.70	24X-4	ER	15	180.64	0.557	2.79
19X-2	ER	130	154.5	0.595	2.98	24X-4	ER	35	180.84	0.526	2.63
19X-3	ER	15	154.85	0.572	2.86	24X-4	ER	57	181.06	0.52	2.60
19X-3	ER	35	155.05	0.532	2.66	24X-4	ER	75	181.24	0.532	2.66
19X-3	ER	55	155.25	0.549	2.75	24X-4	ER	95	181.44	0.586	2.93
19X-4	ER	15	156.35	0.552	2.76	24X-4	ER	115	181.64	0.535	2.68
19X-4	ER	30	156.5	0.537	2.69	24X-4	ER	135	181.84	0.555	2.78
19X-5	ER	17	157.13	0.619	3.10	24X-5	ER	15	182.14	0.55	2.75
19X-6	ER	25	158.21	0.595	2.98	24X-5	ER	35	182.34	0.527	2.64
19X-6	ER	63	158.59	0.674	3.37	24X-5	ER	51	182.5	0.527	2.64
20X-1	ER	12	161.42	0.509	2.55	24X-6	ER	5	183.34	0.572	2.86
20X-1	ER	45	161.75	0.622	3.11	24X-6	ER	28	183.57	0.537	2.69
20X-1	ER	65	161.95	0.71	3.55	25X-2	ER	15	187.03	0.569	2.85
20X-1	ER	85	162.15	0.558	2.79	25X-2	ER	35	187.23	0.569	2.85
20X-1	ER	105	162.35	0.523	2.62	25X-2	ER	55	187.43	0.552	2.76
20X-2	ER	20	163	0.599	3.00	25X-2	ER	78	187.66	0.561	2.81
20X-3	ER	6	163.86	0.597	2.99	25X-2	ER	95	187.83	0.534	2.67
20X-3	ER	29	164.09	0.575	2.88	25X-2	ER	115	188.03	0.532	2.66
20X-4	ER	18	164.78	0.593	2.97	25X-2	ER	135	188.23	0.531	2.66
20X-4	ER	40	165	0.556	2.78	25X-3	ER	15	188.53	0.56	2.80
20X-4	ER	60	165.2	0.558	2.79	25X-3	ER	35	188.73	0.518	2.59
20X-4	ER	80	165.4	0.659	3.30	25X-3	ER	55	188.93	0.559	2.80
20X-4	ER	100	165.6	0.618	3.09	25X-3	ER	72	189.1	0.581	2.91

Table 19. Wenner array electrical resistivity and formation factor results for Hole NGHP-01-03B. (To view the complete table, please see the ASCII files in the supplemental data files.)—Continued

Core, section	Sample	Top (cm)	Depth (mbsf)	Resistivity (W×m)	Apparent formation factor	Core, section	Sample	Top (cm)	Depth (mbsf)	Resistivity (W×m)	Apparent formation factor
NGHP-01-03B—Continued											
25X-4	ER	12	190	0.642	3.21	29X-4	ER	15	205.55	0.569	2.85
25X-4	ER	35	190.23	0.623	3.12	29X-4	ER	35	205.75	0.578	2.89
25X-4	ER	55	190.43	0.592	2.96	29X-4	ER	55	205.95	0.584	2.92
25X-4	ER	75	190.63	0.571	2.86	29X-4	ER	75	206.15	0.58	2.90
25X-4	ER	91	190.79	0.617	3.09	29X-5	ER	15	206.86	0.588	2.94
25X-4	ER	115	191.03	0.601	3.01	29X-5	ER	35	207.06	0.529	2.65
25X-4	ER	135	191.23	0.579	2.90	29X-5	ER	55	207.26	0.623	3.12
25X-5	ER	15	191.53	0.651	3.26	29X-5	ER	75	207.46	0.633	3.17
25X-5	ER	35	191.73	0.615	3.08	29X-5	ER	95	207.66	0.643	3.22
25X-5	ER	55	191.93	0.566	2.83	30X-1	ER	15	210.75	0.514	2.57
25X-5	ER	67	192.05	0.773	3.87	30X-1	ER	34	210.94	0.531	2.66
25X-6	ER	15	193.03	0.624	3.12	30X-1	ER	55	211.15	0.517	2.59
25X-6	ER	35	193.23	0.613	3.07	30X-1	ER	75	211.35	0.571	2.86
25X-6	ER	55	193.43	0.664	3.32	30X-1	ER	95	211.55	0.5	2.50
25X-6	ER	75	193.63	0.617	3.09	30X-1	ER	115	211.75	0.512	2.56
25X-6	ER	95	193.83	0.621	3.11	30X-1	ER	135	211.95	0.57	2.85
25X-7	ER	15	194.03	0.627	3.14	30X-2	ER	15	212.25	0.514	2.57
25X-7	ER	35	194.23	0.634	3.17	30X-2	ER	35	212.45	0.51	2.55
25X-7	ER	55	194.43	0.635	3.18	30X-2	ER	55	212.65	0.516	2.58
25X-7	ER	75	194.63	0.663	3.32	30X-2	ER	70	212.8	0.559	2.80
26X-1	ER	25	196.55	0.591	2.96	30X-3	ER	15	213.75	0.5	2.50
26X-1	ER	45	196.75	0.634	3.17	30X-3	ER	35	213.95	0.497	2.49
26X-1	ER	65	196.95	0.632	3.16	30X-3	ER	55	214.15	0.541	2.71
26X-1	ER	84	197.14	0.59	2.95	30X-3	ER	75	214.35	0.556	2.78
26X-1	ER	105	197.35	0.558	2.79	30X-3	ER	95	214.55	0.543	2.72
26X-1	ER	125	197.55	0.63	3.15	30X-3	ER	115	214.75	0.477	2.39
26X-1	ER	145	197.75	0.721	3.61	30X-3	ER	135	214.95	0.539	2.70
26X-2	ER	15	197.95	0.6	3.00	30X-4	ER	15	215.25	0.562	2.81
26X-2	ER	35	198.15	0.617	3.09	30X-4	ER	35	215.45	0.551	2.76
26X-2	ER	55	198.35	0.668	3.34	30X-4	ER	55	215.65	0.505	2.53
26X-2	ER	66	198.46	0.654	3.27	30X-4	ER	71	215.81	0.488	2.44
26X-3	ER	15	199.45	0.643	3.22	30X-5	ER	15	216.45	0.513	2.57
26X-3	ER	31	199.61	0.614	3.07	30X-5	ER	35	216.65	0.533	2.67
26X-3	ER	57	199.87	0.586	2.93	30X-5	ER	55	216.85	0.485	2.43
26X-3	ER	75	200.05	0.631	3.16	30X-5	ER	75	217.05	0.594	2.97
26X-3	ER	96	200.26	0.631	3.16	30X-5	ER	95	217.25	0.77	3.85
26X-3	ER	116	200.46	0.549	2.75	30X-5	ER	115	217.45	0.535	2.68
26X-4	ER	20	201	0.701	3.51	31X-1	ER	17	220.47	0.451	2.26
26X-4	ER	43	201.23	0.609	3.05	31X-1	ER	45	220.75	0.457	2.29
29X-1	ER	8	200.98	0.594	2.97	31X-1	ER	65	220.95	0.465	2.33
29X-1	ER	27	201.17	0.609	3.05	31X-1	ER	85	221.15	0.547	2.74
29X-1	ER	46	201.36	0.594	2.97	31X-1	ER	105	221.35	0.513	2.57
29X-1	ER	65	201.55	0.563	2.82	31X-1	ER	125	221.55	0.541	2.71
29X-1	ER	85	201.75	0.564	2.82	31X-2	ER	15	221.95	0.506	2.53
29X-1	ER	100	201.9	0.551	2.76	31X-2	ER	35	222.15	0.514	2.57
29X-1	ER	129	202.19	0.571	2.86	31X-2	ER	55	222.35	0.503	2.52
29X-1	ER	145	202.35	0.582	2.91	31X-3	ER	25	223.55	0.503	2.52
29X-2	ER	12	202.52	0.791	3.96	31X-3	ER	70	224	0.542	2.71
29X-2	ER	35	202.75	0.562	2.81	31X-4	ER	15	224.73	0.488	2.44
29X-2	ER	55	202.95	0.606	3.03	31X-4	ER	35	224.93	0.572	2.86
29X-2	ER	75	203.15	0.593	2.97	31X-4	ER	55	225.13	0.482	2.41
29X-2	ER	95	203.35	0.578	2.89	31X-4	ER	75	225.33	0.506	2.53
29X-2	ER	115	203.55	0.595	2.98	31X-4	ER	108	225.66	0.523	2.62
29X-2	ER	143	203.83	0.567	2.84	31X-5	ER	15	226.03	0.585	2.93
29X-3	ER	15	204.05	0.603	3.02	31X-5	ER	35	226.23	0.495	2.48
29X-3	ER	35	204.25	0.595	2.98	31X-5	ER	55	226.43	0.524	2.62
29X-3	ER	55	204.45	0.573	2.87	31X-5	ER	75	226.63	0.526	2.63

Table 19. Wenner array electrical resistivity and formation factor results for Hole NGHP-01-03B. (To view the complete table, please see the ASCII files in the supplemental data files.)—Continued

Core, section	Sample	Top (cm)	Depth (mbsf)	Resistivity (W×m)	Apparent formation factor	Core, section	Sample	Top (cm)	Depth (mbsf)	Resistivity (W×m)	Apparent formation factor
NGHP-01-03B—Continued											
31X-5	ER	100	226.88	0.542	2.71	34X-5	ER	70	255.3	0.557	2.79
31X-5	ER	120	227.08	0.517	2.59	34X-5	ER	128	255.88	0.594	2.97
31X-6	ER	14	227.52	0.548	2.74	34X-6	ER	27	256.37	0.637	3.19
31X-6	ER	55	227.93	0.609	3.05	34X-6	ER	71	256.81	0.67	3.35
32X-1	ER	15	230.05	0.617	3.09	34X-6	ER	118	257.28	0.703	3.52
32X-1	ER	35	230.25	0.59	2.95	34X-7	ER	12	257.72	0.613	3.07
32X-1	ER	57	230.47	0.548	2.74	34X-7	ER	49	258.09	0.666	3.33
32X-1	ER	70	230.6	0.562	2.81	35X-3	ER	36	260.01	0.598	2.99
32X-1	ER	86	230.76	0.564	2.82	35X-3	ER	56	260.21	0.641	3.21
32X-1	ER	110	231	0.544	2.72	35X-4	ER	15	261.3	0.639	3.20
32X-2	ER	15	231.35	0.703	3.52	35X-4	ER	35	261.5	0.596	2.98
32X-2	ER	35	231.55	0.637	3.19	35X-4	ER	55	261.7	0.659	3.30
32X-2	ER	55	231.75	0.583	2.92	35X-4	ER	80	261.95	0.614	3.07
32X-2	ER	75	231.95	0.603	3.02	35X-4	ER	100	262.15	0.675	3.38
32X-2	ER	95	232.15	0.634	3.17	35X-4	ER	125	262.4	0.616	3.08
32X-2	ER	114	232.34	0.632	3.16	35X-5	ER	30	262.95	0.62	3.10
32X-3	ER	15	232.85	0.6	3.00	35X-5	ER	60	263.25	0.605	3.03
32X-3	ER	30	233	0.625	3.13	35X-5	ER	80	263.45	0.627	3.14
32X-3	ER	54	233.24	0.616	3.08	35X-5	ER	100	263.65	0.76	3.80
32X-4	ER	15	234.35	0.688	3.44	35X-6	ER	18	264.33	0.588	2.94
32X-4	ER	35	234.55	0.657	3.29	35X-6	ER	48	264.63	0.614	3.07
32X-4	ER	55	234.75	0.576	2.88	35X-6	ER	75	264.9	0.802	4.01
32X-4	ER	90	235.1	0.656	3.28	35X-6	ER	128	265.43	0.631	3.16
32X-4	ER	105	235.25	0.615	3.08	35X-7	ER	15	265.8	0.633	3.17
32X-5	ER	28	235.98	0.609	3.05	35X-7	ER	35	266	0.879	4.40
32X-5	ER	55	236.25	0.731	3.66	35X-7	ER	55	266.2	0.672	3.36
32X-5	ER	80	236.5	0.629	3.15	35X-7	ER	70	266.35	0.663	3.32
32X-6	ER	55	237.25	0.602	3.01	35X-8	ER	48	267.13	0.759	3.80
32X-6	ER	76	237.46	0.655	3.28	35X-8	ER	73	267.38	0.797	3.99
33X-1	ER	17	239.77	0.591	2.96	36X-1	ER	15	267.85	0.664	3.32
33X-2	ER	20	240.03	0.624	3.12	36X-1	ER	35	268.05	0.608	3.04
33X-2	ER	35	240.18	0.739	3.70	36X-1	ER	55	268.25	0.636	3.18
33X-2	ER	55	240.38	0.582	2.91	36X-1	ER	75	268.45	0.656	3.28
33X-2	ER	82	240.65	0.585	2.93	36X-1	ER	95	268.65	0.632	3.16
33X-3	ER	15	241.23	0.592	2.96	36X-1	ER	115	268.85	0.66	3.30
33X-3	ER	35	241.43	0.655	3.28	36X-1	ER	135	269.05	0.608	3.04
33X-3	ER	55	241.63	0.631	3.16	36X-2	ER	11	269.31	0.548	2.74
33X-4	ER	25	242.83	0.611	3.06	36X-2	ER	35	269.55	0.588	2.94
33X-4	ER	45	243.03	0.637	3.19	36X-2	ER	57	269.77	0.637	3.19
33X-4	ER	65	243.23	0.688	3.44	36X-2	ER	75	269.95	0.721	3.61
33X-4	ER	86	243.44	0.665	3.33	36X-2	ER	95	270.15	0.73	3.65
33X-4	ER	112	243.7	0.699	3.50	36X-2	ER	115	270.35	0.619	3.10
33X-5	ER	20	244.28	0.597	2.99	36X-2	ER	136	270.56	0.7	3.50
33X-5	ER	79	244.87	0.644	3.22	36X-3	ER	12	270.82	0.664	3.32
33X-5	ER	121	245.29	0.6	3.00	36X-3	ER	35	271.05	0.579	2.90
33X-6	ER	20	245.66	0.83	4.15	36X-3	ER	55	271.25	0.688	3.44
34X-2	ER	33	250.43	0.537	2.69	36X-4	ER	15	272.35	0.626	3.13
34X-2	ER	53	250.63	0.557	2.79	36X-4	ER	35	272.55	0.911	4.56
34X-2	ER	83	250.93	0.554	2.77	36X-4	ER	55	272.75	0.617	3.09
34X-2	ER	138	251.48	0.624	3.12	36X-4	ER	75	272.95	0.749	3.75
34X-3	ER	33	251.93	0.56	2.80	36X-4	ER	95	273.15	0.616	3.08
34X-3	ER	83	252.43	0.604	3.02	36X-4	ER	115	273.35	0.676	3.38
34X-4	ER	11	253.21	0.719	3.60	36X-4	ER	135	273.55	0.685	3.43
34X-4	ER	31	253.41	0.68	3.40	36X-5	ER	15	273.85	0.689	3.45
34X-4	ER	75	253.85	0.575	2.88	36X-5	ER	35	274.05	0.644	3.22
34X-4	ER	110	254.2	0.766	3.83	36X-5	ER	55	274.25	0.656	3.28
34X-5	ER	20	254.8	0.57	2.85	36X-5	ER	72	274.42	0.62	3.10

Table 19. Wenner array electrical resistivity and formation factor results for Hole NGHP-01-03B. (To view the complete table, please see the ASCII files in the supplemental data files.)—Continued

Core, section	Sample	Top (cm)	Depth (mbsf)	Resistivity (W×m)	Apparent formation factor	Core, section	Sample	Top (cm)	Depth (mbsf)	Resistivity (W×m)	Apparent formation factor
NGHP-01-03B—Continued											
36X-5	ER	95	274.65	0.66	3.30	38X-2	ER	35	288.05	0.561	2.81
36X-5	ER	115	274.85	0.705	3.53	38X-2	ER	55	288.25	0.57	2.85
36X-5	ER	135	275.05	0.688	3.44	38X-2	ER	75	288.45	0.565	2.83
36X-6	ER	15	275.35	0.736	3.68	38X-2	ER	95	288.65	0.574	2.87
36X-6	ER	32	275.52	0.674	3.37	38X-2	ER	115	288.85	0.548	2.74
36X-6	ER	59	275.79	0.746	3.73	38X-2	ER	135	289.05	0.59	2.95
36X-6	ER	75	275.95	0.68	3.40	38X-3	ER	15	289.35	0.593	2.97
37X-2	ER	15	277.88	0.651	3.26	38X-3	ER	35	289.55	0.647	3.24
37X-2	ER	35	278.08	0.66	3.30	38X-3	ER	55	289.75	0.576	2.88
37X-2	ER	55	278.28	0.643	3.22	38X-4	ER	15	290.85	0.618	3.09
37X-2	ER	75	278.48	0.602	3.01	38X-4	ER	35	291.05	0.635	3.18
37X-2	ER	95	278.68	0.649	3.25	38X-4	ER	55	291.25	0.566	2.83
37X-2	ER	115	278.88	0.613	3.07	38X-4	ER	75	291.45	0.591	2.96
37X-2	ER	135	279.08	0.655	3.28	38X-4	ER	95	291.65	0.594	2.97
37X-3	ER	15	279.38	0.697	3.49	38X-4	ER	116	291.86	0.584	2.92
37X-3	ER	37	279.6	0.645	3.23	38X-4	ER	135	292.05	0.606	3.03
37X-3	ER	55	279.78	0.731	3.66	38X-5	ER	13	292.29	0.566	2.83
37X-4	ER	15	280.88	0.636	3.18	38X-5	ER	35	292.51	0.628	3.14
37X-4	ER	35	281.08	0.616	3.08	38X-5	ER	55	292.71	0.675	3.38
37X-4	ER	55	281.28	0.632	3.16	38X-5	ER	75	292.91	0.693	3.47
37X-4	ER	75	281.48	0.691	3.46	38X-5	ER	95	293.11	0.672	3.36
37X-4	ER	97	281.7	0.677	3.39	38X-6	ER	15	293.31	0.604	3.02
37X-4	ER	115	281.88	0.793	3.97	38X-6	ER	35	293.51	0.59	2.95
37X-4	ER	135	282.08	0.627	3.14	38X-6	ER	55	293.71	0.609	3.05
37X-5	ER	13	282.36	0.583	2.92	39X-1	ER	25	296.05	0.571	2.86
37X-5	ER	35	282.58	0.623	3.12	39X-1	ER	44	296.24	0.629	3.15
37X-5	ER	55	282.78	0.667	3.34	39X-1	ER	65	296.45	0.573	2.87
37X-5	ER	75	282.98	0.705	3.53	39X-1	ER	85	296.65	0.543	2.72
37X-5	ER	97	283.2	0.736	3.68	39X-1	ER	105	296.85	0.622	3.11
37X-5	ER	120	283.43	0.647	3.24	39X-1	ER	125	297.05	0.585	2.93
37X-5	ER	138	283.61	0.666	3.33	39X-1	ER	145	297.25	0.675	3.38
37X-6	ER	15	283.88	0.61	3.05	39X-2	ER	15	297.45	0.565	2.83
37X-6	ER	37	284.1	0.605	3.03	39X-2	ER	35	297.65	0.607	3.04
37X-6	ER	57	284.3	0.677	3.39	39X-2	ER	55	297.85	0.696	3.48
37X-6	ER	75	284.48	0.67	3.35	39X-2	ER	75	298.05	0.689	3.45
37X-6	ER	97	284.7	0.668	3.34	39X-2	ER	95	298.25	0.689	3.45
37X-6	ER	115	284.88	0.621	3.11	39X-2	ER	115	298.45	0.679	3.40
37X-6	ER	135	285.08	0.69	3.45	39X-2	ER	135	298.65	0.721	3.61
37X-7	ER	14	285.37	0.661	3.31	39X-3	ER	15	298.95	0.6	3.00
37X-7	ER	35	285.58	0.602	3.01	39X-3	ER	35	299.15	0.607	3.04
37X-7	ER	56	285.79	0.681	3.41	39X-3	ER	55	299.35	0.642	3.21
37X-7	ER	75	285.98	0.684	3.42	39X-4	ER	15	300.45	0.615	3.08
37X-7	ER	95	286.18	0.64	3.20	39X-4	ER	35	300.65	0.551	2.76
37X-7	ER	115	286.38	0.747	3.74	39X-4	ER	55	300.85	0.554	2.77
38X-1	ER	15	286.35	0.723	3.62	39X-4	ER	75	301.05	0.694	3.47
38X-1	ER	35	286.55	0.619	3.10	39X-4	ER	95	301.25	0.651	3.26
38X-1	ER	55	286.75	0.631	3.16	39X-4	ER	115	301.45	0.589	2.95
38X-1	ER	75	286.95	0.626	3.13	39X-4	ER	135	301.65	0.623	3.12
38X-1	ER	95	287.15	0.605	3.03	39X-5	ER	15	301.95	0.631	3.16
38X-1	ER	115	287.35	0.633	3.17	39X-5	ER	35	302.15	0.659	3.30
38X-1	ER	135	287.55	0.643	3.22	39X-5	ER	55	302.35	0.635	3.18
38X-1	ER	145	287.65	0.564	2.82	39X-5	ER	75	302.55	0.657	3.29
38X-2	ER	15	287.85	0.53	2.65	39X-5	ER	95	302.75	0.629	3.15
						39X-5	ER	115	302.95	0.77	3.85

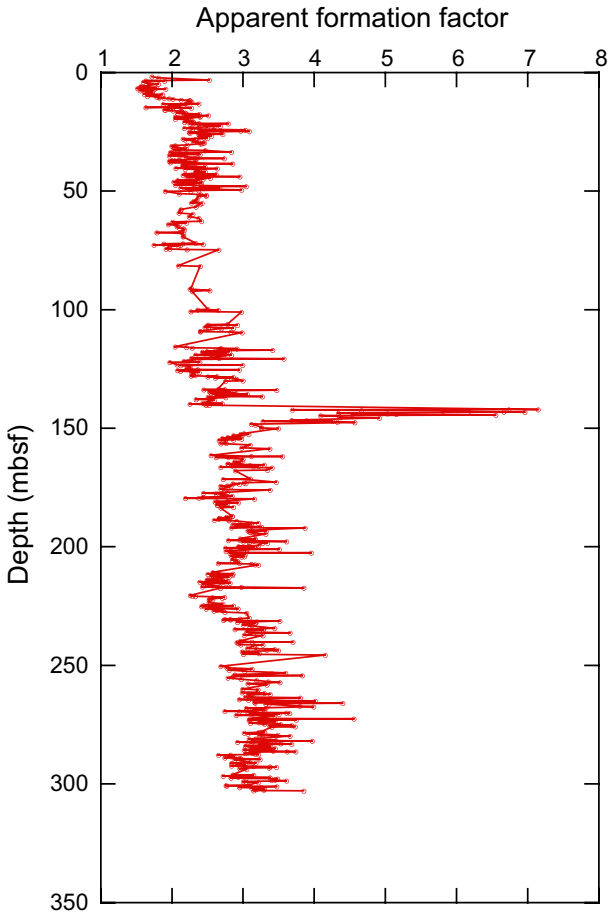

Figure 26. Apparent formation factor versus sub-bottom depth for Hole NGHP-01-03B.

high electrical resistivities from 170–196 mbsf (see "Downhole Logging"). Specific objectives at Site NGHP-01-03 were to confirm and quantify the presence of gas hydrate in the thin layers of high electrical resistivity and possible free gas below the BSR.

Pressure Core Operations and Measurements

Pressure-coring tools were deployed 12 times at Site NGHP-01-03 (table 23): six PCS cores (three in Hole NGHP-01-03B and three in Hole NGHP-01-03C), four FPC cores (one in Hole NGHP-01-03B and three in Hole NGHP-01-03C), and two HRC cores (one in Hole NGHP-01-03B and one in Hole NGHP-01-03C). Figures 28 and 29 show the pressure and temperature history of the cores during deployment, coring, recovery, and chilling (in the ice shuck) of the pressure-coring tools. Figures 30 and 31 show the measurements made on the three successful cores at full pressure and during depressurization. Figure 32 shows the gas and fluid released from the successful cores.

Core NGHP-01-03B-13P (104.9 mbsf), collected above the layers of elevated electrical resistivity, retrieved a full core (1.00 m) at pressure (table 23). The core did not cool properly after recovery as the ice shuck was not filled with ice. The autoclave was placed in the MSCL–P for X-ray and

Table 20. Contact *P*-wave velocity results determined on split cores sections from Hole NGHP-01-03B.

Core, section	Sample	Top (cm)	Depth (mbsf)	Temp (°C)	VP (km/s)	Comment
NGHP-01-03B						
1H-2	VP	75	2.25	23.02	1.470	
1H-3	VP	26	3.26	22.51	1.480	
1H-4	VP	40	4.9	22.87	1.470	
2H-1	VP	90	6.3	22.41	1.475	Weak first break
2H-2	VP	90	7.8	22.48	1.472	Weak first break
2H-3	VP	30	8.7	22.44	1.470	Weak first break
2H-4	VP	50	10.4	22.62	1.446	Weak first break
2H-5	VP	10	11.5	22.49	1.478	Weak first break

Table 21. Thermal conductivity results for Hole NGHP-01-03B.

Core, section	Top (cm)	Depth (mbsf)	Thermal conductivity (W/[m×K])
NGHP-01-03B			
1H-3	75	3.75	0.833
2H-3	75	9.15	0.848
3H-1	75	15.65	0.908
3H-3	75	18.65	0.858
3H-5	75	21.65	0.993
3H-7	43	24.33	0.911
4H-1	25	24.65	0.874
4H-7	46	33.86	0.909
5H-1	75	34.65	0.891
5H-3	55	37.45	0.931
5H-5	50	40.4	0.901
5H-7	43	43.33	0.846
6H-1	75	44.15	0.791
7H-1	75	53.65	0.710
7H-3	55	56.45	0.871
7H-5	54	59.44	1.023
8X-1	75	63.15	0.902
8X-3	75	66.15	0.844
9X-3	44	74.64	0.842
10X-1	30	81.6	0.630
11X-2	43	92.23	0.870
12X-2	23	100.93	0.943
14X-3	51	109.41	0.876
15X-3	50	119	0.863
16X-3	75	128.15	0.882
17X-3	43	136.63	0.900
18X-3	48	145.38	0.840
19X-1	75	152.45	0.961
20X-4	75	165.35	0.953
21X-4	38	175.88	0.703
24X-4	42	180.91	0.786
25X-3	42	188.8	0.899
26X-3	65	199.95	0.878
29X-3	35	204.25	0.828
30X-3	75	214.35	0.866
31X-1	75	221.05	0.862
32X-3	33	233.03	0.947
33X-3	40	241.48	0.856
34X-3	31	251.91	0.907
35X-3	44	260.09	0.918
36X-3	41	271.11	0.956
37X-3	37	279.6	0.886
38X-3	37	289.57	0.860
39X-3	37	299.17	0.878

Table 22. *In situ* temperature estimates from Hole NGHP-01-03B.

Depth (mbsf)	Core	Thermal conductivity (W/[m×K])	Tool	Temp (°C)	Correction applied	Temp (°C)	Estimated uncertainty	Data quality
24.4	B03	0.95	APC3	7.5	0	7.5	0.02	excellent
43.4	B05	0.95	APC3	8.2	0	8.2	0.6	fair (secondary perturbations)
62.4	B07	0.95	APC3	8.75	0	8.75	0.65	fair (secondary perturbations)
153.1	B18X	0.95	DVTP	12.26	0.5	11.87	0.05	good
221.7	B30X	0.95	DVTP	15.01	0.5	14.62	0.05	good
301.4	B300M	0.95	DVTP	18.12	0.5	17.73	0.05	good

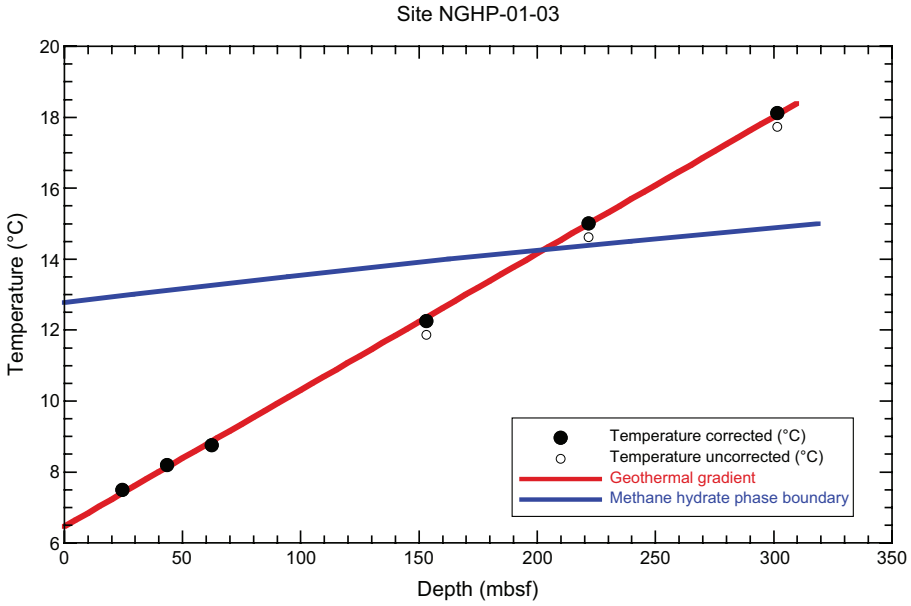

Figure 27. Geothermal gradient and estimated depth to the BSR from *in situ* temperature measurements. [BRS, bottom-simulating reflector]

Table 23. Summary of pressure coring operations at Site NGHP-01-03.

Core ID	Top of core (mbsf)	Length recovered (cm)*	Length curated (cm)*	Pressure at core depth (bar)	Pressure recovered (bar)		Comments
					logged**	gauge***	
NGHP-01-03B							
13P	104.9	100	95	120	65 @11 °C	69	normal operation
22P	174.9	--	80	127	0	--	no pressure
23Y	175.9	88	88	127	96	105	normal operation
27P	198.9	--	100	129	0	--	no pressure; data logger did not record
28E	199.9	--	0	129	0	--	collapsed liner; top o-ring missing
NGHP-01-03B							
04P	170	--	97	126	0	--	valve left open
05Y	175	--	87	127	0	--	flapper valve did not seal
06E	180	--	56	127	0	--	o-ring missing again
07P	184	100	95	127	101 @16 °C	83	normal operation
08Y	190	--	0	128	0	--	did not fire
09Y	197	--	85	129	0	--	liner collapsed
10P	198	--	94	129	0	--	no pressure

Notes:

Water depth at Site NGHP-01-03 is 1086 m. P = PCS, Y = FPC, E = HRC.

*Length measured from X-ray and gamma density analysis, which may not match curated core length.

**Last pressure recorded before data logger disconnected from corer autoclave. Temperature 2–4 °C unless otherwise noted.

***Pressure measured when autoclave pressure transducer connected to external gauge. Pressure measured at 7 °C unless otherwise noted.

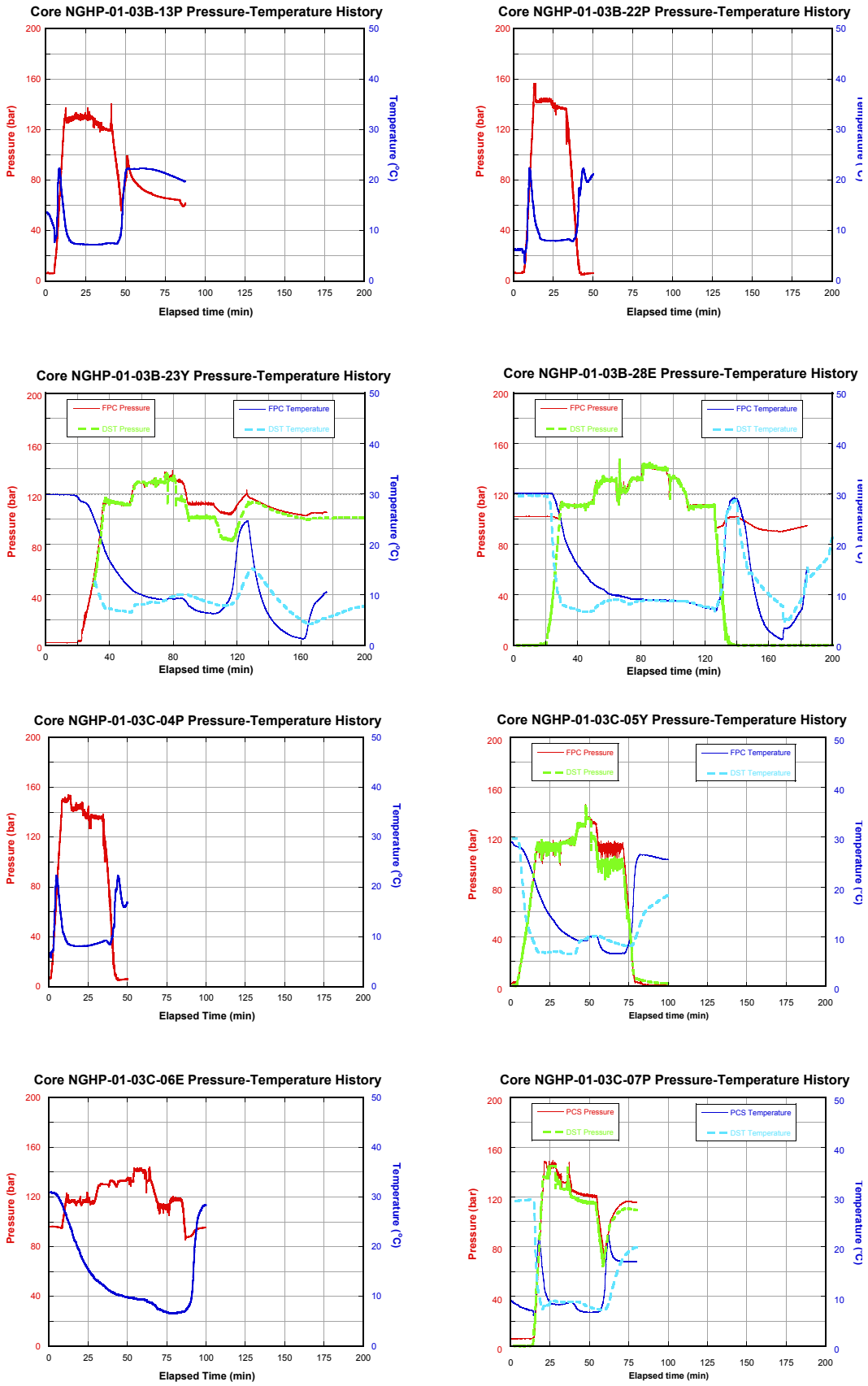

Figure 28. Temperature and pressure versus elapsed time for each pressure corer deployment as recorded by the corer's internal data logger. There are no data for Core NGHP-01-03B-27P. Core NGHP-01-03B-23Y is missing DST data at the beginning of the deployment.

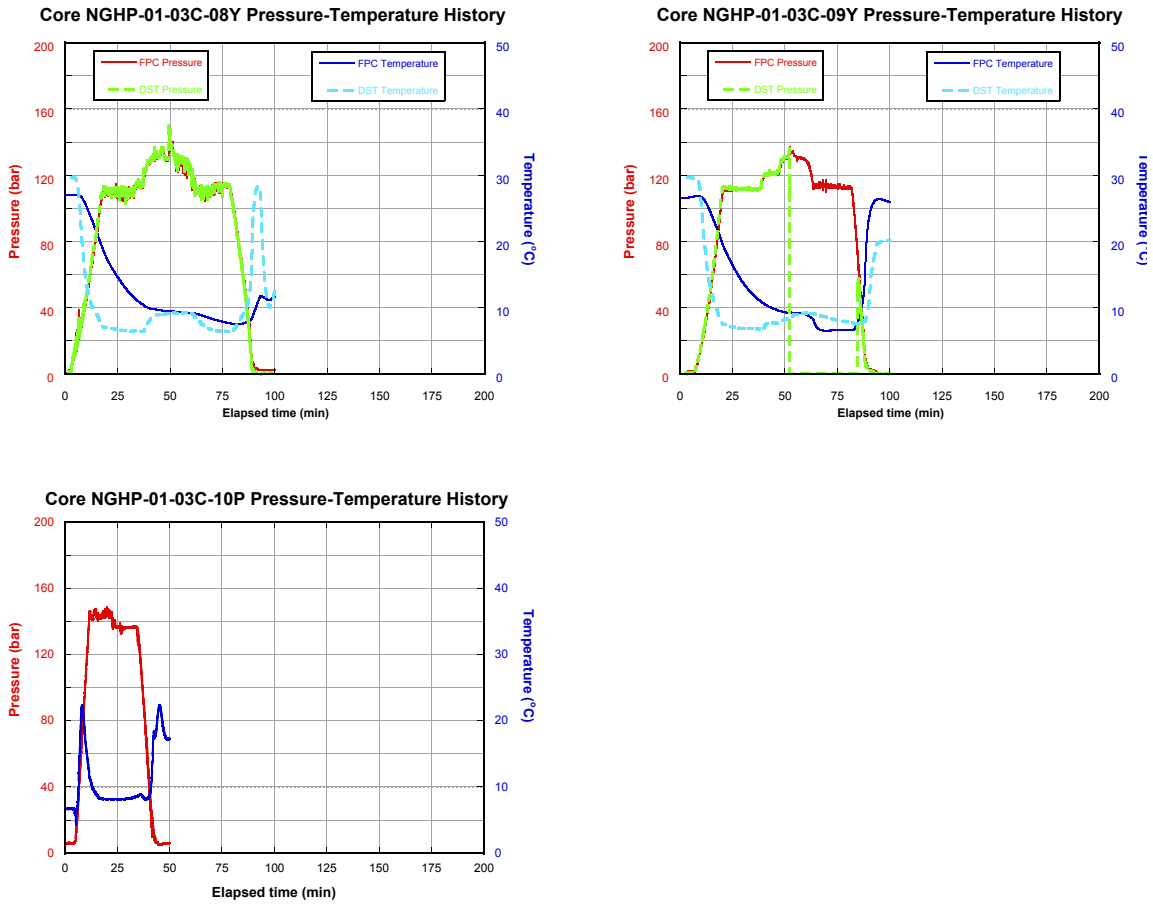

Figure 28. Temperature and pressure versus elapsed time for each pressure corer deployment as recorded by the corer's internal data logger. There are no data for Core NGHP-01-03B-27P. Core NGHP-01-03B-23Y is missing DST data at the beginning of the deployment.—Continued

gamma density measurements, which showed a somewhat stratified core in the x ray of the top half and sediment in the lower half (fig. 31A). The core was depressurized, releasing 1.06 L of methane, which is less than methane saturation at *in situ* temperature and pressure (table 24). After depressurization, the autoclave was again measured in the MSCL–P, and a final X-ray image was collected when the outer barrel was removed, showing the overall expansion of the core due to gas (fig. 31A). One chlorinity measurement was made on this core (538 mM, 82–95 cm), but this sample, taken at the bottom of the core, was probably contaminated with freshwater during core extrusion.

Core NGHP-01-03B-23Y (175.9 mbsf), collected in the zone of elevated electrical resistivity, retrieved a full core (0.88 m) at pressure (table 23). Core NGHP-01-03B-23Y was transferred to the MSCL–P and X-ray images, and gamma density and *P*-wave velocity measurements were collected (fig. 30). Core NGHP-01-03B-23Y was depressurized in the MSCL–P, releasing 4.97 liters of methane, corresponding to 0.9 percent methane hydrate as a percent of pore volume, or 10.8 mL of methane hydrate (table 24). A final MSCL–P scan was collected at atmospheric pressure which showed an intact core but with much lower density (fig. 31B). No chlorinity measurements were made on this core. There is some evidence to indicate that the gas hydrate in this core may have been concentrated in the lower half as indicated by the higher *P*-wave velocities and the nature of the degassing. There is no evidence to suggest that gas hydrate was concentrated in any particular interval. The gas hydrate may have been disseminated, or in finely distributed veins or layers (see "Singapore Pressure Core Studies" in the "Appendix").

Core NGHP-01-03C-07P (184 mbsf), collected in the zone of elevated electrical resistivity, retrieved a full core (1.00 m) at pressure (table 23). The core did not cool properly after recovery as the ice shuck was not filled with ice. The autoclave was placed in the MSCL–P for X-ray and gamma density measurements, which showed a relatively uniform upper core apart from denser layers of iron sulfide or carbonates, and sediment in the lower half (fig. 31C). Core NGHP-01-03-07P released 2.72 liters of methane, corresponding to 0.6 percent methane hydrate as a percent of pore volume or 4.9 mL of gas hydrate (table 24). After depressurization,

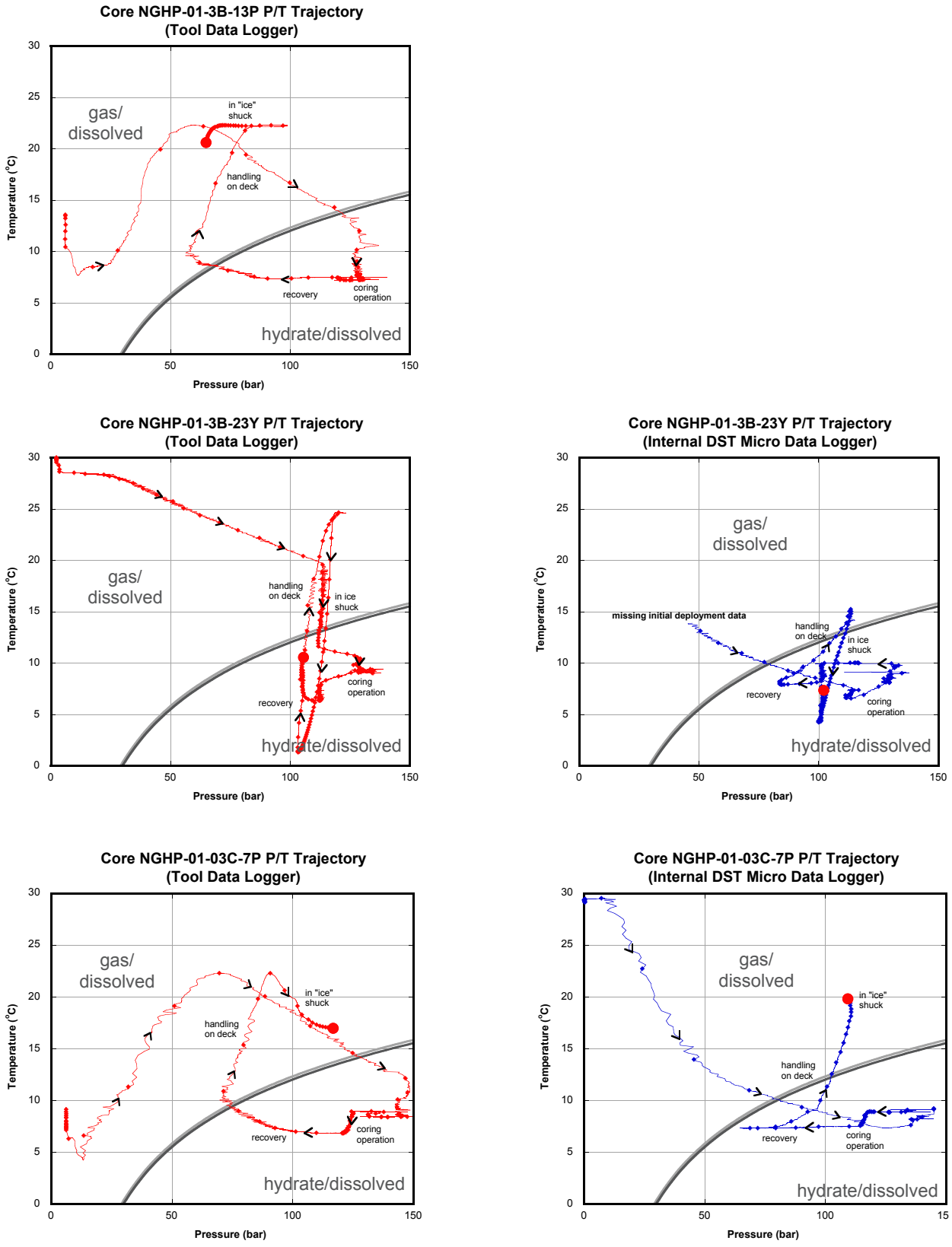

Figure 29. Temperature versus pressure for each successful pressure-corer deployment, showing trajectories relative to gas hydrate stability at 30 ppt and 35 ppt salinity, calculated from Xu (2002, 2004). Each small dot represents a minute. Large dot is final temperature and pressure of autoclave prior to data logger removal. Core NGHP-01-03B-23Y is missing DST data at the beginning of the deployment.

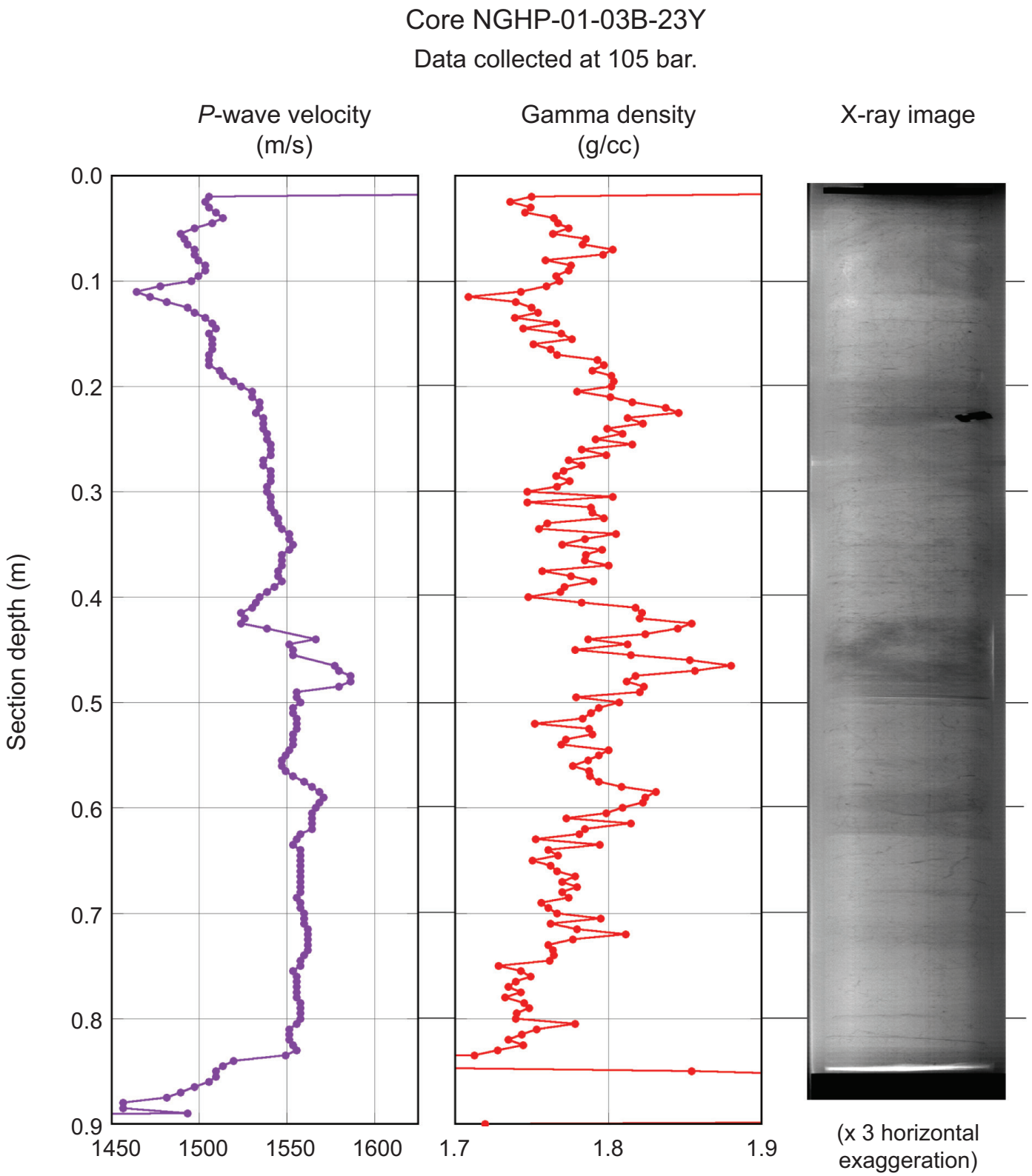

Figure 30. Data collected at near *in situ* pressure and 7 °C for Core NGHP-01-03B-23Y, including X-ray images, gamma density, and P-wave velocity. X-ray images have been stretched 300 percent in the cross-core direction to show detail.

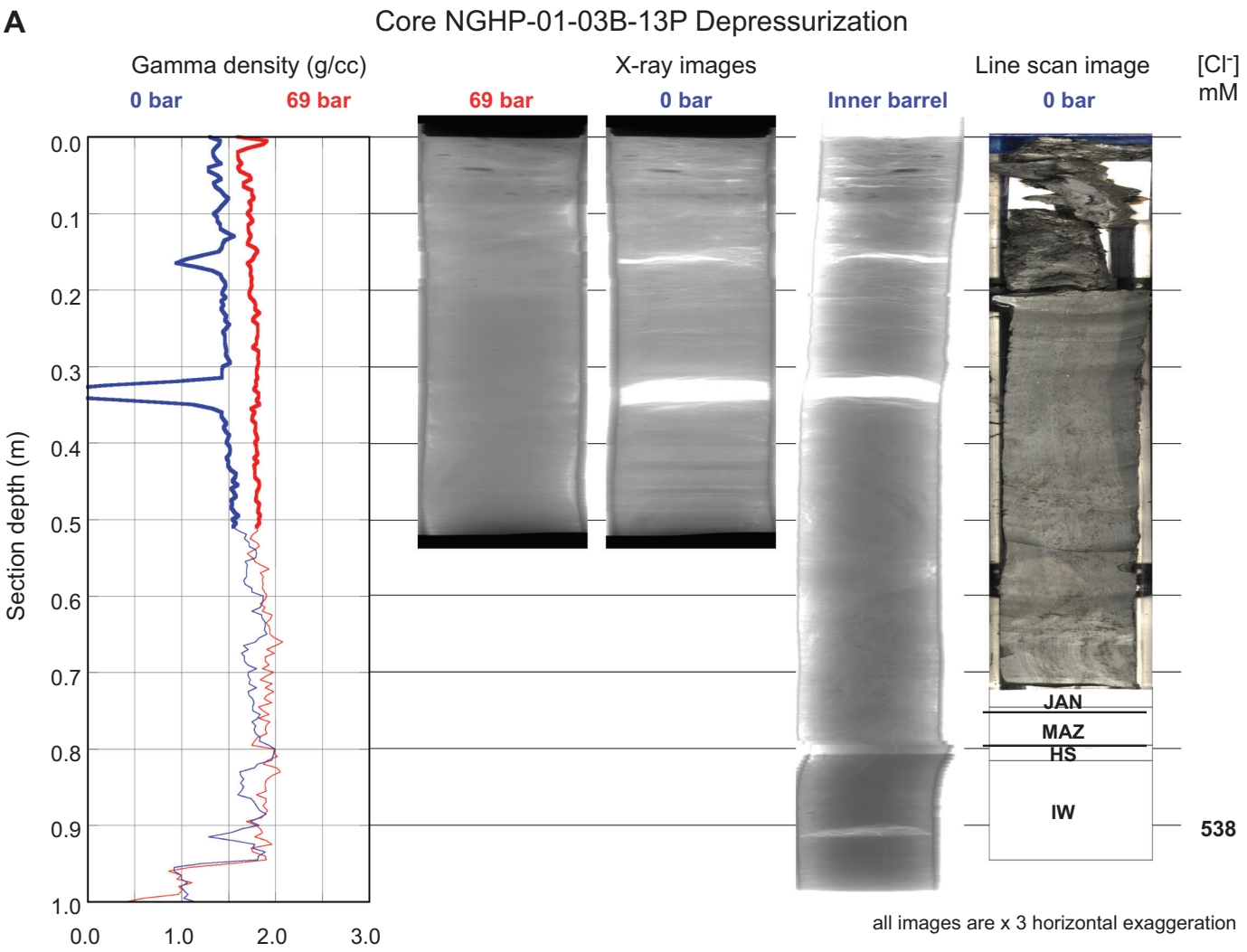

Figure 31. Summary of data taken from successful pressure cores before, during, and after depressurization, including gamma density profiles collected before and after depressurization, X-ray images collected before and after depressurization, and line scan images collected after depressurization.

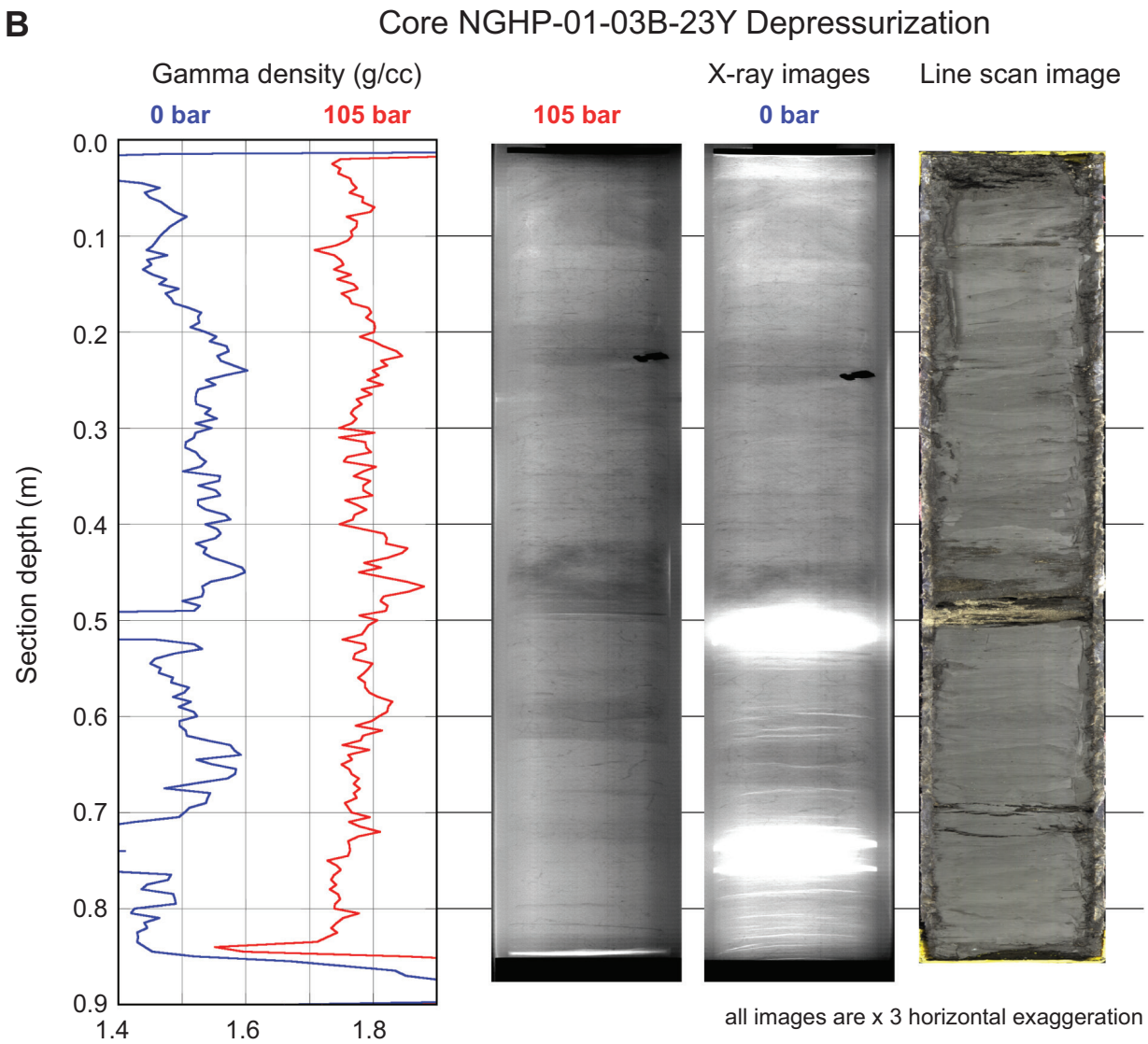

Figure 31. Summary of data taken from successful pressure cores before, during, and after depressurization, including gamma density profiles collected before and after depressurization, X-ray images collected before and after depressurization, and line scan images collected after depressurization.—Continued

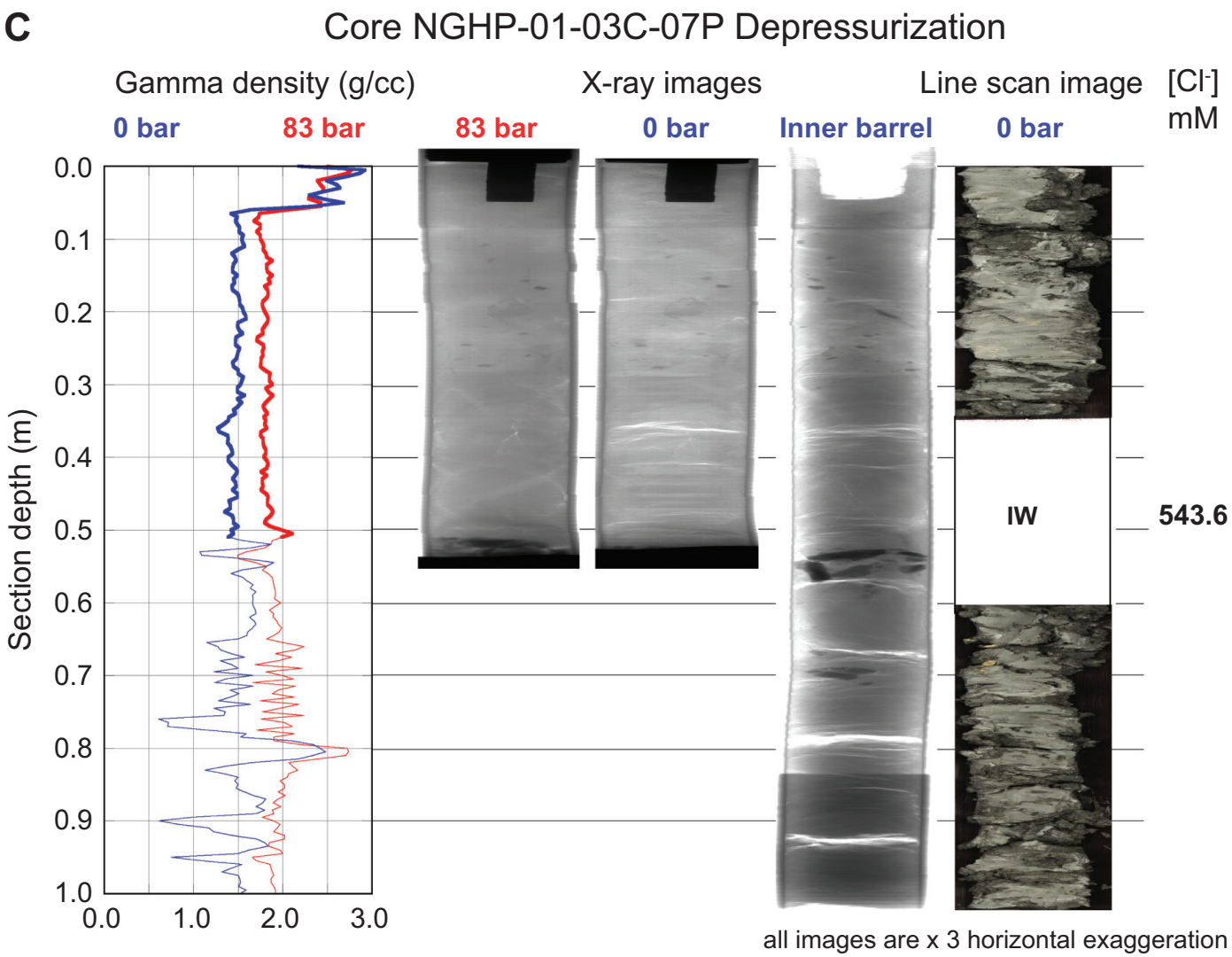

Figure 31. Summary of data taken from successful pressure cores before, during, and after depressurization, including gamma density profiles collected before and after depressurization, X-ray images collected before and after depressurization, and line scan images collected after depressurization.—Continued

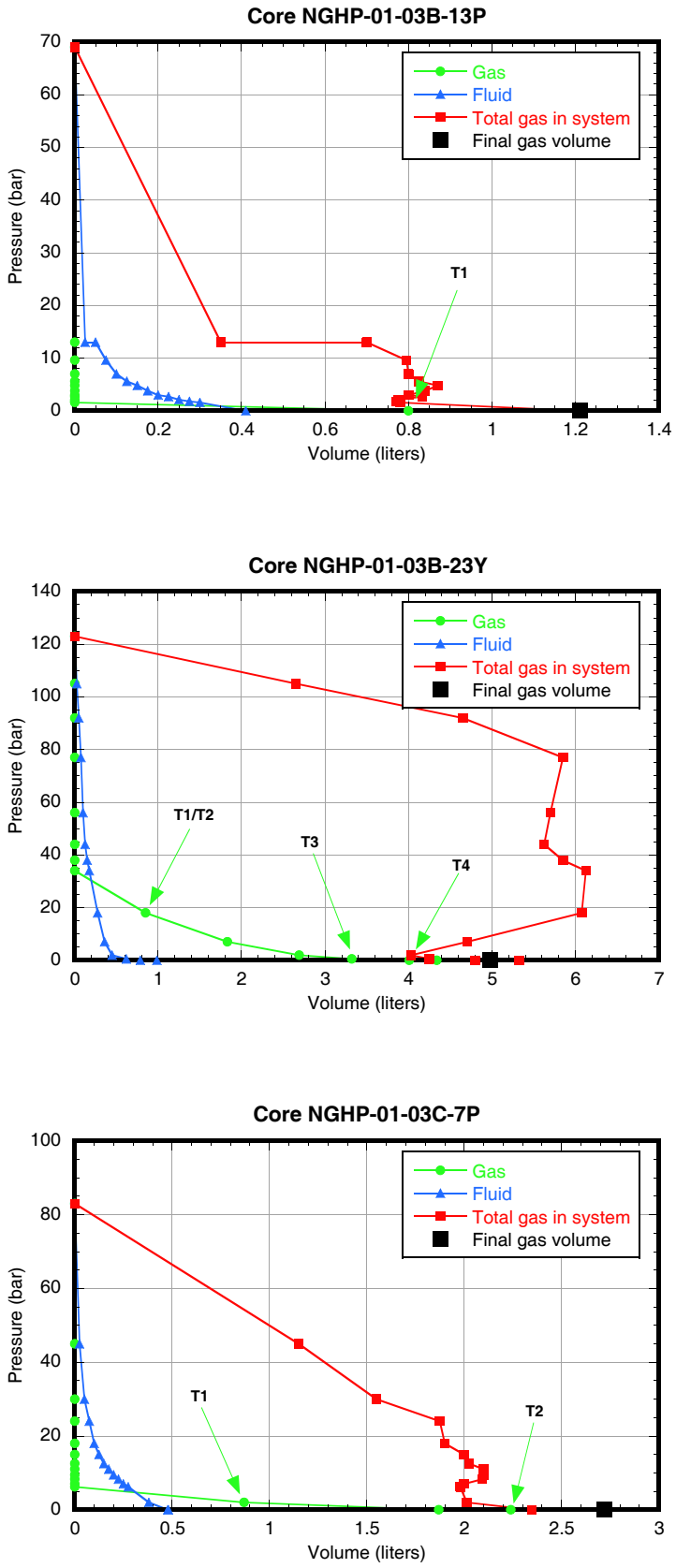

Figure 32. Pressure versus volume for successful pressure cores, also showing placement of gas samples (see "Organic Geochemistry"). [Green circles, collected gas; blue triangles, collected fluid; red squares, total gas in system (calculated as described in "Pressure Coring" section of the "Methods" chapter); large black square, final calculated gas from cores; T(number), gas samples]

Table 24. Methane hydrate volume and concentration in pore space for successful pressure cores at Site NGHP-01-03. Values required for calculation of methane hydrate concentration are also included.

Parameter	Units	NGHP-01-03B-13P	NGHP-01-03B-23Y	NGHP-01-03C-07P
Core diameter	mm	43.2	57	43.2
Sediment length	cm	100	88	100
Sediment porosity	%	60	57	54
Pore volume	*liters*	*0.875*	*1.273*	*0.787*
Volume methane collected	liters	1.06	4.97	2.72
Methane concentration in pore fluids	mM	6.1	0*	11
Total methane in core	*mmol*	*52.6*	*216.3*	*118.3*
In situ salinity	ppt	33.0	33.0	33.0
Methane saturation**	mM	84.2	111.1	115.4
Methane in pore fluids, assuming saturation	*mmol*	*70.0*	*137.0*	*90.8*
Excess methane	*mmol*	*-18.8*	*79.2*	*36.2*
Volume of methane hydrate	*ml*	*0.0*	*10.8*	*4.9*
*Methane hydrate, % of pore volume****	*%*	*0.0*	*0.9*	*0.6*

Notes:

Rows in *italics* are calculated parameters.

*Methane concentration (via headspace) was not measured on these cores. Zero concentration generates a conservative (minimum) estimate of gas hydrate volume.

**Methane saturation calculated from Xu (2002, 2004) using a water depth of 1,086 mbsl, a thermal gradient of 39 °C/km, a seafloor temperature of 6.5 °C, and the above salinities.

***Assuming all gas hydrate evenly distributed throughout the pore space.

the autoclave was again measured in the MSCL–P, and a final X-ray image was collected when the outer barrel was removed, showing the overall expansion of the core due to gas (fig. 31C). One chlorinity measurement was made on this core (543.6 mM, 35–47 cm), which was slightly lower than surrounding background chlorinities at the corresponding depths in Hole NGHP-01-03B of 550 mM. The x rays indicated no anomalous zone during the degassing suggesting that what little gas hydrate had existed was probably disseminated throughout the core.

Gas-Hydrate Concentration, Nature, and Distribution from Pressure Coring

Three of the 12 pressure cores at Site NGHP-01-03 were recovered at sufficient pressures to accurately assess the total concentration of methane and hence the predicted amount of gas hydrate. The calculated methane concentration for these cores is shown in figure 33 in relation to the phase boundaries for Structure I methane hydrate (All pressure cores released nearly pure methane with approximately 20 ppm ethane, confirming the suitability of Structure I methane hydrate for stability calculations; see "Organic Geochemistry"). The cores may or may not have hit the higher resistivity layers seen in Hole NGHP-01-03A near 170–196 mbsf, which were steeply dipping in the resistivity borehole image (see "Downhole Logging"). All of these cores were above the base of gas-hydrate stability and hence there is no information from pressure coring on the possible existence of free gas below this zone. Calculated concentrations of gas hydrate in the pore volume were nowhere over 1 percent, and Core NGHP-01-03B-13P may have been undersaturated with methane.

Downhole Logging

Logging While Drilling

Operations

After tagging the seafloor at 1,092 mbrf (driller's depth), Hole NGHP-01-03A was spudded at 0917 hr on May 22, 2006. LWD tools in the BHA included the GeoVISION resistivity, the EcoScope, the SonicVISION, and the TeleScope MWD. For details on each LWD tool and measurements, see the "Downhole logging" section in the "Methods" chapter.

To avoid washing out the hole near the seafloor, Hole NGHP-01-03A was spudded at a relatively low flow rate. The first 10 m were drilled at 100 gpm with a rotation rate of 20 rpm and a ROP of 25 m/h. Below 10 mbsf, the rotation rate was increased to 30 rpm; over the range of 30–35 mbsf, the rotation rate was increased to 60 rpm and the flow rate was increased until the LWD tools turned on (~370 gpm), continuing to drill with a ROP of 25 m/h. The target depth of 300 mbsf (1,392 mbrf) was reached at 0110 hr on May 23. The tools were back to the rig floor at 0715 hr, and all the data were downloaded and the tools rigged down by 1005 hr on May 23. (The depths in mbsf mentioned above are referenced to the seafloor depth tagged by the driller.)

Gas Monitoring with Real Time LWD/MWD Data

The LWD logs were acquired in the first hole drilled at Site NGHP-01-03 to plan coring and pressure-coring operations in subsequent holes. As Hole NGHP-01-03A was drilled without coring, the LWD data had to be monitored for safety to

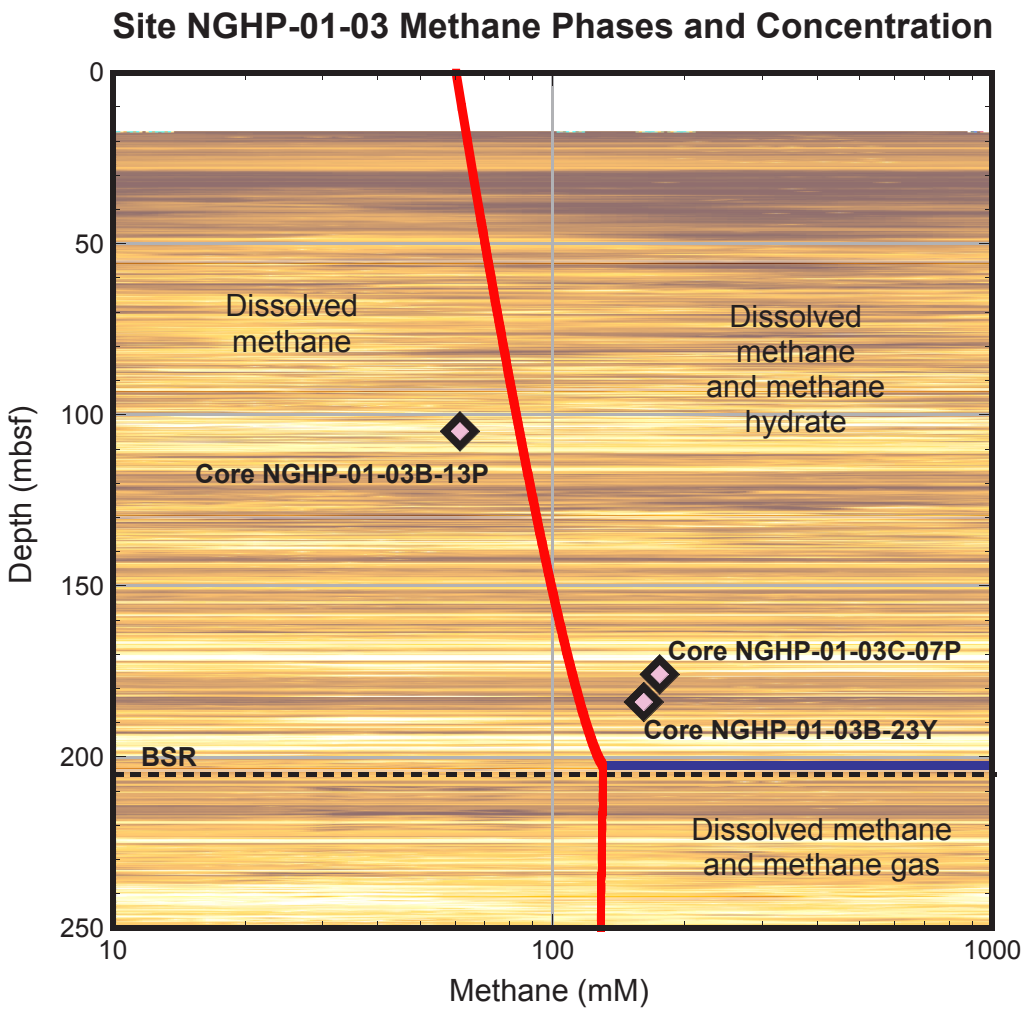

Figure 33. Methane phase diagram for Site NGHP-01-03, with total methane concentration measured from the three successful pressure cores at Site NGHP-01-03. The seafloor shipboard-calculated temperature (6.5 °C) and thermal gradient (39 °C/km) were taken from "Downhole Temperature Measurements" in "Physical Properties", the salinity was the average background salinity around the depths of the pressure cores (33 ppt; from table 5), and methane saturation was calculated according to Xu (2002, 2004). Background is LWD deep borehole resistivity (RAB) image. [LWD, logging-while-drilling; RAB, resistivity-at-bit]

detect gas entering the wellbore. As explained in the "Downhole Logging" section of the "Methods" chapter, the primary measurement used in the gas monitoring was the "annular pressure while drilling" (APWD) measured by the EcoScope tool in the borehole annulus. We looked for sudden decreases of more than 100 psi in the annular pressure, which could be due to low-density gas entering the wellbore. We also monitored pressure increases of the same magnitude, which could be due to fluid acceleration caused by a gas kick (Aldred and others, 1998).

Figure 34 shows the measured borehole fluid pressure profile in Hole NGHP-01-03A after subtraction of the hydrostatic pressure trend. This residual pressure curve shows only minor fluctuations that are well below the 100 psi level that would have required preventive action. We also monitored the coherence of the sonic waveforms acquired by the SonicVISION tool, focusing on the sound velocity in the borehole fluid. Gas indicators are loss of coherence in the waveforms and a slower sound velocity for the drilling fluid. We found no significant decrease of sonic waveform coherence throughout the interval drilled.

LWD Log Quality

Figure 34 also shows the quality control logs for Hole NGHP-01-03A. The two curves for rate of penetration (ROP) are an instantaneous rate of penetration (ROP_RM) and a rate of penetration averaged over the last five feet (1.5 m, ROP5_RM). The occasional large peaks in the instantaneous rate of penetration are artifacts due to depth fluctuations during pipe connections. The average ROP is about 20 m/h, which is sufficient to record high resolution GeoVISION resistivity images (for details, see "Downhole Logging" in the "Methods" chapter).

The density (DCAV) and ultrasonic caliper logs (UCAV) show an average borehole diameter that is around 11 in at 35 mbsf and decreases to about 10 in below 105 mbsf. The bit size (dashed line in fig. 34) is 9 7/8 in, and most of the borehole below 105 mbsf is in gauge. The density correction, calculated from the difference between the short- and long-spaced density measurements, is everywhere less than 0.2 g/cm^3 (fig. 34), suggesting that the density measurements should be of good quality.

Figure 35 is a summary of the LWD gamma ray, density, neutron porosity, and resistivity logs measured in Hole NGHP-01-03A. (SonicVISION results are not shown because they were processed on shore.) The gamma ray and resistivity logs measured by the GeoVISION (red and orange curves) and EcoScope LWD tools (green and blue curves) generally agree. The GeoVISION and EcoScope gamma ray curves have the same shape, but are offset by about 20–30 gAPI; this difference is most likely due to tool calibration. LWD gamma ray tools are calibrated with a total gamma ray standard that has a defined relative proportion of the radioactive elements (potassium (K), thorium (Th), and uranium (U)). If this relative proportion in the formation was different from the standard, the tool calibration would not be entirely accurate.

Figure 36 shows a comparison of the ring resistivity measured by GeoVISION with the attenuation and phase resistivity curves obtained by the EcoScope tool at different frequencies and coil spacings. For a given coil spacing, the phase-shift EcoScope resistivities have higher vertical resolution than the attenuation resistivities and thus show more detail.

Figure 35 also shows two bulk density curves: RHOB is the average density obtained by the EcoScope tool while rotating, while IDRO (image-derived density) is the value of density measured when the sensors were in closest contact with the formation. The two density curves are very close. The large variability of the densities above 105 mbsf, and particularly of the image-derived values, may be due to the hole enlargements shown on the caliper logs (fig. 34). However both curves show a good agreement with core-derived measurements in this interval. At greater depth, the log densities are generally higher than the core data while following the same trend. The lower core measurements values could be due to the sediment expansion as the samples are brought to the surface.

The bottom-simulating reflector (BSR) that should mark the bottom of the gas-hydrate stability zone was estimated to be at a depth of 209 mbsf in this hole. The only change in the LWD logs near this depth is a change from a general trend of decreasing density and resistivity to an increasing trend at 211 mbsf (fig. 35).

The depths relative to seafloor were fixed for all the LWD logs by identifying the step change in the GeoVISION gamma ray log at the seafloor. For Hole NGHP-01-03A, the gamma ray logging pick for the seafloor was at a depth of 1,087 mbrf, 5 m above the initial depth estimated by the drillers (1,092 mbrf). The rig floor logging datum was located 10.5 m above sea level.

LWD Porosities

Sediment porosities can be determined from analyses of recovered cores and from downhole measurements (see "Physical Properties" and "Downhole Logging" in the "Methods" chapter). Sediment porosities were calculated from the LWD density and neutron logs in Hole NGHP-01-03A. Core-derived physical property data, including porosities (see "Physical Properties"), can be used to calibrate and evaluate the log-derived sediment porosities.

Because the density log (RHOB) is generally less noisy than the image-derived values (IDRO, see fig. 35), we used this curve to calculate porosity (ϕ) with the standard density-porosity relation: $\phi = (\rho_g - \rho_b) / (\rho_g - \rho_w)$. We first used a constant water density (ρ_w) equal to 1.03 g/cm^3 and a grain/matrix density (ρ_g) equal to 2.75 g/cm^3. After revisiting the sites for coring, density measurements on core samples and pore water chemistry analysis allowed us to correct this first estimate for grain density and water salinity, using Fofonoff (1985) to calculate the pore water density. Despite these corrections, the "corrected density porosity" curve is barely distinguishable from the original density porosity estimate (fig. 35). The resulting density log-derived porosities from Hole NGHP-01-03A range from about 60 percent at 30 mbsf to about 50 percent at 245 mbsf.

The LWD neutron porosity log from Hole NGHP-01-03A (fig. 35) yielded sediment porosities ranging from an average value near the seafloor of about 65 percent at 30 mbsf to about 55 percent at 245 mbsf. Porosities measured by the neutron log are expected to be higher than those computed from the density log in clay-rich sediments, because the neutron log essentially quantifies hydrogen abundance, and counts hydrogen in clay minerals as porosity. However, the neutron porosity measured by the EcoScope tool shown in figure 35 is the "best thermal neutron porosity" (BPHI). It has been corrected to reduce the effect of clay (Adolph and others, 2005), and it is only marginally higher than the density porosity. While the density porosities are consistently less than the neutron porosity in the deep portion of the hole, the density porosities approach the neutron porosity at depths above 105 mbsf. This shallow interval is where the hole is enlarged (see the caliper logs in fig. 35), suggesting that the logged values of density may be too small above 105 mbsf.

Both neutron and density-derived porosity logs are in good agreement with the porosity measurements made on core samples. The generally higher log-derived values above ~60 mbsf are likely due to the hole enlargement.

LWD Borehole Images

The GeoVISION and EcoScope LWD tools generate high-resolution images of borehole log data. The EcoScope tool produces images of density and hole radius (computed on the basis of the density correction, which depends on the borehole standoff). The GeoVISION produces a gamma ray image and shallow, medium, and deep depth of investigation resistivity images.

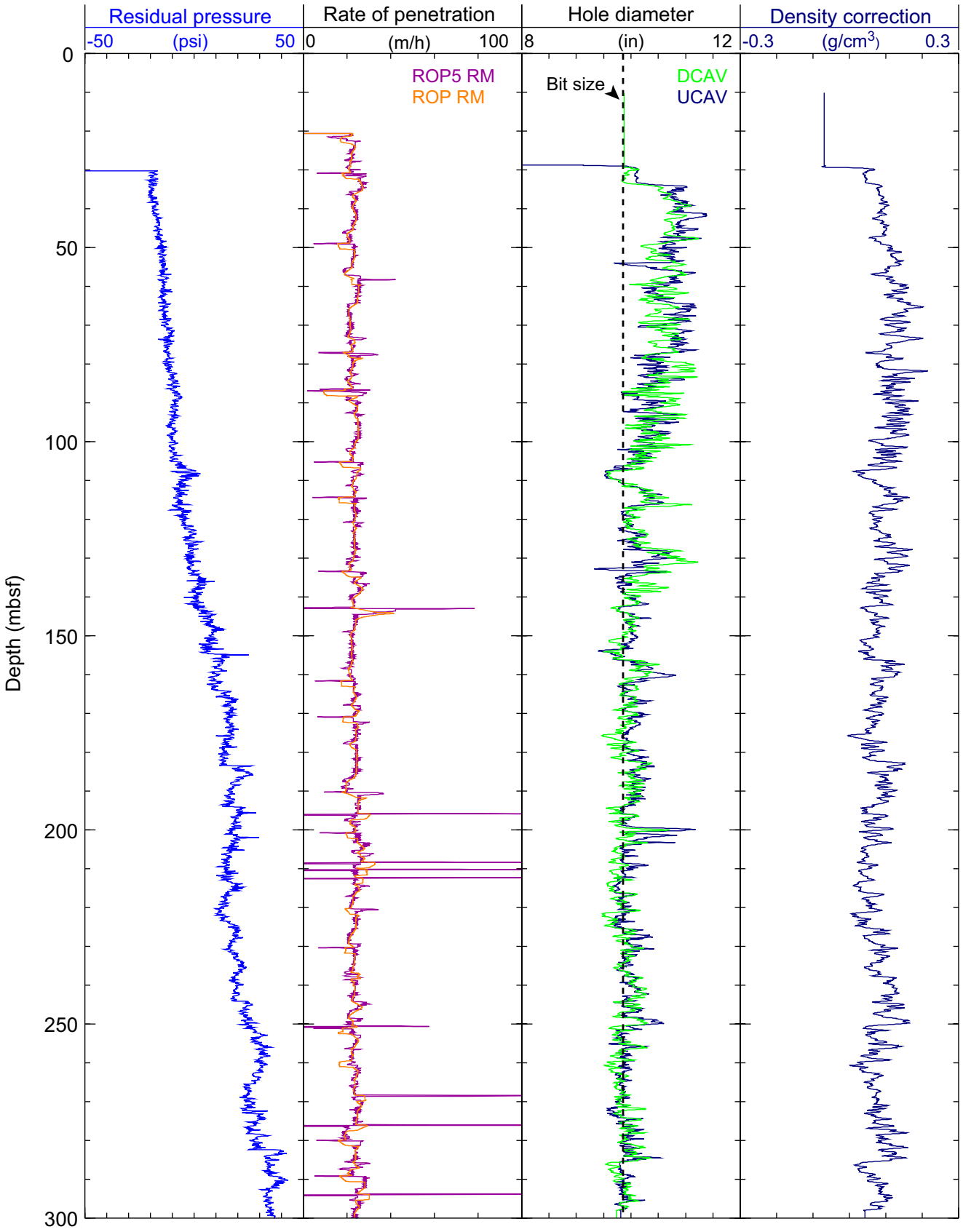

Figure 34. Monitoring and quality control LWD/MWD logs from Hole NGHP-01-03A. [LWD/MWD, logging-while-drilling/measurement-while-drilling; ROP, Rate of penetration; ROP_RM, Instantaneous rate of penetration; ROP5_RM, Rate of penetration averaged over a 5-ft interval; UCAV, Ultrasonic caliper; DCAV, Density caliper]

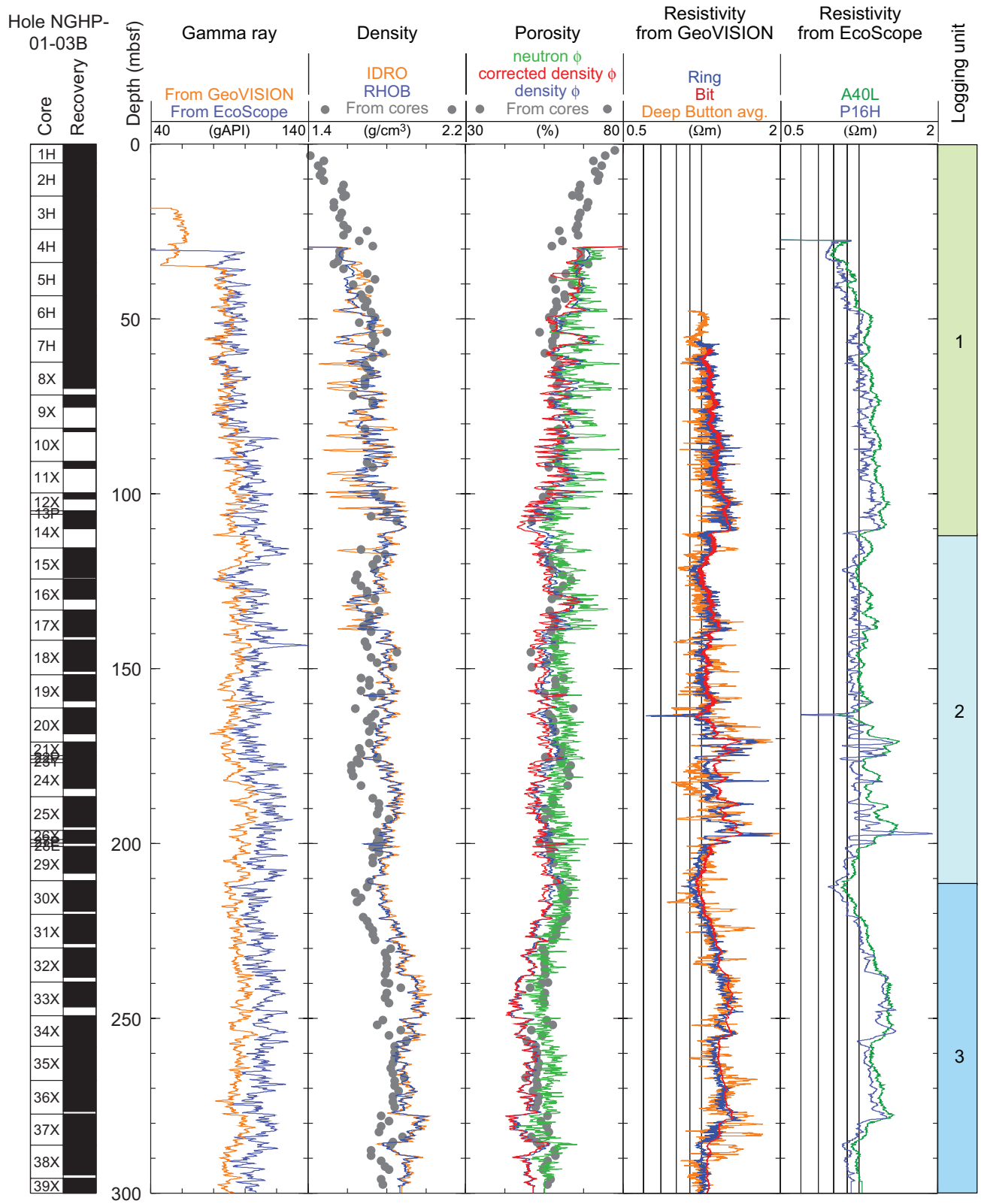

Figure 35. Summary of LWD log data from Hole NGHP-01-03A. [LWD, logging-while-drilling; gAPI, American Petroleum Institute gamma ray units; IDRO, Image-derived density (EcoScope); RHOB, Bulk density (EcoScope); neutron, Thermal neutron porosity (EcoScope); corrected density, density porosity with core derived grain densities (EcoScope); density, density porosity; RING, Ring resistivity (GeoVISION); BIT, Bit resistivity (GeoVISION); Deep Button avg., Button deep resistivity (GeoVISION); A40L, Attenuation resistivity measured at 400 kHz and a transmitter-receiver spacing of 40 in (EcoScope); P16H, Phase-shift resistivity at 2 MHZ and a transmitter-receiver spacing of 16 in (EcoScope)]

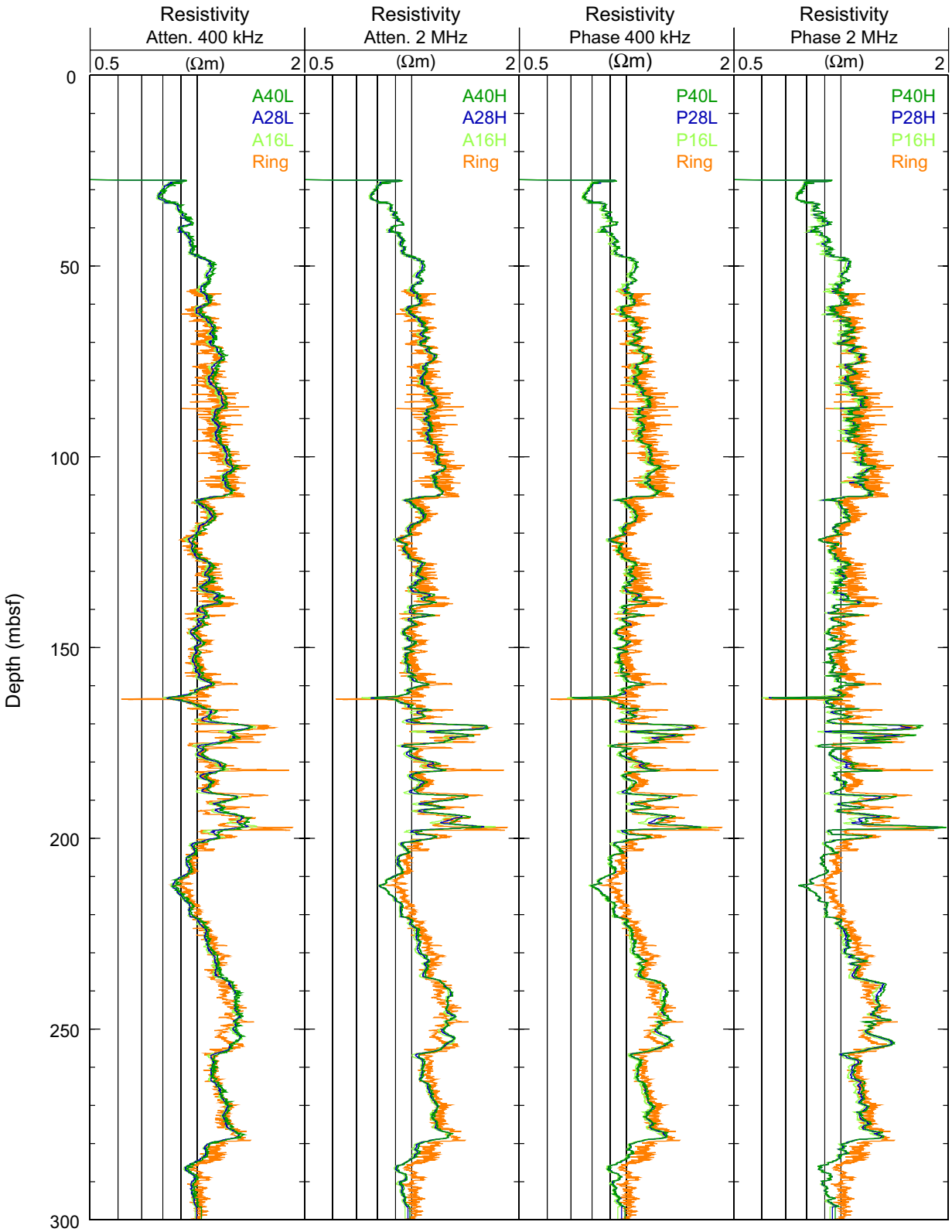

Figure 36. Comparison of LWD resistivity curves from Hole NGHP-01-03A. [LWD, logging-while-drilling; RING, Ring resistivity (GeoVISION); AXXL, Attenuation resistivity measured at a frequency of 400 kHz, where XX is the transmitter-receiver spacing in inches (EcoScope); AXXH, Attenuation resistivity measured at a frequency of 2 MHz, where XX is the transmitter-receiver spacing in inches (EcoScope); PXXL, Phase-shift resistivity measured at a frequency of 400 kHz, where XX is the transmitter-receiver spacing in inches (EcoScope); PXXH, Phase-shift resistivity measured at a frequency of 2 MHz, where XX is the transmitter-receiver spacing in inches (EcoScope)]

Figure 37 shows some of the LWD images collected by the EcoScope and GeoVISION tools. It should be noted that the display in figure 35 is highly compressed in the vertical direction. The unwrapped images are about 80 cm wide (for a 10 in diameter borehole) and the vertical scale is compressed relative to the horizontal by a factor of about 55:1. These high-resolution images can be used for detailed sedimentological and structural interpretations and to image gas-hydrate distribution in sediments (for example, in layers, nodules, fractures). Gas-hydrate-bearing sediments exhibit high resistivities within intervals of uniform or low bulk density. Layers with high resistivities and high densities are likely to be low porosity, compacted, or carbonate-rich sediments. The two resistivity images in figure 37 correspond to two depths of investigation (for details, see "Downhole Logging" in the "Methods" chapter).

Wire-Line Logging

Operations

After drilling Hole NGHP-01-03C to 300 mbsf ended at 0930 hr on July 3, 2006, the hole was conditioned for logging with several sweeps of sepiolite and a complete wiper trip. One last DVTP measurement was made, and the hole was displaced with 110 bbl. of 10.5 ppg barite before pulling the bit to logging depth at 1,144 mbrf (=57 mbsf). At 1715 hr the top drive was removed and the logging equipment was brought to the rig-floor.

Rig up of the first tool string, the triple combo, started at 1850 hr and the tool was complete and lowered into the hole at 1950 hr. The bottom of the toolstring passed the bit without problem at 2050 hr but then could not pass below 1,154 mbrf, with about 20 m of tool-string still inside the pipe. After several unsuccessful attempts at passing the obstruction, the tool was brought back inside the pipe and the bit raised to 1135 mbrf, to figure if the obstruction was inside or outside the pipe. At 2150 hr, the tool was completely in open hole and reached the bottom of the hole at 1,387 mbrf at 2225 hr, when we started the log up. By 2320 hr the tool was completely inside the pipe, without encountering any obstacle, and the logging pass was complete at 2335 hr, when the gamma ray log identified the seafloor at 1,087 mbrf. The caliper had shown that the hole was irregular, with some ledges and washout, but was of sufficient quality to expect good data from the FMS-sonic and VSP runs. At 0035 hr on July 4, 2006, the toolstring was back to the surface, and it was disassembled at 0135 hr, when we started the FMS-sonic rig-up.

The FMS-sonic tool-string was complete at 0215 hr, and rigged into hole (RIH) at 0230 hr. It reached the bit at 0340 hr, but again could not go deeper than 1154 mbrf, 10 m below the bit. All attempts at passing this obstruction failed, and at 0425 hr it was decided to bring the tool back to the surface and lower the drill string to where the caliper from the triple-combo indicated a larger hole.

The tool string was back on deck at 0530 hr and partially rigged down while the bit was set at 1,192 mbrf. It was then rigged back up and RIH at 0710 hr, and it passed the bit without trouble before reaching the bottom of the hole (1,387 mbrf) at 0835 hr. Two full passes were made over the entire open hole available, but the caliper arms could not close or open properly at the end of the first pass, and only poor quality FMS data were recorded during the second pass. This pass was complete at 1040 hr when the tools were brought back inside the pipe, and they were at the surface at 1125 hr.

The FMS-sonic string was rigged down at 1205 hr, and the VSI tool for the final VSP run was ready at 1230 hr. After RIH at 1350 hr, the VSI was at the bit, at 1,192 mbrf, at 1335 hr. Once again the tool string had trouble exiting the pipe, and it could not go deeper than 1,194 mbrf. It was then completely in open hole, but its top was only ~2 m below the bit. At 1450 hr, no progress had been made; as time was running short before the end of daylight, there was also some concern that damage could have been done to the tool because of its light weight and its location near the bit. Hence it was decided to abort the VSP, and after bringing the tool back inside the pipe with significant overpull, the VSI was back to the surface at 1535 hr. The only discernable damage was to the wire line immediately above the tool. At 1550 hr the VSI was rigged down, and the rig floor was clear at 1630 hr for transit to Site NGHP-01-07.

Wire-Line Log Quality

Figure 38 shows the basic logs measured by the triple combo in Hole NGHP-01-03C. In the left panel, the hole size calculated from the caliper log shows an irregular hole, with an alternance of washouts and ledges where the hole can be significantly smaller than the bit size. Despite the irregular size, the caliper arm appears to have lost contact with the borehole wall in only a few places, indicating that the quality of the data should be only moderately affected. An indication of the general good data quality is the good agreement between the density log and the core measurements. While this naturally coincides with a good agreement between the porosity measurements on core samples and the density-derived porosity log, the neutron porosity log indicates much larger values. This difference is due to the large hole in some intervals, but it is mainly related to the large amount of clay in this formation, which is not corrected for in the neutron porosity log.

The sonic logging waveforms and coherence data in figure 39 also confirm that the monopole and the upper dipole waveforms were not seriously affected by the irregular hole and displayed a strong coherence over most of the interval logged. However the compressional velocity (V_p) is very close to the velocity in the borehole fluid and required further processing to derive a reliable profile. A subtle V_p decrease with depth at ~210 mbsf could indicate a mild BSR. Above 180 ~mbsf, the shear velocity of these unconsolidated sediments is too low for the flexural arrival to be recorded within the 20 ms recording window.

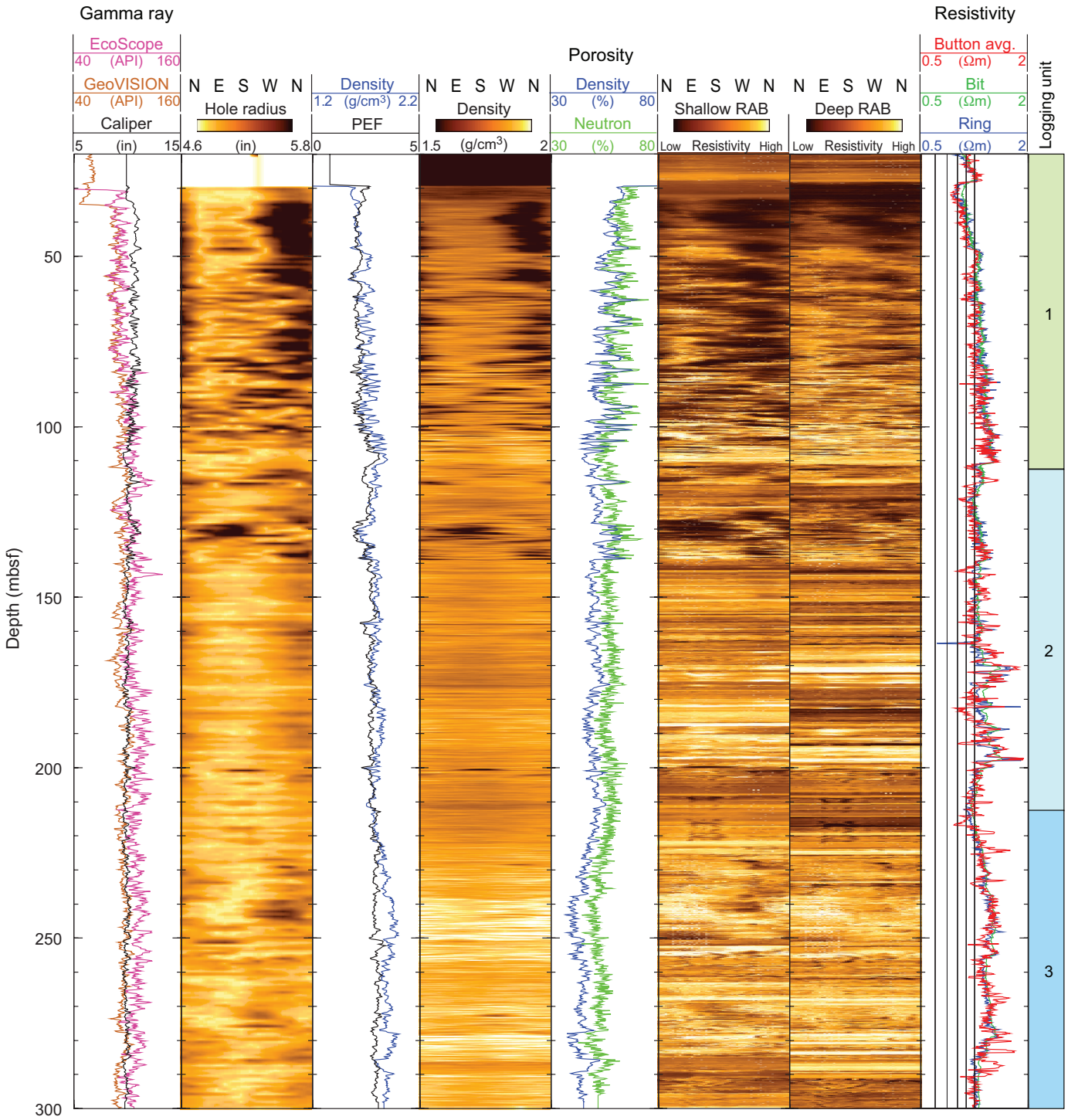

Figure 37. LWD image data from Hole NGHP-01-03A. [LWD, logging-while-drilling; API, American Petroleum Institute gamma ray units; RAB, resistivity-at-bit image obtained by the GeoVISION tool]

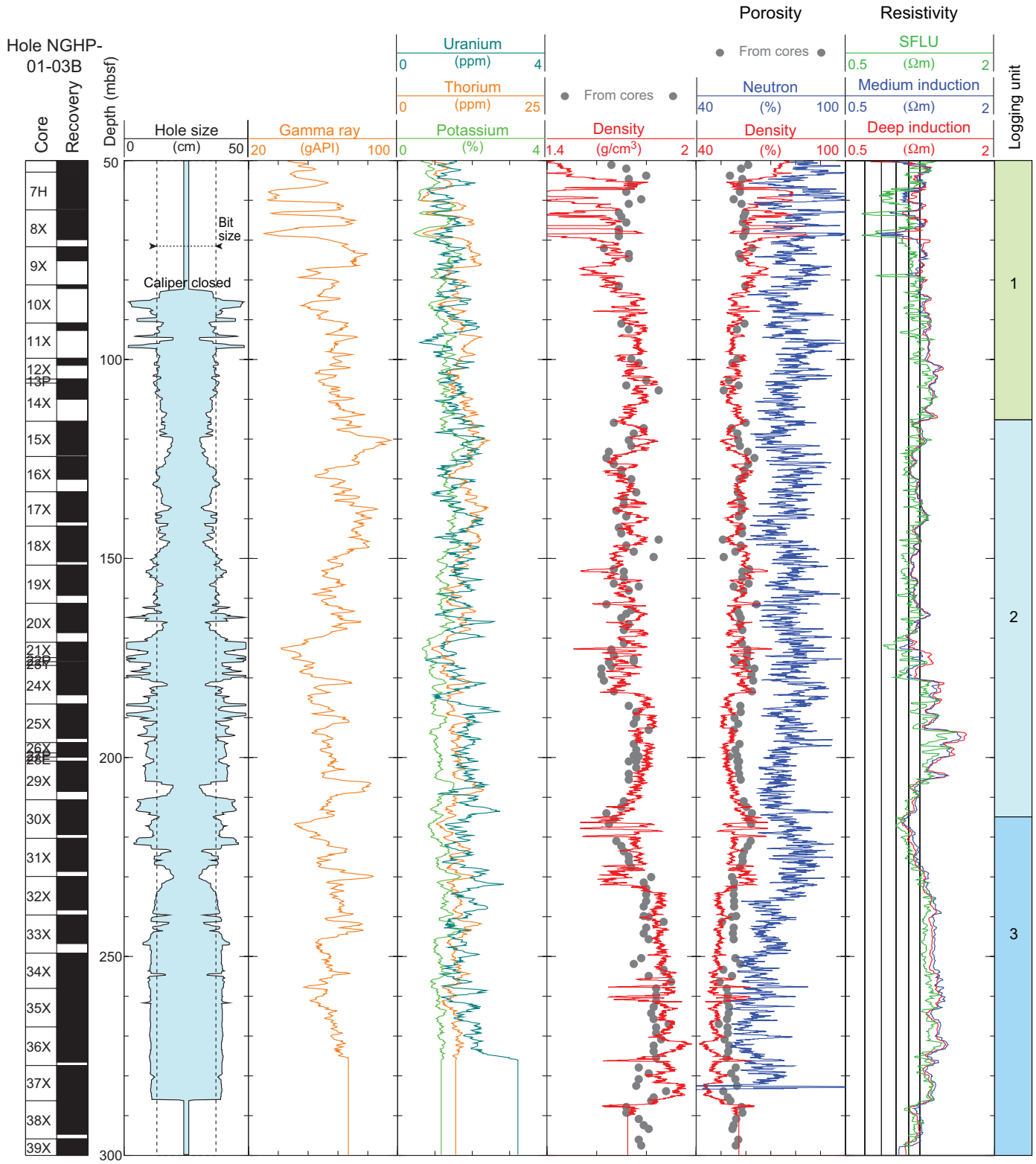

Figure 38. Summary of the wire-line logs recorded in Hole NGHP-01-03C. [SFLU, Spherically focused log]

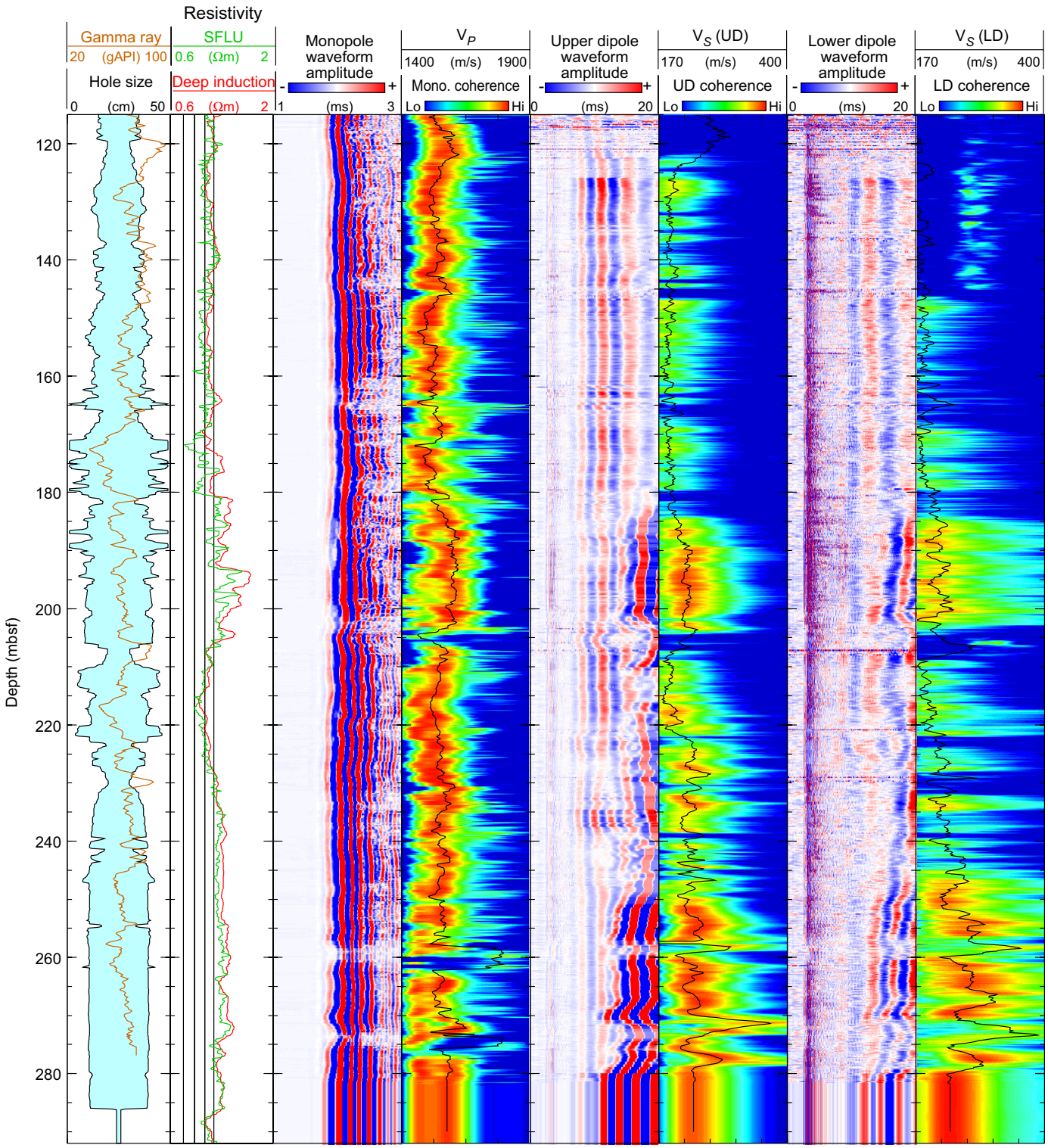

Figure 39. Sonic waveform data, *P*-wave and *S*-wave velocities measured by the DSI wire-line log in Hole NGHP-01-03C. [V_p, P-wave velocity; V_S, *S*-wave velocity; LD, Lower dipole; UD, Upper dipole] Note: The hole size and the gamma ray and resistivity logs are shown for quality control and correlation.

Logging while Drilling and Wire-Line Logging Comparison

Figure 40 shows a comparison of the LWD and wire-line logging data recorded at Site NGHP-01-03. The most obvious difference is between the shape of the holes measured by the LWD tool string and the two wire-line runs. This difference is ultimately responsible for most of the discrepancies observed between the other data sets. While the LWD measurements are made very briefly after the bit enters the formation, the coring process provides much more time and disturbances for the hole to deteriorate before the wire-line logs are acquired. Despite this, most of the LWD and wire-line logs display very similar trends, in particular the density and resistivity data. The largest difference is between the neutron porosity logs, which is due to the correction for clay content which is applied to the LWD data but not the wire-line neutron log. In this clay-rich formation, such correction is necessary to derive a reliable porosity estimate, which is confirmed by the good agreement between the LWD neutron porosity log and the core-derived porosity measurements. The difference between the two wire-line gamma ray logs and the LWD log is mostly due to differences in the calibration of the tools. The only difference between the LWD and wire-line resistivity curves, which follow remarkably similar trends, is between ~165 and 175 mbsf, where the LWD data indicate higher resistivities. This might possibly reflect some local heterogeneity in the minor gas-hydrate occurrences at this site.

Logging Units

The combined analysis of the gamma ray, density, porosity, resistivity, and velocity logs recorded by the wire-line and LWD tools can help delineate three logging units (see figs. 35, 37 and 38):

Logging unit 1 (~20–115 mbsf) is characterized by the steady increase with depth in density and resistivity, indicating increasingly consolidated sediments. Gamma ray values also increase slightly with depth within this logging unit, which coincides with Lithologic Unit I (see "Lithostratigraphy").

The top of Logging unit 2 (~115–215 mbsf) is defined by a sharp drop in resistivity with depth, and the rest of the unit is characterized a high variability in the resistivity logs which could be related to the heterogeneously distributed low amount of gas hydrate that could be present in the formation. The highest resistivity values above 200 mbsf could coincide with the bottom of the gas-hydrate stability field, which was estimated around ~220 m in this area.

The top of Logging unit 3 at ~215 mbsf is also defined by a drop in resistivity, while the rest of the unit is characterized by a renewed increase in resistivity and density with depth. Below 250 mbsf, the data become mostly uniform.

Gas-Hydrate and Free Gas Occurrence

As previously discussed (see "Downhole Logging" in the "Methods" chapter), the presence of gas hydrate is generally characterized by increases in electrical resistivity and acoustic velocity that are not accompanied by a corresponding porosity decrease. A decrease in porosity alone in a water-saturated sediment can result in an increase in resistivity and acoustic velocity. Resistivity logs in Hole NGHP-01-03A show a general negative correlation with porosity (fig. 35), suggesting that little or no gas hydrate is present.

To make a quantitative estimate of the amount of gas hydrate at Hole NGHP-01-03A, we followed the procedure described in "Downhole logging" in the "Methods" chapter, to apply the Archie relationship to the resistivity and porosity logs recorded in Hole NGHP-01-03A. The procedure and the results are shown in figure 41. The pore fluid resistivity (R_w) was estimated from Fofonoff (1985) using a linear temperature profile based on the temperature measurements made at this site (6 °C at the seafloor and a gradient of 30 °C/km, see "Physical properties") and water salinity measured at this site. The estimated m curve is derived from R_w, the porosity (ϕ) and resistivity (R_t) logs ($m_{est} = -\log F/\log\phi$, where $F = R_t / R_w$). The chosen value of $m = 2.2$ is given by the baseline of this curve in the low-resistivity water-saturated formation. Using the porosity log and Archie's equation ($R_0 = (a\, R_w) / \phi^m$), we derive the predicted resistivity of the water-saturated formation R_o. A qualitative influence of gas hydrate on the resistivity log is indicated by the difference between the R_0 and the measured resistivity R_t. The actual water saturation, assumed to be the numerical complement of the hydrate saturation, is $S_w = (R_0/R_t)^{1/n}$, where n=2 (Pearson and others, 1983). We used the density porosity computed from the image-derived density (IDRO) and the resistivity from the 16 in, phase-shift, high-frequency propagation resistivity (P16H) measured by the EcoScope tool. We used the P16H curve because it is the resistivity with the highest vertical resolution measured by the EcoScope.

As noted earlier, porosity and resistivity curves in Hole NGHP-01-03A generally mirror each other, so that the computed water-saturated resistivity R_0 is very close to the measured resistivity R_t and the water saturation S_w is close to 100 percent throughout most of the logged interval (fig. 41). The only exceptions where the computed S_w is less than 100 percent are in the uppermost section of the hole, above 105 mbsf, and in three more intervals (128–140 mbsf, 165–177 mbsf, and 193–203 mbsf). As noted earlier, it is likely that the logged densities are too low in the interval above 105 mbsf because of poor hole conditions, and a corresponding overestimate of porosity could make the computed water-saturated resistivity R_0 less than the measured resistivity R_t. This is also probably the case in the interval 128–140 mbsf, where the hole is enlarged and the density may have been underestimated. On the other hand, the two intervals at 165–177 mbsf and 193–203 mbsf correspond to peaks in the measured resistivity and are more likely to correspond to gas hydrate-bearing intervals.

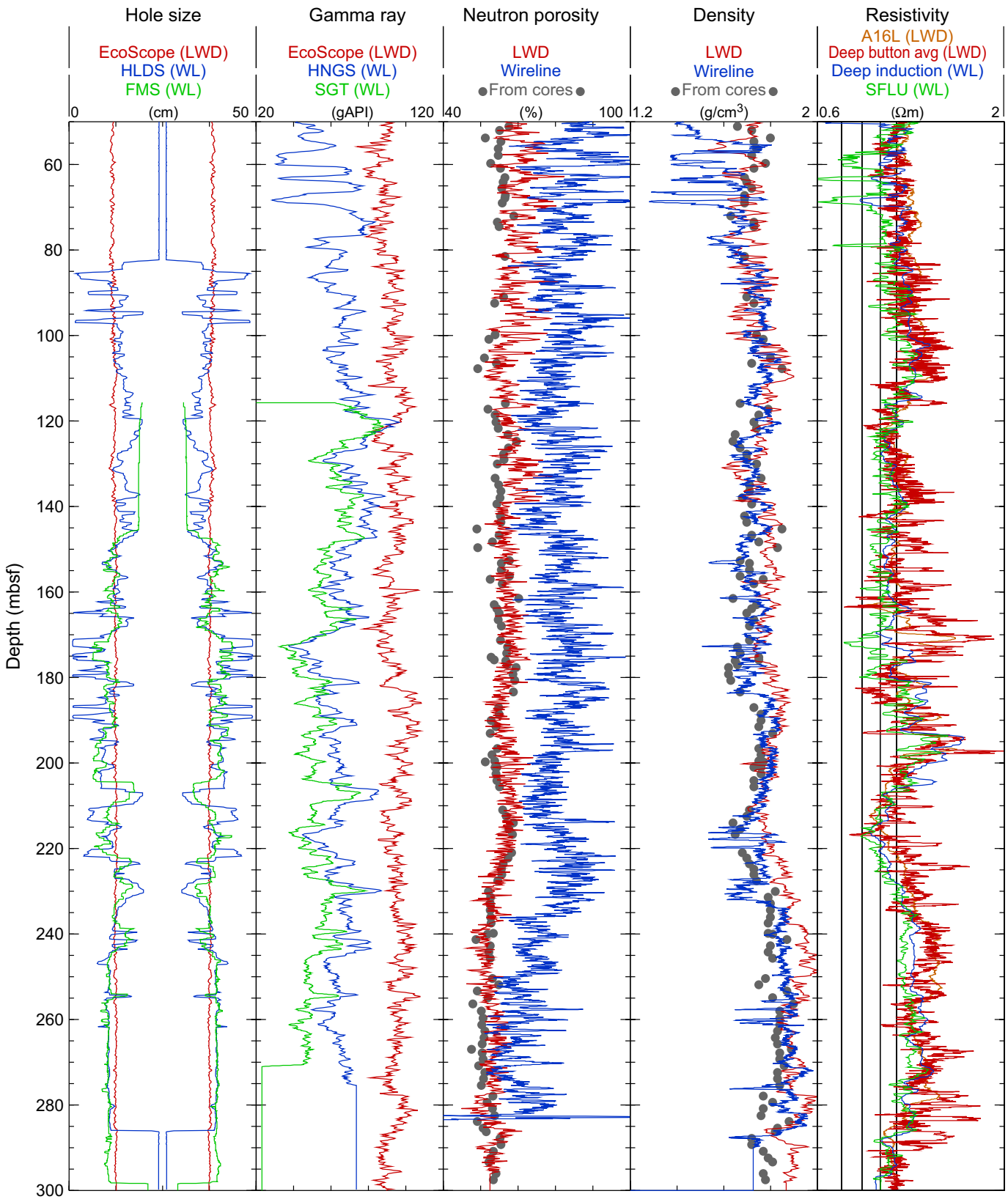

Figure 40. Comparison of LWD (Hole NGHP-01-03A) and wire-line log data (Hole NGHP-01-03C). [LWD, logging-while-drilling; WL, wire-line; HLDS, Hostile Environment Litho-Density Sonde; HNGS, Hostile Environment Gamma Ray Sonde; SGT, Scintillation Gamma Ray Tool; SFLU, Spherically focused log]

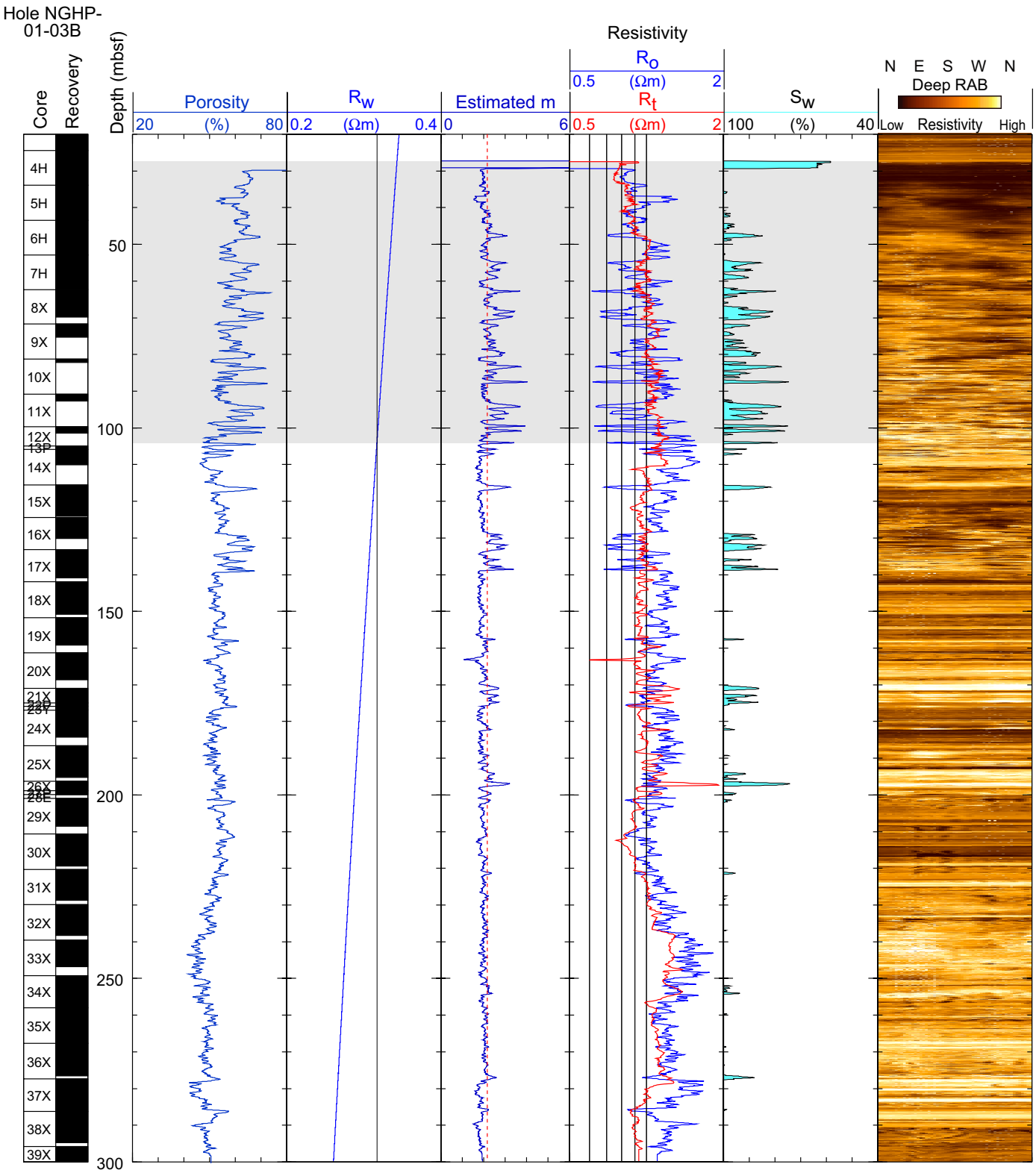

Figure 41. Water saturations from Archie's equation and LWD porosity and resistivity logs in Hole NGHP-01-03A. The gray area indicates degraded data quality. [LWD, logging-while-drilling; R_w, Formation water resistivity; R_0, Computed formation resistivity for 100 percent water saturation; R_t, Measured resistivity; S_w, water saturation]

References Cited

Adolph, B., Archer, M., Codazzi, D., el-Halawani, T., Perciot, P., Weller, G., Evans, M., Grant, J., Griffiths, R., Hartman, D., Sirkin, G., Ichikawa, M., Scott, G., Tribe, I., and White, D., 2005, No more waiting—Formation evaluation while drilling: Oilfield Review, Autumn 2005, p. 4–21.

Aldred, W., Cook, J., Bern, P., Carpenter, B., Hutchinson, M., Lovell, J., Rezmer-Cooper, I., and Leder, P.C., 1998, Using downhole annular pressure measurements to improve drilling performance: Oilfield Review, Winter 1998, p. 40–55.

Bjerrum, L., 1972, Embankments on soft ground: Proceedings of the ASCE Specialty Conference on Performance of Earth and Earth-Supported Structures, Purdue University, v. II, p. 1–54.

Davis, E.E., Hyndman, R.D., and Villinger, H., 1990, Rates of fluid expulsion across the northern Cascadia accretionary prism—Constraints from new heat flow and multichannel seismic reflection data: Journal of Geophysical Research, v. 95, p. 8869–8889.

Duan, Z., Møller, N., Greenberg, J., and Weare, J.H., 1992, The prediction of methane solubility in natural waters to high ionic strengths from 0° to 250 °C and from 0 to 1600 bar: Geochimica et Cosmochimica Acta, v. 56, p. 1451–1460.

Fofonoff, N.P., 1985, Physical properties of seawater: Journal of Geophysical Research, v. 90, no. C2, p. 3332–3342.

Holtz, R.D., and Kovacs, W.D., 1981, An introduction to geotechnical engineering: Englewood Cliffs, N.J., Prentice-Hall, Inc., 733 p.

Hunt, R.E., 1984, Geotechnical engineering investigation manual: New York, McGraw-Hill Book Company, 983 p.

Kvenvolden, K.A., and Lorenson, T.D., 2000, Methane and other hydrocarbon gases in sediment from the southeastern North American continental margin, *in* Paull, C.K., Matsumoto, R., Wallace, P.J., Black, N.R., Borowski,W.S.,Collett, T.S., Damuth, J.E., Dickens, G.R., Egeberg, P.K., Goodman,K., Hesse, R.F., Hiroki, Y., Holbrook, W.S., Hoskins, H., Ladd, J. ,Lodolo, E., Lorenson, T.D.,Musgrave, R.J., Naehr, T.H., Okada, H., Pierre, C., Ruppel, C.D., Satoh, M., Thiery, R., Watanabe, Y., Wehner, H., Winters, W.J.,and Wood, W.T., Gas hydrate sampling on the Blake ridge and Carolina rise; covering leg 164 of the cruises of the drilling vessel *JOIDES Resolution*, Halifax, Nova Scotia, to Miami, Florida, sites 991–997, 31 October–19 December 1995: Proceedings of the Ocean Drilling Program, Scientific Results, v. 164, p. 29–36.

Ladd, C.C., Foote, R., Ishihara, K., Schlosser, F., and Poulos, H.G., 1977, Stress-deformation and strength characteristics—State-of-the-art report: Proceedings of the Ninth International Conference on Soil Mechanics and Foundation Engineering, Tokyo, v. 2, p. 421–494.

Lambe, T. W. and Whitman, R.V., 1969, Soil mechanics: New York, John Wiley and Sons, 553 p.

Musgrave, R.J., Bangs, N.L., Larrasoana, J.C., Gracia, E., Hollamby, J., and Vega, M.E., 2006, Rise of the base of the gas hydrate zone since the last glacial recorded by rock magnetism: Geology, v. 34, no. 2, p. 117–120.

Novosel, I., Winters, W.J., Boldina, O.M., Labails, C., and Geli, L., 2007, Thermal conductivity of sediment recovered from the IMAGES VIII/PAGE 127 Gas Hydrate and Paleoclimate Cruise on the *R/V Marion Dufresne* in the Gulf of Mexico, 2–18 July 2002, *in* Winters, W.J., Lorenson, T.D., and Paull, C.K., eds., Initial report of the IMAGES VIII/PAGE 127 gas hydrate and paleoclimate cruise on the RV Marion Dufresne in the Gulf of Mexico, 2–18 July 2002: U.S. Geological Survey Open-File Report 2004–1358.

Pearson, C.F., Halleck, P.M., McGuire, P.L., Hermes, R., and Mathews, M., 1983, Natural gas hydrate deposits—A review of *in situ* properties: Journal of Physical Chemistry, v. 87, p. 4180–4185.

Reeburgh, W.S., 1976, Methane consumption in Cariaco Trench waters and sediments: Earth and Planetary Science Letters., v. 28, p. 337–344.

Sloan, E.D., 1998, Clathrate Hydrates of Natural Gases (2d ed.): New York (Marcel Dekker), 705 p.

Tréhu, A.M., Bohrmann, G., Rack, F.R., Torres, M.E., Delwiche, M.E., Dickens, G.R., Goldberg, D.S., Gracia, E., Guerin, G., Holland, M., Johnson, J.E., Lee, Y.J., Liu, C.S., Long, P.S., Milkov, A.V., Riedel, M., Schultheiss, P., Su, X., Teichert, B., Tomaru, H., Vanneste, M., Watanabe, M., and Weinberger, J.L., 2003, Proceedings of the Ocean Drilling Program, Initial Reports, v. 204: College Station, Tex., Ocean Drilling Program, 81 p. [CD-ROM; available from: Ocean Drilling Program, Texas A&M University, College Station, Tex. 77845-9547, USA.]

Xu, W., 2002, Phase balance and dynamic equilibrium during formation and dissociation of methane gas hydrate, *in* International Conference on Gas Hydrates, 4th, Yokohama, Japan, May 2002, Proceedings: Yokohama, Japan, International Conference on Gas Hydrates, p. 195–200.

Xu, W., 2004, Modeling dynamic marine gas hydrate systems: American Mineralogist, v. 89, p. 1271–1279.